Thermodynamic Analysis of a Combined LiBr-H$_2$O Absorption System with a Single Effect Evaporation Cycle

BY

Ahmed Mohammad Shaaban

A Thesis Presented to the

DEANSHIP OF GRADUATE STUDIES

KING FAHD UNIVERSITY OF PETROLEUM & MINERALS

DHAHRAN, SAUDI ARABIA

In Partial Fulfillment of the
Requirements for the Degree of

MASTER OF SCIENCE

In

Mechanical Engineering

March 2017

KING FAHD UNIVERSITY OF PETROLEUM AND MINERALS

DHAHRAN, SAUDI ARABIA

DEANSHIP OF GRADUATE STUDIES

This thesis, written by Ahmed Mohamed Shaaban under the direction of his thesis advisor and approved by his thesis committee, has been presented to and accepted by the Dean of Graduate Studies, in partial fulfilment of the requirements for the degree of MASTER OF SCIENCE IN MECHANICAL ENGINEERING.

_____

Dr. Mohamed A. Antar

(Advisor)

_____

Dr. Zuhair M. Gasem

(Department Chairman)

Med Habib 20/3/2017

_____

Dr. Mohamed A. Habib

(Member)

_____

Dr. Salam A. Zummo

(Dean of Graduate Studies)

_____

Dr. Gandhidasan P.

(Member)

26/3/17

_____

Date

ii

© Ahmed Mohammad Shaaban

March 2017

This Dissertation is

Dedicated to

My Beloved Parents

for their prayers and encouragement

Acknowledgements

I thank Allah for giving me the strength to complete my thesis. I would like to thank my family, especially my parents for their support and motivation. I acknowledge and appreciate my pervious advisor Dr. Maged A. I. El-Shaarawi for his valuable guidance, dedication to my work, and for providing the needed support and information in the thesis work. I really appreciate his kindness while being my advisor. I wish him good Health.

I would like to thank the most respectful professor Dr. Mohammed A. Antar my current advisor for his continuous guidance in the thesis and my personal life. I appreciate Dr. Antar for substituting Dr. Maged during his illness in a short notice. I hope our relation extends after finishing the master degree.

I would also like to thank, Dr. Mohamed A. Habib, Dr. Gandhidasan P. for their motivation and valuable time and effort that they dedicated on my research. Deep gratitude is also due to my distinguished friends in KFUPM, Basssel Alaa, Sherif Rashwan, Ahmed Abd El-Monem, Ahmed Yassin, Hamza Kamal, Ahmad El-Rashidi, Abd El-Rahman Etman.

Acknowledgment is due to King Fahd University of Petroleum & Minerals for supporting this research.

Table of Contents

List of Figures

List of Tables

Nomenclature

A	:	Area	m^2
BPE	:	Boiling Point Elevation	°C
C$_P$	:	Specific heat capacity	kJ/°C.kg
COP	:	Coefficient of Performance	-
CR	:	Circulation Ratio	-
COPc	:	Carnot Coefficient of Performance	-
Ex		Exergy	kW
h	:	Specific enthalpy	kJ/kg
HP	:	High pressure of absorption system	kPa
LP	:	Low pressure of absorption system	kPa
LMTD	:	Logarithmic mean temperature difference	°C
ṁ	:	Mass flow rate	kg/s
PR	:	Performance Ratio	-
Qa	:	Water quality	-
Q	:	Heat transfer	kW

s	:	Specific entropy	kJ/kg.°K
SHE	:	Solution Heat Exchanger	-
T	:	Temperature	°C
U	:	Overall heat transfer coefficient	kW/ m^2 °C
W	:	Pump work	kW
X	:	Salinity	g/kg

Subscripts

abs	:	Absorber
b	:	Brine
cond	:	Condenser
cw	:	Cooling water
desal	:	Desalinated
d	:	Distilled / Desalinated
evap	:	Evaporator
f	:	Feed/ saturation liquid

fg	:	The difference between vapor and liquid properties at saturation
g	:	Saturation vapor condition
gen	:	Generator
ra	:	Ratio
ref	:	Refrigerant
o		Ambient conditions/out
out	:	Out
s	:	Steam
ss	:	Strong LiBr solution
sp		Solution pump
sw	:	Seawater
v	:	Vapor
ws	:	Weak LiBr solution
in	:	Input

Greek Letters

ε	:	Effectiveness
ρ	:	Density

η :   Efficiency

Ψ :   Fluid stream exergy

Thesis Abstract (English)

NAME   :   **Ahmed Mohammad Shaaban**

Title   :   **Thermodynamic analysis of a combined LiBr-H_2O absorption system with a single effect evaporation cycle**

MAJOR FIELD   :   **Mechanical Engineering**

DATE OF DEGREE   :   **2017**

Thermodynamic analysis of hybrid H_2O-LiBr Absorption cooling and single effect desalination (SEE) system is investigated for standalone and combined systems. Engineering Equation Solver EES® software is utilized to calculate and evaluate the performance of the standalone and combined modes. The results showed that the increase of generator temperature from 75 °C to 90 °C has boosted COP, and PR by 10.86%, and 32.37%, respectively, at pressure of 40 kPa in the SEE unit. Moreover, the increase of evaporator temperature from 2 °C to 6 °C has increased COP, and PR by 3.2%, and 31%, respectively. However, the increase of condenser temperature from 30 °C to 45 °C has decreased COP, and PR by 10.6%, and 80%, respectively. In addition, the increase of absorber temperature from 30 °C to 45 °C has decreased COP, and PR by 4%, and 51%, respectively. On the other hand, the combined system performance which is called Overall Energy Utilization Factor (EUF) is boosted to a value of 1.6 which is almost double the performance of the standalone absorption system, where the COP value is 0.766. The drawbacks of the system are that the generator temperature must be over 78 °C to produce potable water through SEE system. Furthermore, desalination plant must be operated as long as the cooling plant is working to keep the cooling conditions for LiBr condenser in order to have a heat rejection component of the cycle.

Thesis Abstract (Arabic)　　　　ملخص الرسالة

الاسم	**:**	**أحمد محمد شعبان**
عنوان الرسالة	**:**	**التحليل الحراري لدورتين الهجين بين دورة الامتصاص بستخدام بروميد الليثيوم مع الماء و دورة التبخر تأثير واحد**
التخصص	**:**	**الهندسة الميكانيكية**
تاريخ التخرج	**:**	**2017**

تم دراسه التحليل الحراري لدورتين الهجين بين دورة الامتصاص بستخدام بروميد الليثيوم مع الماء (H_2O-LiBr) و دورة التبخر تأثير واحد (SEE) لكل نظام علي حدة و هجين. استخدم برنامج (EES) لحساب و تحليل الاداء و الكفاءه للانظمه المختلفه. النتائج اظهرت ان بزياده حراره ال(Generator) من $75°C$ الي $90°C$، تم رفع معامل الاداء (COP) و نسبه الاداء (PR) بنسبه 10.86% و 32.37% ، بالترتيب، عند ضغط 40kPa. بالاضافه، بزياده حراره ال(Evaporator) من $°C$ 2 الي $6°C$ تم رفع معامل الاداء (COP) و نسبه الاداء (PR) بنسبه 3.2% و 31% ، بالترتيب. ومع ذلك ، بزياده حراره ال(Condenser) من $30°C$ الي $45°C$ ، انخفض معامل الاداء (COP) و نسبه الاداء (PR) بنسبه 10.6% و 80%، بالترتيب. بالاضافه، بزياده حراره ال(Absorber) من $30°C$ الي $45°C$ ، انخفض معامل الاداء (COP) و نسبه الاداء (PR) بنسبه 4% و 51% ، بالترتيب. من الناحية أخرى، تحليل الاداء لنظام الهجين المسمي بمعامل استخدام الطاقه العاليه الاجماليه (EUF) ،تم رفع كفاءته لقيمة 1.6 وهو ما يقرب من ضعف كفاءة أداء نظام امتصاص مستقلا، حيث ان قيمه (COP) كانت 0.766. من عيوب النظام ان حراره ال(Generator) يجب ان تكون اعلي من $°C$ 78 لانتاج مياه محلاه من خلال وحدة SEE. علاوة على ذلك، نظام التحليه يجب ان يعمل طالما نظام الامتصاص يعمل للحفاظ على شروط التبريد ل (LiBr Condenser) ، للحفاظ علي طرد الحراره من النظام كك

Chapter 1: **Introduction**

Nowadays, the world is facing three major problems that affect the existence and the comfort of humans. These problems are; high energy demand, global warming, and water scarcity.

Firstly, energy demand has been increased in many regions all over the world, especially in the Gulf area. The International-Institute-of-Refrigeration-in-Paris (IIR) has predicted that 15% of worldwide electricity production used in the HVAC devices [1]. Moreover, about 45% of the electricity consumption is employed in air-conditioning systems in the commercial buildings. New technology has been used to decrease the electricity consumption in HVAC systems specially in the Vapor Compression Systems (VCS), where compressors are highly consuming energy devices. The new technology is called absorption system, where it replaces the high energy consuming compressor with an absorber and generator operated by low grade energy.

Secondly, the global warming problem is observed as increasing the average temperature of the earth atmosphere. This temperature increase is due to the greenhouse effect, where some hazard gases as carbon dioxide, carbon monoxide, and chlorofluorocarbons preserve the heat produced from industrial applications. Scientists reported that more than 95.5% of the global warming is being caused by human behavior. Researchers implemented many techniques to decrease the poisoned exhaust for factories, and discovered new chemical mixtures to replace the hazard chlorofluorocarbons used in refrigeration and cooling, hence, reducing the greenhouse effect.

Thirdly, the water shortage problem has been amplified during last years, this problem is threatening the existence of the human beings, where more than one billion people cannot drink

potable clean water [2]. Moreover, some areas, like the Arabian Gulf regions, have no access to natural pure drinking water. World Health Organization (WHO) considered any country water resources less than 1000 m3/y/capita is lower than the scarcity line [3]. Researchers who are working in the desalination field helped in solving the water shortage problem by developing new desalination technologies every now and then. Researchers investigated in the solar cooling and desalination systems to have a unique design, this design can produce both cooling effect and fresh water. The combination of absorption cooling and thermal desalination systems have a promising results. The absorption subsystem uses free solar or waste energy as an input energy and rejects the energy to the desalination through the absorption condenser. This energy evaporates water vapor from the hot brine to produce potable safe water for drinking[4].

1.1 Refrigeration Absorption System

During the past century, scientists discovered the detrimental effect of CFCs which is known in the market as Freon. It is dangerous to our health and causes depletion in the ozone layer that protects us from the harmful ultraviolet rays [5]. CFCs compound are used extensively in refrigeration process, where the boiling point of the solution varied from -49 °C to 92 °C depending on the compound. European Community and other 24 countries approved the Montreal Protocol to legalize the usage of the CFCs fluid. Researches succeeded to replace the CFCs substances with other mixtures for air conditioning and refrigeration processes. In addition, the high operating energy cost needed for the simple VCS and the high cooling requirements led to alternative systems like absorption systems. Absorption cooling systems was the solution to decrease fossil fuel consumption needed for refrigeration and to reduce gas emissions accompanied with the production of electricity. The generator input energy source can be obtained from either waste heat

produced from any industrial/manufacturing processes or from natural solar radiation that is collected by the means of thermal solar collectors.

Absorption cooling system has been developed in 1700`s, where it was known as ice maker that depends on the evaporation of water from sulfuric acid solution vessel [6]. In 1859, absorption cooling using water-ammonia (NH_3-H_2O) as the working fluid, was introduced by Ferdinand Carre to solve the corrosion effect of sulfuric acid [7], where it was used in refrigeration systems before. Water-ammonia absorption cycle has been used for cooling and heating demand. This system has an advantage, where its freezing temperature can reach -77 °C, where it can be used in storing food and ice production [8]. However, an extra device (rectifier) is needed to strip away the evaporated water (volatile absorbent) with ammonia (refrigerant). Without a rectifier the evaporated absorbent (water) would accumulate in the evaporator, hence decreasing the system performance. Thereafter, H_2O-LiBr solution was introduced as a new working fluid that can operated at a lower generator temperature with a higher performance than ammonia solution.

Principle of operation

Absorption system consists of a binary solution of refrigerant and absorbent material [8]. They are located inside two evacuated vessels connected together through pipes as shown in Figure 1-1. The right vessel contains binary solution of refrigerant and absorbent while the left vessel contains only liquid refrigerant. Due to the low pressure, solution in the right vessel will absorb refrigerant vapor from the left vessel causing pressure to decrease more, whereas the temperature of the liquid refrigerant reduced because of vaporization effect. This phenomenon called the refrigeration effect (left vessel). While the solution the right vessel is diluted as it the absorbent absorbed vapor, hence

absorption phenomenon occurs. This phenomenon is an exothermic reaction so heat is rejected to the surrounding as shown in Figure 1-1a. At this state, the process will stop because of the saturation of the refrigerant, so heat must be added to the right vessel (solution) to evaporate the vapor from the diluted solution as shown in Figure 1-1b. Thereafter, the evaporated refrigerant will flow to the left vessel and condenses by rejecting heat to the surrounding.

This simple cycle is an intermittent operation where refrigeration effect cannot be occurred continuously. Subsequently, a modification done to ensure the simultaneously operation where absorption process occurs at low pressure, while the separation process occurs at a higher pressure as shown in Figure 1-2.
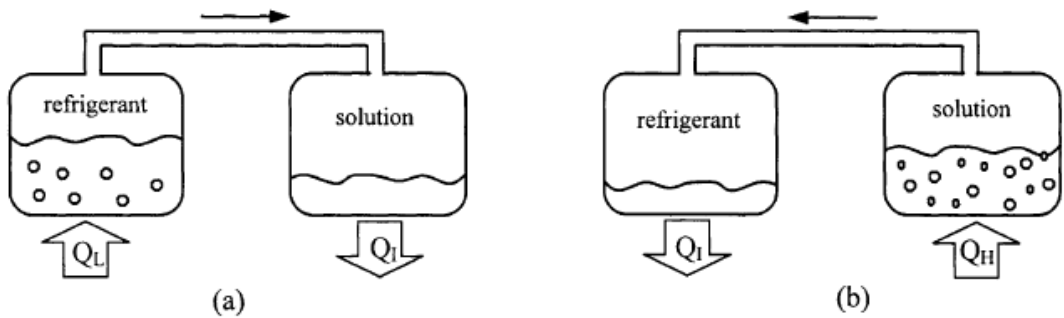
Figure 1-1 Principle of operation of intermittent absorption system [8]

4
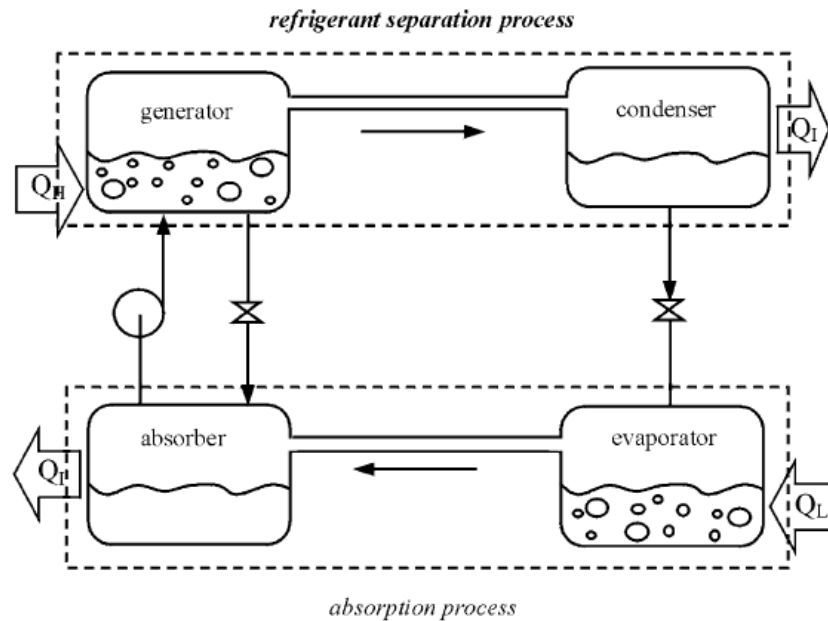
Figure 1-2 Absorption refrigeration cycle continuous operation [8]

1.1.1 Aqueous Lithium Bromide Solution

H_2O-LiBr solution is a mixture of water and lithium bromide salt that is used in refrigeration and air conditioning applications. It has more advantages than ammonia solution, such as it does not need rectifier as the refrigerant is water, and it is less volatile than LiBr (salt). In addition, the coefficient of performance (COP) of H_2O-LiBr is higher and the working fluid is safer than ammonia. However, using water as a refrigerant would limit the cooling temperature to be above 0°C. Another drawback, the high concentrated solution is exposed to the crystallization phenomenon which could decrease system performance.

The generator output temperature needed is high in water-ammonia mixture (125°C- 170°C), that can be supplied from concentrated parabolic collectors not from simple flat plate collector, hence increasing the initial and maintenance cost of tracking system. On the other hand, the

5

generator output temperature of H_2O-LiBr varies from (70°C- 110°C), which is lower than water-ammonia mixture that can be achieved by any type of thermal solar collector especially flat-plate collector [9].

The performance of the system can be measured by the coefficient of performance (COP), which is defined as the cooling capacity to the total energy input of the whole system.

In the terms of construction and COP, H_2O-LiBr absorption system can be categorized into three types [10], [11];

Single effect absorption system   COP = 0.6-0.88

Double effect absorption system   COP = 1.5-1.65

Triple effect absorption system   COP = 2.1-2.3

The main benefits of absorption systems over other types are as follow;

1. Energy free (Solar energy/ waste energy).
2. Less maintenance. (No compressor)
3. Environment friend solution.
4. Longer lifetime than vapor compression system (VCS).
5. Less vibration than VCS

However, absorption systems need large construction area, and they have lower COP than VCS.

Working fluid properties for absorption system:

The performance of the absorption system mainly depends on the thermodynamic and chemical properties of the binary solution. The binary mixture must be totally miscible and homogenous in the vapor and liquid phases.

The mixture should satisfy the following safety and thermodynamic properties [6];

- Non-toxic and non-inflammable solution for safety issues.

- Chemically-stable (To avoid any unwanted formation of gases).

- Homogenous mixture and no solid salt exist (crystallization), as salt formation could block the internal solution flow and decrease the thermal performance.

- Non-explosive solution for safety.

- Non-corrosive solution for durability.

- High elevation boiling temperature difference between pure refrigerant (water) in (LiBr absorption system) and binary mixture at a constant temperature.

- The refrigerant has high heat of vaporization.

- Volatility ratio (The refrigerant –water- should be more volatile than the salt-absorbent- to be easily separated in LiBr solution)

- Moderate pressures are used in the system to decrease the wall thickness and the pumping power to circulate the flow.

Comparison between H_2O-LiBr and H_2O-NH_3 solutions are shown in

Table 1-1.

Table 1-1 Comparison between H_2O-LiBr and H_2O-NH_3 solutions [12]

	H2O-LiBr absorption cooling system	H_2O-NH_3 absorption cooling system
COP	Higher COP than other solutions	Lower COP than LiBr solution
Complexity	Simple design	Complex design needs extra components than LiBr solution
Temperature limits	Cannot reach subzero temperature	Works efficiently at subzero temperatures
Generator temperature	Lower input heat is needed, generator temperature varies from 70 °C – 88 °C	Higher input heat is needed, generator temperature varies from 90 °C – 180 °C
System Pressure	Low pressure needed	Higher pressure is needed hence more pumping power
Hazard	Safe mixture	Ammonia is dangerous

For the stated reasons, LiBr solution is the best option for low-grade energy to be used in most of air-conditioning applications with higher COP.

1.2 Thermal Desalination system

The scarcity of fresh water resources in different areas especially in the Arabian Gulf region is threatening the human existence [13]. The water consumption average rate in Gulf Countries is estimated to be 400 liters per day per person according to WHO. Therefore, researchers worked on the desalination field to provide potable water from saline water[14]. The total water resources across the world are expected to be 43,750 km^3/year, where the largest share goes to the American continent with a 45%. Figure 1-3 shows the percentage of fresh water from the total water resources. Figure 1-4 shows the distribution of fresh water resources with sectors consumption.
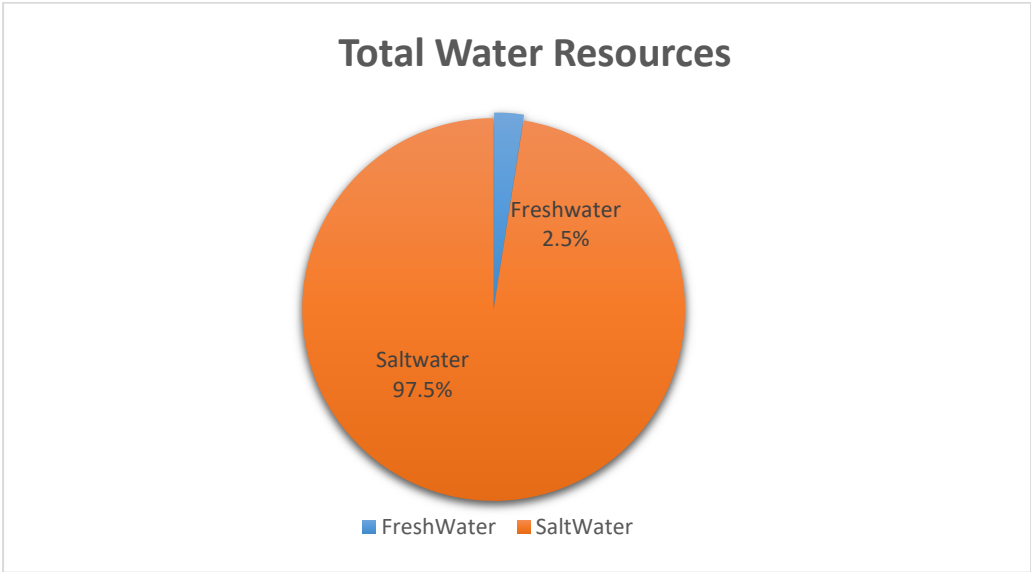
Figure 1-3 Total water resources worldwide
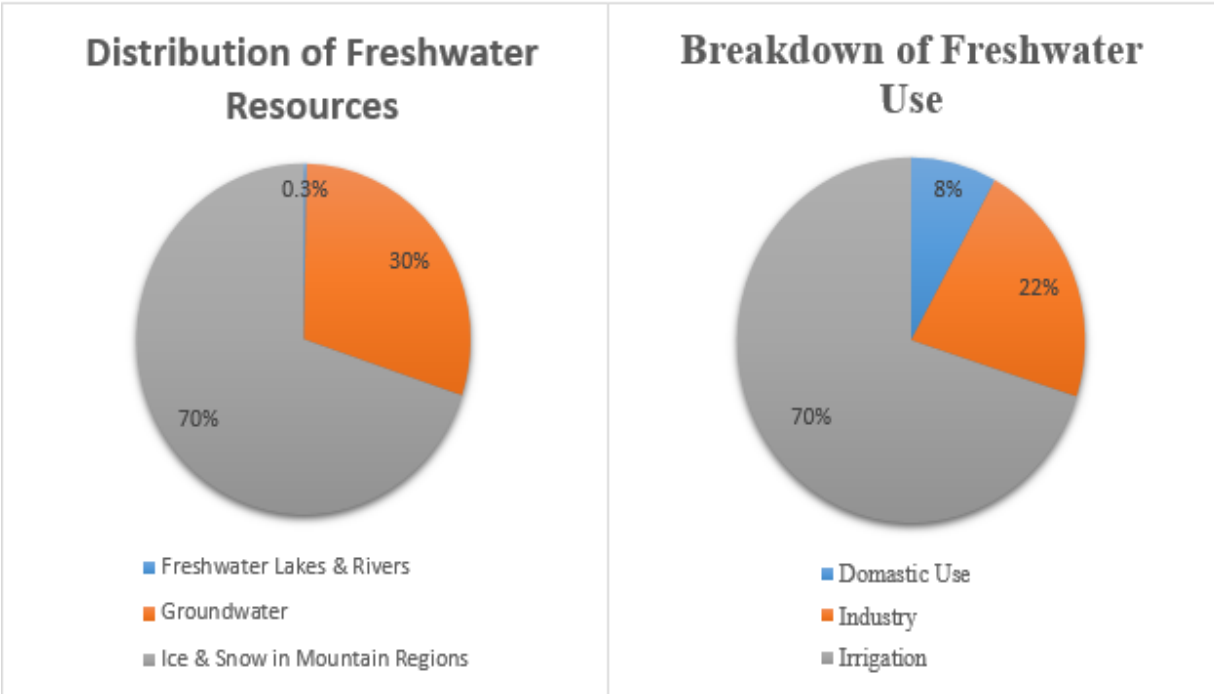
Figure 1-4 Freshwater resources distribution and freshwater usage sectors

The Gulf Cooperation Council (GCC) countries are the largest consumer for desalinated water, where 65% of the desalinated water produced there, starting from 1938 [2].Desalination process is the separation of saline or brackish water into brine (high concentrated salty water) and pure water (free salt) by mechanical, or thermal, or electrical technique as shown in Figure 1-5 [15].

The natural thermal desalination mainly depends on the natural circulation of the rain, where the sun evaporates water from lacks, seas, and oceans to a pure water vapor that accumulates and condenses again through the clouds.
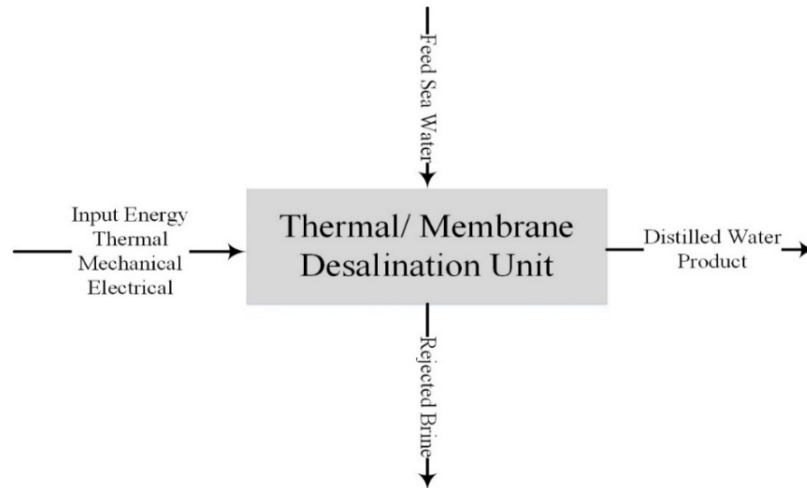
Figure 1-5 The principle of desalination process

Nowadays there are more than fourteen thousand desalination plants all over the world producing billions of gallons of fresh water per day. However, most of the existing desalination plants are operated by fossil fuel, where the fuel price is expensive and produces harmful emissions pollution. In addition, the emissions cause a greenhouse effect that changes the natural climate.

Many countries have the shortage of both fresh water and fossil fuel hence renewable energy as solar, wind energies gained great attention as they can reduce the pollution and greenhouse effect. Solar energy solved many problems in power production and thermal desalination lately, especially in the solar belt regions. Solar collectors are the devices used to collect sun rays, where solar collectors can be classified by the mean of absorbing the rays. The main thermal solar collectors are flat plate collector(FPC), evacuated tube collector (ETC), parabolic reflectors, and compound parabolic collector (CPC), where air or water are used as a working fluid to transfer heat to the application. On the other hand, photovoltaics collectors are used to collect sun rays to

be converted to electricity, where electricity can be used to operate desalination plants or any systems [4].

Many thermal desalination techniques are implemented and modified to meet the required distilled water demand. The popular techniques are mainly multi-stage flash (MSF) and multi-effect evaporation (MEE) plants, where they can produce a high distilled water flow rate compared to other techniques. Table 1-2 shows the most available desalination units in the industry [15]. Single effect desalination system will be discussed in the following section.

Table 1-2 Water Desalination Techniques

Thermal desalination process	Membrane desalination process
Single / Multi Effect Desalination (SEE/MED).	Reverse Osmosis (RO).
Multi-Stage Flash Desalination (MSF).	Membrane Distillation (MD).
Vapor Compression Evaporation (VC).	Electro-Dialysis (ED)
Humidification and Dehumidification (HDH)	

1.2.1 Single Effect Evaporation System

Single Effect Evaporation Desalination System (SEE) is the simplest form from Multi Effect Desalination System (MED), where it is used in marine vessels and in remote regions [16]. Figure 1-6 shows the configuration of SEE unit, where the basic components for SEE are an evaporator, a preheater/condenser, and connecting pipes. The evaporator consists of heat exchanger tubes,

distributing salty water pipes, demister, brine drum (container). The condenser consists of shell and tubes heat exchanger, distilled water collector.

The condenser acts as a preheater as it preheats the salt water charge entering the condenser with the condensed water vapor by losing its latent heat. The preheated salt water is sprayed over the evaporator hot tubes to evaporate a percentage of it, while the other portion (brine) is pumped out of the system. The evaporated water vapor portion is directed to the condenser to be condensed and collected as a pure water.
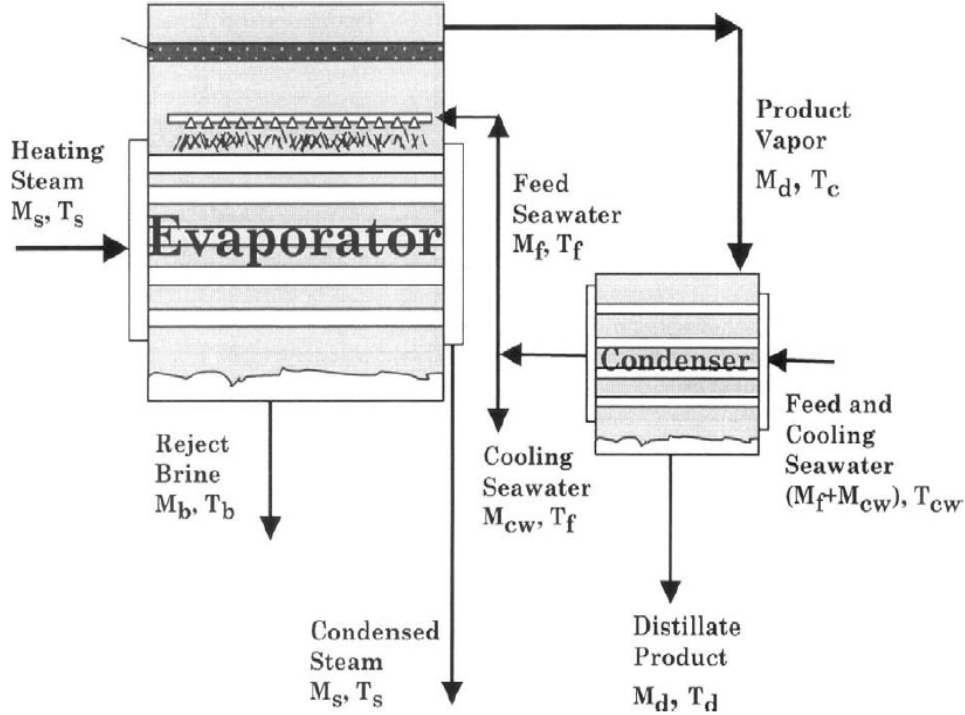
Figure 1-6 Single Effect Evaporation System (SEE) configuration [16]

It must be taken into account;

- The feed seawater charge must be deaerated and chemically treated before being injected into the system. Water treatment is needed to prevent foaming and scaling inside tubes of the condenser, and outside tubes of the evaporator.

- The non-condensable gases in the condenser space should be expelled out to preserve the heat transfer capacity and to keep the system pressure constant for a performance ratio.

1.3 Objectives and Methodology

1.3.1 Objectives

The main purpose of this research is to study the performance of a combined system that can provide a cooling effect and potable drinking water by the following procedures

1. Investigate the performance of the single effect evaporative desalination subsystem.

2. Model the single effect evaporative desalination subsystem.

3. Investigate the performance of a single stage aqueous LiBr absorption subsystem.

4. Model the single stage aqueous LiBr absorption subsystem.

5. Couple the two basic subsystems.

6. Model the coupling of the absorption and the desalination system.

1.3.2 Methodology

In this thesis, thermodynamic analysis of the combined absorption cooling and desalination plant will be reviewed and discussed, afterward the results will be, analyzed and reported as the following steps:

1. Literature review on the thermal desalination cycles especially the proposed system.

2. Literature review on the absorption cooling H_2O-LiBr absorption refrigeration cycle.

3. Mass and energy balance will be conducted using Engineering Equation Solver (EES) for standalone and combined cycles.

4. A parametric study will be investigated at different input parameters to show the analysis of system performance.

Chapter 2: **Literature Review**

2.1 Cooling System

Fan, et al [1] presented a technical review on solar sorption that includes both absorption and adsorption cooling technologies. Absorption cooling is a process where material transfers from one phase to another-from a liquid solution to vapor-form. However, adsorption cooling is a process of separation of a substance from one phase, where accumulation is on another surface. More research work is needed to improve the COP through enhancing the mass and heat transfer and the systems design to utilize the rejected energy.

Aphornratana and Sriveerakul [17] made practical study on a single-type absorption refrigeration cycle with an aqueous LiBr solution. They constructed the system with different temperatures range of generator, condenser, and evaporator as 65-85 °C, 25-45 °C and 3-11 °C respectively. The results showed that the COP increased by 60% by using solution heat exchanger that reduced the heat needed in the generator, also decreased cooling effect needed in absorber. Moreover, the measured solution circulation ratio was more than the theoretical solution circulation ratio by 2-5. Parametric studies done with temperature range for different devices. The researchers showed that the generator can be run at a low temperature at 65 °C with a reasonable performance.

Kurem and Horuz [18] studied a comparison between the basic cycles of vapor absorption refrigeration operating with aqueous LiBr and aqueous ammonia solutions. They focused on the COP, the cooling capacity and the temperature limitation of the solutions. The study showed that

aqueous LiBr gives more COP and less system complexity. However, LiBr solution disadvantage is the temperature limitation as the refrigerant is water, where ice formation is counted at low temperature, moreover, crystallization zone due to low solution temperature with high LiBr concentration. On the other hand, aqueous ammonia system is more complex where water is a volatile substance and can escape with ammonia vapor from the generator. The escaped water accumulates in the evaporator leading to raise the temperature, hence decreasing cooling effect and COP. Consequently, rectifier and analyzer accompanied with the system to eliminate the pervious phenomena. The analysis indicated that the COP increased with increasing the generator temperature as the flow rate of refrigerant increased thus boosting the cooling effect.

Horuz and Callander [19] examined the performance of a commercial vapor absorption refrigeration system (VAR) that is heated by the aid of natural gas. The hot flue gases were supplied to the aqueous ammonia VAR unit, where the cooling capacity was designed to be 10 kW. The results showed that the lower combustion emissions, the lower refrigerant flow rate produced (ammonia), hence low COP. In addition, the higher the chilled water inlet, the higher cooling capacity. Moreover, decreasing the condenser cooling water temperature more than absorber cooling water temperature will increase the system efficiency.

Asdrubali and Grignaffini [20] evaluated experimentally the performance of an aqueous LiBr absorption refrigerator cycle. They used 3 variable electrical resistances with a nominal power of 10 kW each, as heating sources in the generator. The experiment showed that the maximum COP was achieved at 70°C, hence, solar energy is the best choice for the heating mode. Furthermore, the excessive increase of the input temperature to the generator would decrease the COP of the cycle. On the other hand, the change of the feed flow rate had no effect on the COP because the

system compensates the decreasing flowrate by increasing the temperature difference between inlet and outlet of the generator.

Hammad and Audi [21] explored the performance of an aqueous double LiBr absorption system using solar flat plate and concentrator collectors as heat input to the generator in Amman, Jordan. They focused on the factors affecting the COP of the system. They proved that the COP increased with the increase of solar intensity; hence, increasing the generator temperature. In addition, the temperature difference between ambient and evaporator has direct effect on the operation. It was found that the peak measured COP of the system during August and September days was 0.55, while the ideal COP was 1.6.

Raja and Shanmugam [22] explored different factors affecting the single effect absorption system to minimize the total cost. They found from the literature that aqueous LiBr solution is the most common working fluid as is the cheapest across the absorption systems and has no ozone depleting possibility. It was found that vapor mass flux increased by increasing the absorber pressure. Moreover, evacuated tubes and flat plates are the most common and economical for this design. The authors implemented a new design to increase system`s efficiency and decrease initial and running cost. The generator is placed inside a hot tank for a steady operation to decrease heat loss to the surrounding in the simple cycle, hence, decreasing the thermal insulation needed. In addition, the solar collector was located over the tank to take the advantage of Siphon theory, hence, removing the solar circulating pump. Moreover, low boiling temperature for the solution can be achieved by decreasing the working pressure. Although the COP would be greater by using a wet cooling tower, but a dry one is used to prevent the problem of legionella.

Lansing [23] modeled a single stage H_2O-LiBr absorption refrigeration unit at Goldstone energy. He discussed the operation for the refrigeration system and focused on the mathematical formulation. He suggested to heat the solution in the generator to a temperature above 80 °C, hence, keeping an efficient operation. The experiment showed that the COP for the cycle was 0.776 with temperatures 90, 40, 7 and 40 °C for the generator, the absorber, the evaporator and the condenser, respectively.

Bolocan, et al [24] fabricated an ammonia-water absorption refrigeration prototype system that is operated by a low-temperature energy. EES software is used to simulate the performance of the system. The results showed that the highest COP is 0.43, where this value is less than the predicted one because of no insulation used and the liquid separator need to be modified.

Prasartkaew [7] investigated the performance of a renovated single stage H_2O-LiBr absorption system. The study was operated with strong LiBr concentration (after vaporization of the refrigerant) of 59% and the heat supplied to the generator was from electric heaters, where the generator temperature was 85 °C and the maximum refrigeration capacity was 7 kW. He conducted the experiment with three generator temperatures 80 °C, 85 °C and 90 °C, where at 80 °C the temperatures of the whole cycle were stable. On the other hand, the cooling capacity of the system was 50%, 72% and 75% from the rated refrigeration capacity when the inlet hot water to the generator was 80 °C, 85 °C and 90 °C, respectively. The COP for the three cases varied as follow 0.52, 0.58 and 0.53.

Sencan, et al [25] performed thermodynamic analysis of H_2O-LiBr absorption system for heating and cooling functions. They calculated and simulated the energy balance, and the exergy loss across every component on FORTUN 90 software to improve each component. Exergy loss

reduces the performance of the system because of solution mixing loss, low mass and heat transfer across the single components, and circulating loss. Moreover, the mixing losses accompanied with the evaporation process of the water refrigerant in the generator, where additional energy is needed for a superheated refrigerant vapor, hence, higher exergy loss. Therefore, exergy efficiency can be enhanced by a proper heat source selection with the right working mixture. It was shown that the cooling and heating COP increased with a higher heat source temperature, however the exergy efficiency decreased as the input energy and the exergy losses increased. In addition, the COP increased with the temperature rise in the chilled water at the evaporator as more cooling capacity can be created. However, the exergy efficiency decreased as the cooling effect decreased with higher chiller water temperature.

Ketfi, et al [26] modeled and simulated a single stage H_2O-LiBr absorption cooling system in Algeria using Matlab and EES software. The system used a binary solution with a cooling capacity of 17.6 kW. The COP performance of the cycle, the exergy destructed in each component and the second law of thermodynamics COP-II were investigated to recognize the best working conditions. The paper showed that the COP rises sharply as generator temperature increases from 67 °C to 75 °C and keeps constant from 75 °C to 100 °C.

Majdi [27] compared the performance of a modified single stage H_2O-LiBr absorption cycle with a thermal ejector Figure 2-1, and a basic H_2O-LiBr cycle. He utilized the kinetic energy of the vapor produced from the generator to enhance the performance and to decrease the cost of using double stage system. The Engineering Equation Solver (EES) software is used to calculate the performance of both systems. The results illustrated that the thermal heat load of both the evaporator and the condenser increased by increasing the temperature of the generator, however it inversely proportional to the condenser temperature. The entrainment mass ratio is constant at

different generator temperature. The COP is boosted by the new modification from 8%-60% by changing the condenser temperature from 24 °C to 45 °C, and from 30%-84% by increasing the evaporator temperature 0 °C -10 °C. The maximum COP achieved for the simple cycle and modified cycle is 0.83 and 1.6, respectively at evaporator temperature of 10 °C.
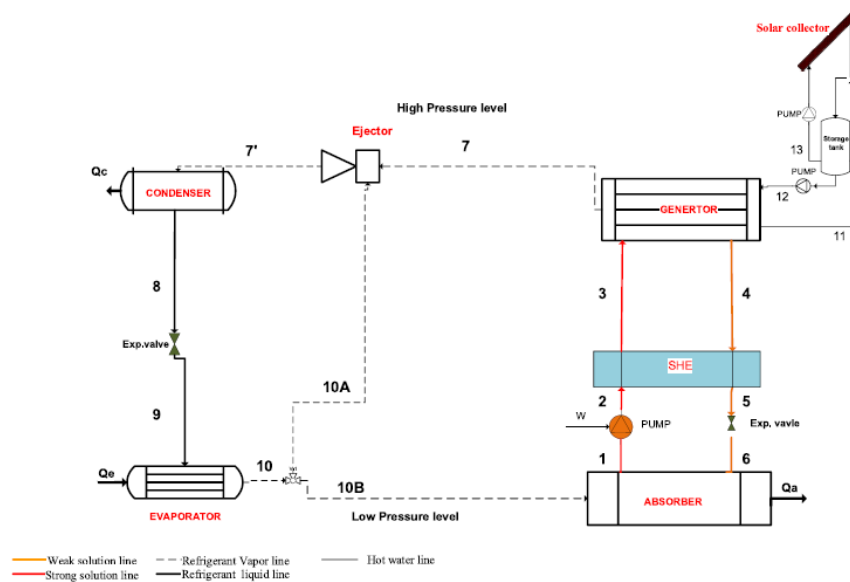
Figure 2-1 System configuration of single-stage combined absorption–ejector refrigeration system [27]

Agyenim, et al. [28] designed a solar cooling prototype using H_2O-LiBr absorption technique in Cardiff University. They explored the COP of both the prototype and compared it with numerical results. The average thermal COP for the proposed system was 0.58 using 12 m^2 vacuum tube solar collector arrays in a hot summer day with average hourly radiation of 800 W/m^2. The system was feasible and it produced 7.5 °C chilled water at an electrical COP of 3.64.

Florides, et al [29] designed and constructed a LiBr absorption refrigeration system. They performed a sensitive analysis using a computer program to evaluate system performance. The

analysis shows that as the generator temperature increases the COP decreases at a certain operating conditions, because the high pressure increases with the generator temperature that has a direct relation on the concentrated LiBr flowrate and the produced refrigerant. Moreover, the system performance can be enhanced by increasing the effectiveness and the area of solution heat exchanger. The authors concluded that the absorber exit temperature must be maintained at a lower level, where if the exit temperature was around 30 °C that would result an outlet LiBr percentage 58% from the absorber. On the other hand, the cost of 10 kW absorption cooling system was calculated to be $5255 including all auxiliary components.

Kaushik and Singh [30] studied the first and second law of thermodynamic for LiBr vapor absorption refrigeration system. The authors designed the absorption system with a cooling effect of 5.25 kW. They computed the heat transfer across every component and the COP of the system. The results showed heat transfer across generator, absorber, condenser, and COP of the system are 5.96 kW, 5.724 kW, 5.48 kW, and 0.881, respectively. Energy and exergy analysis for both single and parallel flow two-stage LiBr solution absorption system are studied [31], [32]. Results show that the highest COP and exergy efficiency of a single stage absorption system are 0.78, 11.48%, respectively. However, the highest COP and exergy efficiency of a two-stage absorption system are 1.373, 11.576%, respectively. Moreover, the COP of the two systems increased and the exergy efficiency decreased by increasing the evaporator temperature.

Karamangil, et al [33] studied the performance of a single absorption refrigeration cycle using ammonia–water (NH_3–H_2O), lithium bromide (H_2O–LiBr) and NH_3–$LiNO_3$ as a working fluid pairs. They investigated the thermodynamic analysis using a simulating visual software package that is created by Delphi programming. The COP increased by 66%, 14% and 6% by using solution heat exchanger (SHE), refrigerant heat exchanger (RHE) and solution–refrigerant heat exchangers

(SRHE) respectively, as the mass flow rates and temperature differences between the inlet fluids for SHE are larger than the other heat exchangers. The effectiveness of SHE has the greatest effect on the system, the COP is 0.55 at 0.7 effectiveness. For H_2O–LiBr cycle, the temperature range is smaller than NH_3–H_2O cycle and less than 100 °C because of crystallization phenomena. On other hand, NH_3–$LiNO_3$ mixture has an advantage over other solutions, the generator temperature can be operated efficiently at low temperature at 75 °C or less.

Wonchala, et al [34] studied the performance of aqueous LiBr absorption cooling machine. They evaluated first and second laws of thermodynamics, and circulation ratiowhich is a design parameter that measures the physical dimensions for the system. The results show when the generator exit temperature was varied from 60 °C to 110 °C, the heat rejection from the absorber, and condenser increased by 65%, while cooling effect increased by 1200%. Moreover, the circulation ratio was improved by increasing the generator temperature, where the circulation ratio decreased to a value of 6 at generator temperature of 100b°C. However, the circulation ratio was not affected by the effectiveness of solution heat exchanger.

Gomri [35] compared the COP and the exergy efficiency of two systems; single and double effect vapor absorption systems. Thermodynamic analyses including mass of conservation, 1st and 2nd law of thermodynamics are modeled on Fortran software to study the performance of the two systems. The cooling load was kept constant at 300 kW. The COP of the two systems increased by increasing generator temperature, however the COP has a limit and starts to decrease slightly. The COP has an optimum value which increased by increasing the mean temperature of the evaporator. On the other hand, the exergy efficiency for each component has a value depending on optimum generator temperature, where by increasing the generator temperature the exergy efficiency starts to decrease. The maximum value of the COP was in the range of 0.74- 0.79 and

1.22-1.42 for single and double effect systems, respectively. The highest energy quality (exergy) efficiency was in range of 12.5%–23.2% and 14.3%-25% for single and double effect systems, respectively. The paper showed that the COP of double effect absorption system is roughly double the COP of single effect absorption system, but the energy quality of double effect system increases slightly over single effect system.

Kaushik and Arora [36] developed a computational model to calculate COP and exergy efficiency of single stage and series flow two-stage H_2O-LiBr absorption refrigeration systems. The results indicated that the range of COP was 0.6-0.75, while the exergy efficiency range was 1-1.28. The COP of the series flow two-stage system is almost 60-70% greater than the single stage system. Moreover, the optimum generator temperatures for single, and double stage systems are 91 °C, 150 °C at constant temperature of 37.8 °C for the condenser and absorber. On the other hand, the exergy efficiency increases by increasing the generator temperature till a certain limit of 80 °C for single stage and 130 °C for double stage, then the efficiency starts to deteriorate.

Al-Ugla, et al. [37] studied the performance of 24-hour operating solar H_2O-LiBr absorption air conditioning system. They suggested three alternative designs (cold storage, heat storage, and refrigerant storage) to operate the solar cooling system -no solar energy available- at night. The results showed that the best option was the refrigerant storage since the operating pressure is low, so no critical requirements needed, less insulation are needed, and the solar collector field area are much smaller compared with the other two types. The COP of a system with heat storage, cold storage, and refrigerant storage was 0.788, 0.7703, and 0.7703, respectively.

Romero, et al [38] compared the maximum COP and enthalpy coefficient of performance between H_2O-LiBr and some aqueous ternary hydroxide mixtures (NaOH: CsOHK: KOH) with

this proportional quantity (40:24:36). The analysis was calculated at steady state. The maximum Carnot COP of ternary solution was 1.5 more than the enthalpy COP. On the other hand, the COPe of ternary solution was between 1.2-2.2, which are quite high for absorption system compared with simple LiBr system. The generator and absorber temperatures ranges could reach 170 °C and 100 °C receptively. However, this new ternary solution has lower mass and heat transfer coefficient because of low density and viscosity, the hazard of corrosion at high temperatures.

Liao and Radermacher [39] studied the crystallization phenomena associated with H_2O-LiBr absorption system. Too high solution concentration of aqueous LiBr over a certain range or too low solution temperature lead to crystallization. Crystallization phenomena means the formation and appearance of solid crystals in the solution. It usually occurs in a strong solution injected inside the absorber, where high concentration of LiBr salt exists. This salt accumulates inside the connecting pipes that leads to blocking the flow and affecting the system performance. Therefore, the concentrated solution temperature should be raised over the saturation temperature, so that the crystalized salt will dissolve again in the mixture but within a time.

Farshi, et el [40] studied the crystallization possibilities for three different configurations - series, parallel and reverse parallel models of double H_2O-LiBr absorption refrigeration systems. A computer program using EES software is utilized to calculate the performance of the systems. The results showed in case of series flow configuration, the possibility of crystallization increased by increasing the evaporator, and main generator (higher temperature) temperatures. However, in parallel and reverse parallel configurations, the crystallization probability is low, but caution must be taken in experimental work as the operating conditions may change.

Kaita [41] developed thermodynamic equations valid for H_2O-LiBr solution at very high temperature. The author developed the equations by gathering a measured data of heat capacity and vapor pressure. The equations can calculate enthalpy, entropy, and vapor pressure for the solution. Those equations are applicable for concentration range of 46% - 60%, and temperature range of 40 °C-210 °C. Therefore, this analysis is useful in modeling the triple effect H_2O-LiBr absorption system.

2.2 Desalination System

Shatat, et al [42] showed a comprehensive review on the different types of the desalination plants and the coupling with solar energy. Kalogirou [43] revealed that desalination used 10,000 tonnes/year of oil to produce 1000 m^3/day, that is reflected to be a highly consumption rate of fuel, therefore solar energy can be used as a sustainable, low operation cost, emission free source. The researchers divided the desalination process into two categories; thermal desalination and membrane desalination processes, moreover additional technologies including ion exchange and freezing processes. Thermal desalination process mainly depends on heating the sea or brackish water where evaporation takes place then condensation of the potable pure vapor is collected. The main thermal water desalination technologies available in the literature and the industry are Multi-effect desalination (MED), Multi-stage flash desalination (MSF), vapor compression evaporation (VC) and humidification-dehumidification (HDH). On the other hand, membrane technology depends on the property of the membrane accompanied with micro-filtration as well as nano-filtration for purification of seawater and removing of viruses, monovalent and multivalent ions. Solar MED and MSF desalination plants are recommended for a large production scale.

Casimiro, et al [44] presented a hybrid system contains a single effect evaporation system (SEE) operated by a Rankine cycle hybrid system. They modeled the whole system using TRNSYS software at steady state. The paper focused on the mathematical model of the single effect evaporation system and described the feasibility study by using concentrated solar power plant. The simulation by FORTRAN program showed that SEE has very low performance ratio. Though, this system will aid the simulation for more complex cycles.

El-Dessouky, et al [16] developed a numerical model to calculate the performance of a certain design for a SEE. This system used a line of steam as the input heating source for the cycle. The saline seawater is pumped into the condenser (preheater) to recover heat and condense the salt-free evaporated water. Afterward, the heated seawater has sprayed over the steam tubes inside the evaporator for the evaporation process. They assumed in the calculation that steam temperature is more than the brine by 7 °C and the feed seawater by 12 °C. The study indicated that the performance ratio decreased slightly by the boiling temperature. In addition, the specific heat transfer area decreases for the evaporator and condenser by the increasing of the boiling temperature. This feature happened because of the enhancement of the heat transfer coefficient as a result of lessening the thermal resistances. The decrease of the inlet seawater temperature boosts the driving thermal force in the condenser thus lowering the specific heat transfer area. The thermal performance ratio of single effect evaporation process is less than 1.

Mistry, et al. [45] developed a detailed multiple effect distillation (MED) system in a modular method. Equation-oriented solvers were used such as EES, and JACOBIAN software to simplify the code complexity. The developed model was compared with other forward MED configurations. The variation outputs between the models are too close. Moreover, developed code

was simpler with fewer assumptions. The result showed that the number of effect greatly increase PR normally with the same increment trend.

The combination between adsorption heat pump (ADVC) and SEE have adsorption heat pump (ADVC) investigated to check the performances of the systems[46], [47].the results of hybrid ADVC system were compared with a thermal vapor compression (TVC), an absorption vapor compression (ABVC), and a mechanical vapor compression (MVC). The PR for single effect evaporation coupled with ADVC, TVC, ABVC, and MVC was 7.25, 1.29, 2.74, and 9.68, respectively.

2.3 Combined System

Parham, et al [48] discussed the performance of four different configurations of absorption heat transformer integrated with water desalination system. The input waste heat to the generator is produced from a textile factory, where heat is used to operate the absorption system, and the generated heat from the unit is directed to the desalination cycle. The maximum distilled water flow rate achieved is 0.243 kg/s.

Ibrahim and Dincer [49] performed an experimental analysis of a combined system of solar cooling and desalination systems in Cairo, Egypt. The desalination technique used was solar still module at a sub-pressure to increase the evaporated yield. H_2O-LiBr absorption refrigeration system is operated intermittently to match the fluctuating solar radiation. PV solar cells are used to supply the generator heaters with the required input energy for refrigerant evaporation process. The results showed that August had the best performance with system efficiency of 40 %. The maximum COP obtained was 0.125 at evaporation temperature of 4.7 ℃. The unexpected low performance was due to the high heat losses from the system. Abdulrahim and Darwish [50]

studied the effect of the combination of low temperature multi-effect desalination and LiBr absorption cycles. They modeled and simulated the combined system on IPSEpro software. The results show that the evaporated distilled water increases with increasing the cooling load at constant gain output ratio (GOR). Moreover, increasing the cooling load increases the solar plate area and fluid flow rate.

Chiranjeevi and Srinivas [51] examined the performance of integrated humidification and dehumidification (HDH) desalination system with aqueous ammonia vapor absorption refrigeration cycle (VAR). The Overall Energy Utilization Factor (EUF) is considered to study the performance of the coupling effect. The highest value of EUF is 0.358 at strong solution concentration, and evaporator temperature of 0.47, and 10 °C, respectively. However, the separator temperature is kept at 100 °C.

Fathalah and Aly [52] investigated the performance of a hybrid system consist of a E-W tracking solar subsystem, a single stage absorption subsystem and a multi-effect desalination subsystem providing a comfort zone plus a potable water in a remote area. The authors demonstrated the mathematical model and the governing equations for the three subsystems. They performed the experiment in Jeddah, Saudi Arabia using parabolic trough collectors with caloria HT-43 as a working fluid, a LiBr absorption cycle for cooling and a MED system for providing a potable water. The results indicated that the increase in the generator`s temperature from 150 °C to 190 °C will increase the heat loses and decrease the COP of the collector from 0.743 to 0.71 at a constant evaporator temperature. However, the overall COP for the system will be boosted from the collector`s COP from 46% to 103% at the same temperatures, hence, producing fresh water ranged from 453-865 gal/h. During a fixed cooling load of 100 TR, the desalination plant produced 40 m^3 fresh water with a heat storage capacity of 286 MJ/K and 3235 m^2 for the PTC. The measured

overall COP for the three subsystems increased up to 1.444, which is higher than the basic LiBr absorption refrigeration cycle.

Mandani, et al. [53] studied the effect of a hybrid system by coupling a single effect H_2O-LiBr absorption with a SEE. They performed energy and mass balance on the whole process to calculate the performance ratio, conversion ratio and the specific mass flow rate of cooling water. The desalination system utilized the refrigerant water vapor produced from the generator to evaporate the seawater. The results showed that the performance ratio for the proposed system varies between 2.4 and 2.8, which is more than the single thermal vapor compression system by 50-70%. Moreover, the study mainly focused on the effect of increasing steam temperature on the specific heat transfer area and the specific mass flow rate for cooling water, they reported that higher steam temperature leads to lower specific mass flow rate and specific area.

Chiranjeevi and Srinivas [54] studied the effect of coupling two stage humidification and dehumidification (HDH) desalination system and single stage absorption refrigeration system. The results showed that the cooling effect used in the desalination humidification process enhanced the distilled water productivity. The combined system produced 670 L/h as distilled water, and 75 kW cooling effect at an air volume of 1 m^3/s. Moreover, the cycle EUF for the cooling and desalination system is 0.58. However, the plant EUF including the solar panels and the cooling and desalination system is 0.33.

Gude and Nirmalakhandan [55] investigated the performance of a combined low temperature desalination and solar air conditioning systems. Absorption refrigeration system is operated by solar collector system and a grid power as a backup system. The system required solar collectors with area 25 m^2 and thermal energy storage volume of 10 m^3. The heat delivered to the desalination

cycle is rejected from the absorption condenser. The results showed that the cooling capacity of the proposed system is 3.25 kW, and distilled water is 4.5 kg/h.

The proposed study is aimed at providing a thorough investigation on the combination of H_2O-LiBr absorption and single effect evaporation desalination system. The interaction between different components is studied. To the best of the author knowledge, such detailed investigation is not found in the open literature. The raised study indicates the effect of the temperature changing of various LiBr components on the performance analysis (COP, PR, EUF) of the whole system using Engineering Equation Solver EES$^®$ software [56].

Chapter 3: **Single Effect Evaporation Desalination Subsystem**

3.1 Introduction

The single effect evaporative (SEE) desalination system is the simplest form of MED, where it is used in marine vessels, and less densely populated remote areas to produce potable fresh water. The basic components for SEE are an evaporator, a condenser, and connecting pipes. The evaporator consists of heat exchanger tubes, distributing water pipes, water droplet removal demister, brine drum (container). Whereas the condenser consists of shell and tubes heat exchanger, distilled water collector, and a seawater pump. The simplicity is one of the advantages of the system, where only one condenser and one evaporator working under a certain pressure. However, the productivity of the system is not as much as produced from MSF or MED systems.

Many studies have been conducted in the SEE system field by controlling and monitoring the performance of each component to develop the MED system for mega distilled water production.

The system description for SEE subsystem and the governing equation with the theoretical validation used will be discussed in the following sections. In addition, the parametric study will be conducted to select the best parameters for a higher performance.

3.2 System Description
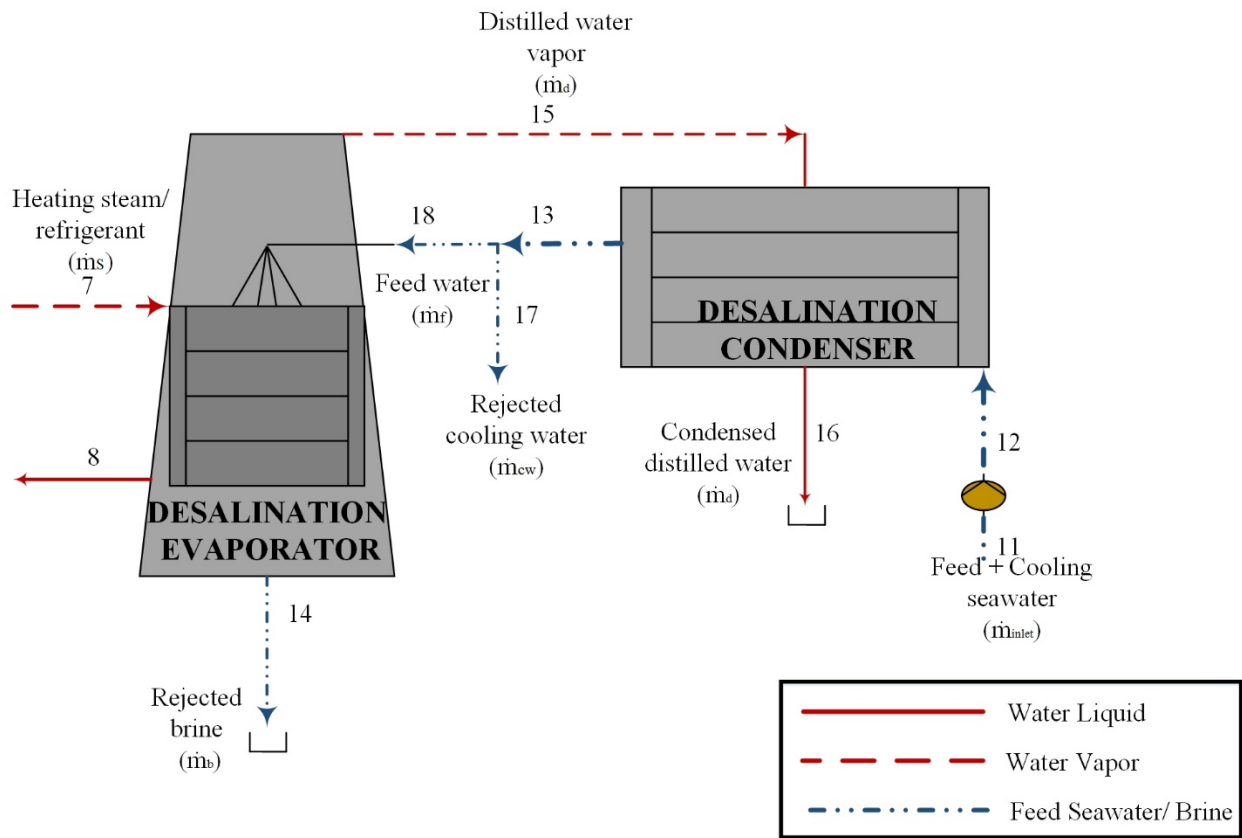
Figure 3-1 Single effect evaporative desalination subsystem

The desalination SEE plant is shown in Figure 3-1,where feed seawater is pumped at (11) through a pump and is directed to the condenser for preheating and exchanging heat with the hot desalinated condensing vapor (15). This is an important step since it helps condensing the product and preheating the feed seawater to recover energy at the same time. Thereafter, a part of the feed seawater is sprayed over the tube bundles (18) in the evaporator where the hot steam (7) runs through, whereas the rest of the feed seawater is pumped back to the sea (17). Afterwards, a portion of the feed seawater is evaporated in the evaporator producing pure vapor. This vapor is directed

to the condenser (15) to be condensed and collected as pure distilled water (16). The rest of the seawater that did not evaporate is rejected as brine at (14).

Temperature variation through the whole cycle is illustrated in Figure 3-2 showing the heating procedures, BPE, and thermal losses across the heat-exchangers.
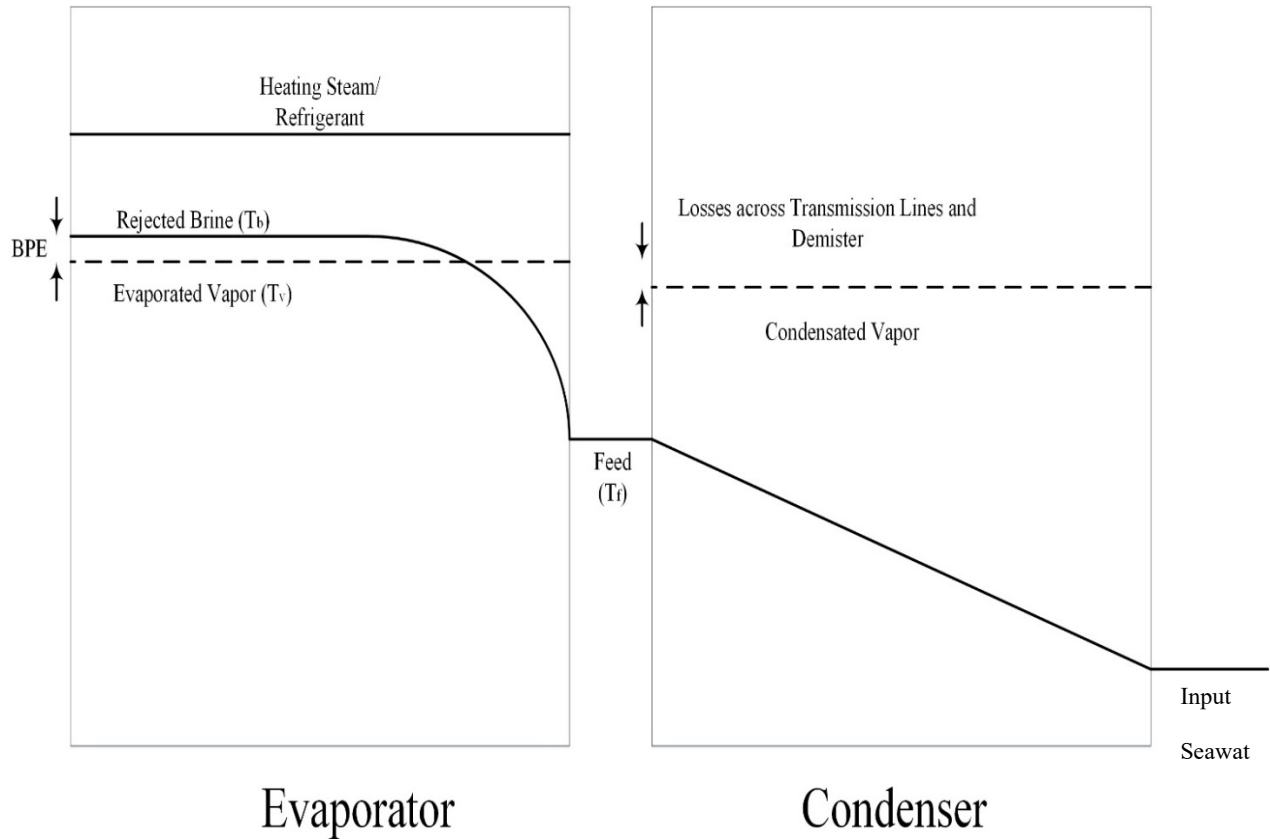
Figure 3-2 Temperature variation across SEE condenser and evaporator

3.3 Mathematical Model

3.3.1 Assumptions

Thermodynamic study has been performed by applying mass and energy balance equations with the following assumptions:

- The cycle operates under steady-state and steady-flow conditions.

- No heat loss from the heat exchangers to the ambient.

- No pressure drop across the piping and fittings.

- Only water vapor is evaporated in the desalination evaporator.

- Pressure is kept constant in the SEE subsystem.

3.3.2 Governing Equations

3.3.2.1 Mass Balance

Mass balance is carried out across the evaporator and condenser of the SEE subsystem.

The general law of conservation of mass

$$\sum \dot{m}_{in} = \sum \dot{m}_{out} \tag{3-1}$$

Mass balance at the cooling water rejection process.

$$\dot{m}_{13} = \dot{m}_{17} + \dot{m}_{18} \tag{3-2}$$

Mass balance across the evaporator.

$$\dot{m}_f = \dot{m}_b + \dot{m}_d \tag{3-3}$$

Salt concentration balance across the evaporator.

$$\dot{m}_f \times X_f = \dot{m}_b \times X_b + \dot{m}_d \times X_d$$

(3-4)

where, $X_d = 0$ (Vapor is salt-free)

3.3.2.2 Energy Balance

Energy balance is written for seawater pump, evaporator, and the desalination condenser.

Seawater Pump

The pumping power required to overcome pressure resistances through the system is given by:

$$W = \dot{m}_{11} \times (h_{12}-h_{11}) \tag{3-5}$$

The Desalination Evaporator

Heat balance is written for the evaporator, where warm seawater gains heat from the heating steam that condensed inside the tubes and thus releases its latent heat.

$$Q_{desl.evap} = \dot{m}_{ref} \times (h_7-h_8) \tag{3-6}$$

$$Q_{desl.evap} = (\dot{m}_d \times h_{15}) + (\dot{m}_b \times h_{14})-(\dot{m}_f \times h_{18}) \tag{3-7}$$

$$= (\dot{m}_f \times (h_{f,v} - h_{18})) + (\dot{m}_d \times h_{g,v}) + (\dot{m}_b \times h_{g,v})$$

$$Q_{des.evap} = U_{des.evap} \times A_{des.evap} \times (T_{ref}-T_b) \tag{3-8}$$

Boiling Point Elevation is the difference between saturated vapor and brine boiling temperature.

$$T_b = BPE + T_v \tag{3-9}$$

The Desalination Condenser

Heat is transferred between inlet new charge of seawater and the evaporated portion from the seawater.

$$Q_{desal.cond} = \dot{m}_d \times h_{fg,v} \tag{3-10}$$

$$Q_{desal.cond} = \dot{m}_{11} \times (h_{13}-h_{12}) \tag{3-11}$$

$$Q_{desal.cond} = U_{cond} \times A_{cond} \times LMTD_{cond} \tag{3-12}$$

$$\text{Where,} \quad LMTD_{cond} = \left(\frac{T_{cw,o}-T_{cw,in}}{\ln\left(\frac{Tv-T_{cw,in}}{Tv-T_{cw,o}}\right)}\right) \tag{3-13}$$

3.3.2.3 Performance Analysis

The system performance is evaluated through calculated the Performance Ratio (PR). The PR is counting the amount of distilled water that we collected over the refrigerant mass flow rate that causes the evaporation;

$$PR = \dot{m}_d / \dot{m}_{ref} \tag{3-14}$$

3.4 Validation

To establish credibility of the results presented for SEE subsystem, results produced by this model are compared with the thermodynamic analysis developed by El-Dessouky, and Ettouney [16]. The input parameters for SEE are presented in Table 3-1. Thermodynamic formulas by El-Dessouky, and Ettouney are compared using EES model, and percentage deviation is shown in

Table 3-2.

Table 3-1 Input Parameters Data of SEE by El-Dessouky and Ettouney [16]

Input Parameter	Quantity
Distillate water ($\dot{m}_d$)	1 kg/s
Boiling temperature (T_b)	75 °C
Feed temperature (T_f)	70 °C
Intake seawater temperature (T_{cw})	30 °C
Steam temperature (T_s)	75 °C
Feed salinity (X_f)	42 g/kg
Brine salinity (X_b)	70 g/kg

Table 3-2:Validation between by El-Dessouky, and Ettouney [16] formulas and EES code

Output Parameters	El-Dessouky, and Ettouney Formulas	Current model	Deviation (%)
BPE (°C)	0.903	0.9753	8.01
Tv (°C)	74.097	74.02	0.10
PR (-)	0.97	0.99	2.06

$\dot{m}_b$ (kg/s)	1.5	1.5	0.00
$\dot{m}_f$ (kg/s)	2.5	2.5	0.00
$\dot{m}_s$ (kg/s)	1.03	1.009	2.04
Q_{evap} (kW)	2372.9	2347	1.09
Q_{cond} (kW)	2323.6	2323	0.03

The developed code results are very close to those of El-Dessouky, and Ettouney approch where the maximum deviation does not exceed 2%. However, the deviation for BPE is 8%, because the EES software used the most updated properties for seawater, while El-Dessouky, and Ettouney approach utilize an old formula. Moreover, the absolute deviation is within 1 °C as BPE varies from 0 °C to 1 °C, so it doesn't affect the cycle analysis.

3.5 Parametric Study of SEE Subsystem

A parametric study is performed using EES software to evaluate the performance of SEE subsystem with different input parameters.

The following inputs are considered constant during the whole study as shown in Table 3-3.

Table 3-3: Input parameters of SEE subsystem

Input Data	Quantity
$\dot{m}_{11}$	16 kg/s
$\dot{m}_{ref}$ / $\dot{m}_s$	1 kg/s
T_7	100 °C
T_{11}	25 °C
Steam/refrigerant Pressure (HP)	10 kPa
SEE System Pressure	40 kPa
Percentage seawater mass entering the evaporator ($\dot{m}_{percentage}$)	0.3 kg/s
X_f	42 g/kg

Figure 3-3 shows the effect of steam/refrigerant temperature variation on the output distillate water at different top brine temperature. It is obviously shown that the distillate water increased by increasing the input steam temperature, as the amount of heat added increased (h_7-h_8) at constant T_8. Consequently, the amount of evaporated water vapor from the feed seawater increased. The top brine temperature of the system has a great influence on the system productivity, where the saturation temperature (top brine temperature) is function of system pressure. Consequently, the

evaporation process increases by decreasing the saturation temperature/pressure, where distillate water is 0.93, 0.825, and 0.76 kg/s at top brine temperature of 76, 86, 94 °C, receptively.
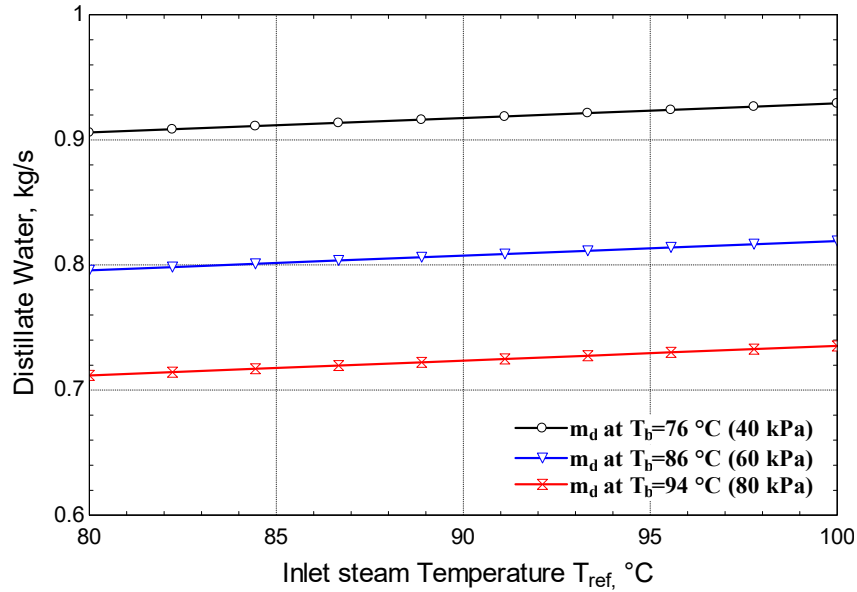
Figure 3-3 Effect of inlet steam temperature on the produced distillate water at different top brine temperature

Figure 3-4 shows the effect of the refrigerant temperature on the performance ratio (PR) and evaporator surface area. The figure illustrates that the PR increases by increasing the inlet refrigerant temperature as when increasing the refrigerant temperature, the degree of superheated vapor increased (h_7) at constant steam output conditions (state 8). Therefore, the enthalpy difference across the condenser (h_7-h_8) increases. Moreover, the evaporated refrigerant mass flow rate increased slightly, so the evaporated water from the seawater increased with a higher rate than the increase in the refrigerant mass flow. However, the evaporator area decreased with increasing

the refrigerant temperature since it leads to an increase in the temperature difference and in the overall heat transfer coefficient. Therefore, it leads to a smaller area at constant heat transfer rate.
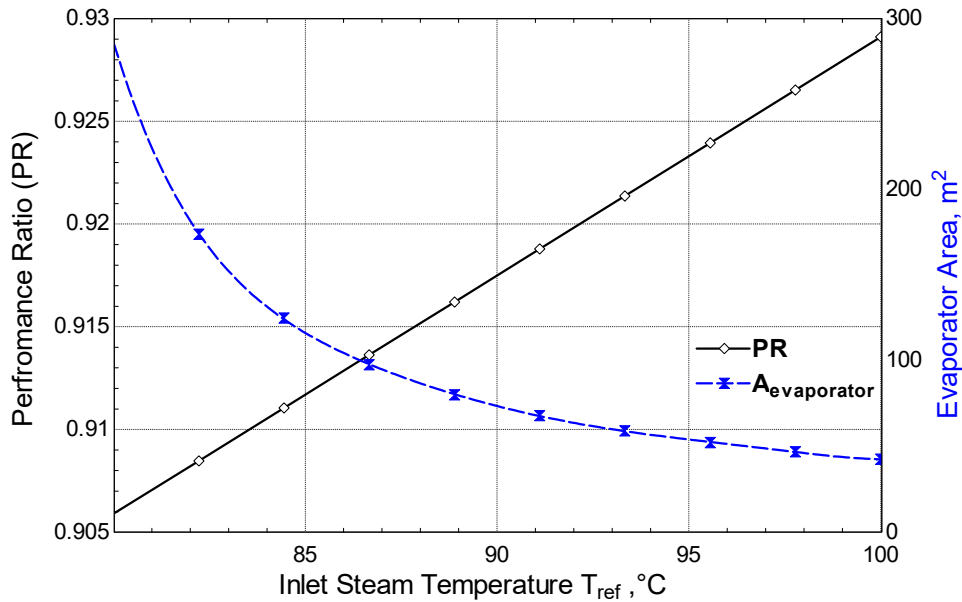
Figure 3-4 Effect of inlet refrigerant temperature on the PR and the evaporator area

Figure 3-5 shows that the temperature of the inlet cooling seawater entering the condenser has a direct effect on the PR. Increasing the inlet cooling water temperature from 15 °C to 30 °C leads to an increase in the PR from 0.82 to 0.987. This result occurred as the input cooling water gained almost constant latent heat from the condensed distilled water that boost its temperature more at state number 13 in Figure 3-1. Therefore, the feed water reached the evaporator at a higher temperature. Afterward, the high feed temperature at state 18 gained a constant amount of heat that increases the evaporation process of water-vapor, hence, producing more distilled water at constant steam mass, so the PR increased.
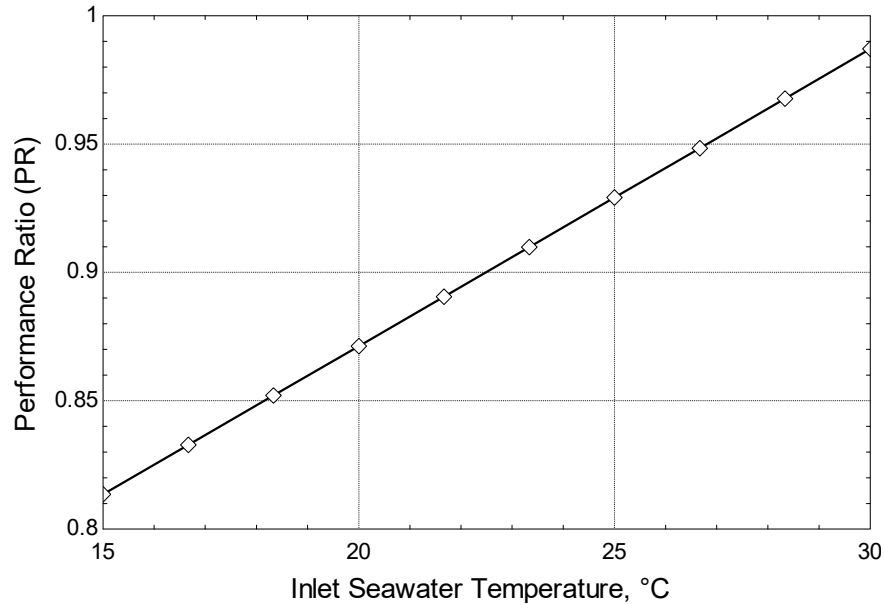
Figure 3-5 Effect of cooling seawater temperature on PR

The effect of evaporator and condenser areas with respect to the inlet cooling water temperature is discussed in Figure 3-6. The increasing the cooling seawater temperature from 15 °C to 30 °C would require higher condenser area. The needed area for the condenser increases as the temperature difference in the condenser diminished at virtually constant latent heat applied to the seawater so the condenser area will compensate for the temperature difference to keep Q_{cond} constant. However, the cooling seawater temperature had no effect on the evaporator area as steam, system pressure, and brine temperature are kept constant during the operation with a constant heat input to the evaporator.
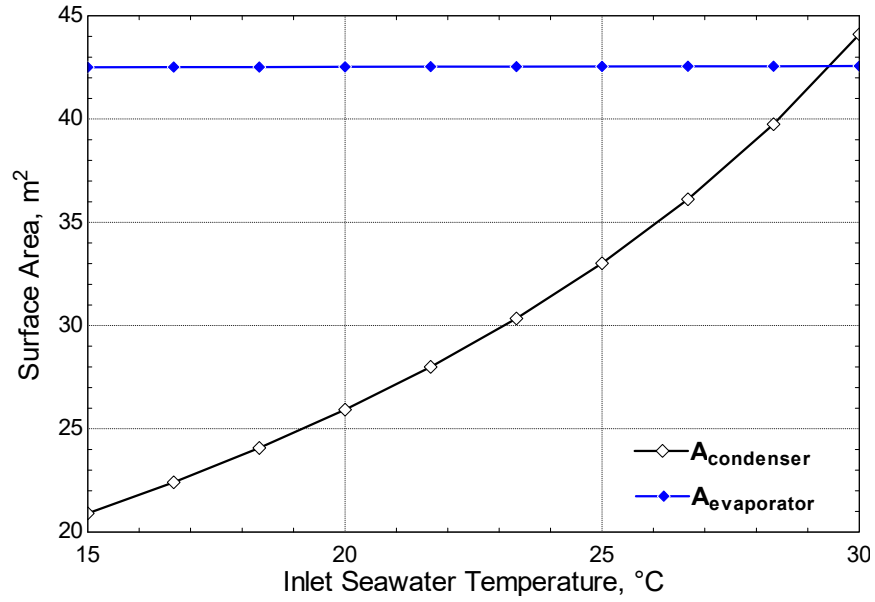
Figure 3-6 Effect of cooling seawater temperature on condenser and evaporator areas

System pressure is considered to be one of the main factors that affect the performance of the system. The evaporation and the brine temperatures of the seawater depend mainly on the saturation temperature at a certain system pressure. By increasing the brine boiling temperature - through controlling the system pressure- the evaporated water ($\dot{m}_d$) and the PR will decrease considerably as shown in Figure 3-7.

The evaporation temperature of the feed seawater will increase by increasing boiling point temperature, hence, most of the input heat will be consumed as a sensible heat to increase the feed seawater temperature to the saturation not to evaporate it. In addition, the PR decreased by increasing input feed mass flow rate as the heat added to the feed seawater flow rate through the condenser and evaporator would increase feed temperature sensibly and less water will evaporate at constant steam mass flow rate. On the other hand, the evaporator area increases by increasing the brine boiling temperature as the temperature difference (T_7-T_b) decreased with constant heat

44

input to the system. However, the condenser area is inversely proportional to the brine temperature because the condensation process decreased by increasing brine boiling temperature/pressure. The rate of heat transfer through the condenser is decreased by increasing the brine boiling temperature as the enthalpy of vaporization decreased by increasing system pressure. The decrease in the condenser area rebalances the increase in the temperature difference, as shown Figure 3-8.
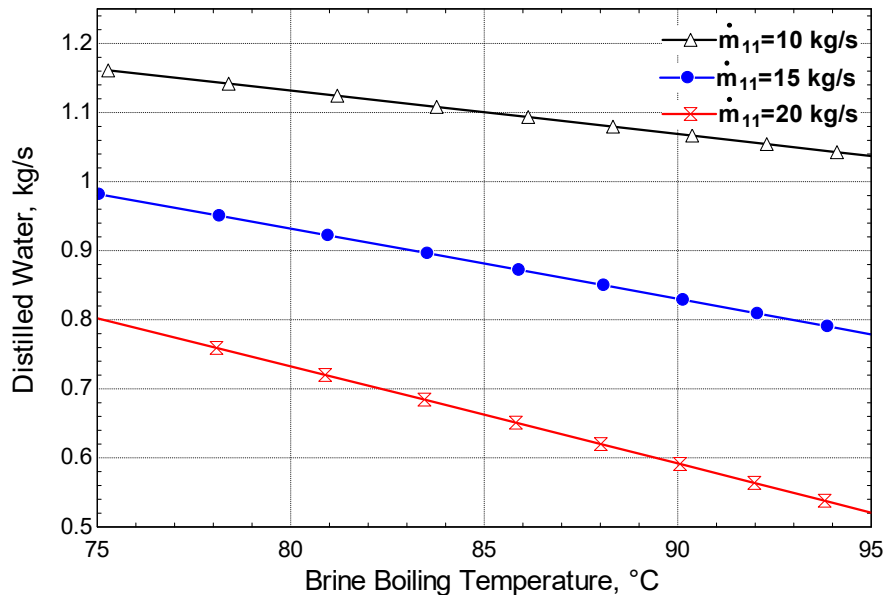
Figure 3-7 Effect of brine temperature on distilled water
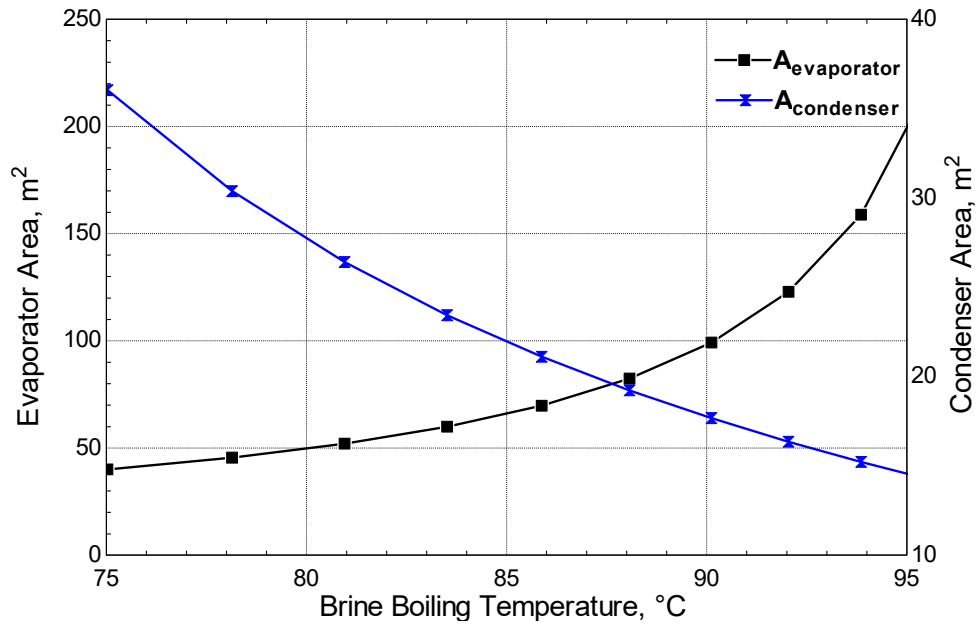
Figure 3-8 Effect of brine temperature on the evaporator and condenser Areas

Figure 3-9 shows the effect of the percentage of seawater pumped in the evaporator with the distilled water ($\dot{m}_d$). The distilled water decreases by increasing the feed mass to the evaporator at constant heat input. The input heat is used as a sensible energy to increase the temperature of the bulk feed seawater to the boiling brine temperature. However, a less energy is used to evaporate feed water leading to less vapor quantity, hence, less distilled water produced, so the output fresh water and PR decreases.
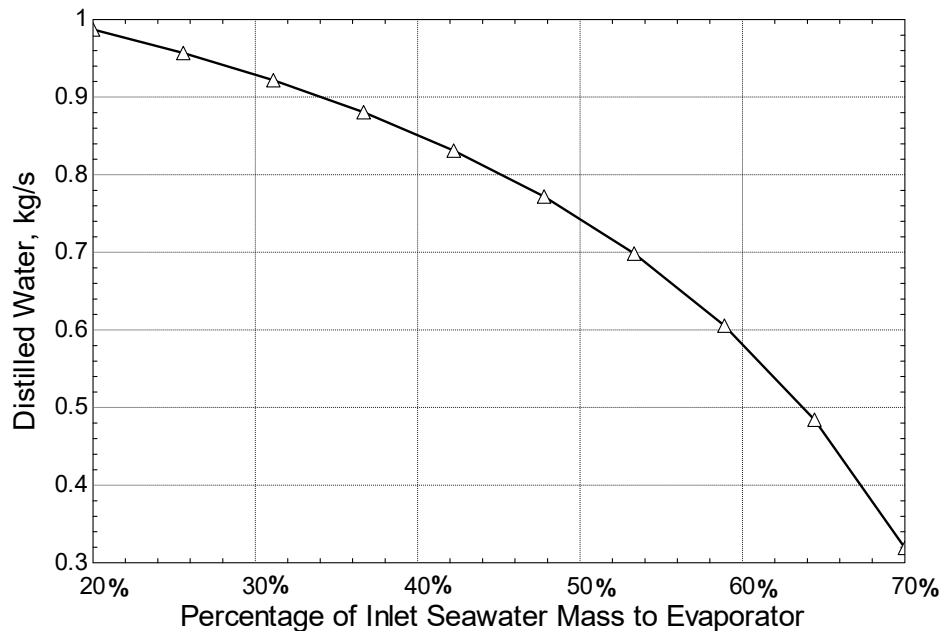
Figure 3-9 Effect of increasing the inlet feed seawater on The distilled water

Chapter 4: **Single Stage of Aqueous Lithium Bromide Absorption Subsystem**

4.1 Introduction

Absorption refrigeration systems have been used since the late 19th century. Later, more attention has been given to modify these systems because of the oil prices and the increasing of greenhouse emissions problem produced from simple vapor compression systems (VCS) operation. The high consumption of electricity of compressors in VCS can be replaced by an absorption system with a generator, absorber, and a solution recirculating pump.

Absorption systems are environmentally friendly since they use safe working fluids for atmosphere especially ozone layer as H_2O–LiBr solution. Moreover, this technique reduces the combustion emissions associated with the compressors operation of VCS. The working fluid pair H_2O–LiBr has a high enthalpy of vaporization and is a non-toxic solution. In addition, it uses low grade energy like solar energy or waste heat from any industrial application to be utilized as an input feed heat to the generator. These systems are effective during the summer peak as they provide the required cooling effect at a hot daytime if solar energy is used.

Many improvements are needed in the absorption field to improve the COP of the system to be implemented commercially in small and large scales. Single stage LiBr solution system works at very low pressure of 1-10 kPa. Thus, a hermetic design must be offered to prevent air leakage to the low pressure system. The system works with two pressures; the high pressure in the generator and the condenser, while the low pressure is in the absorber and the evaporator [57].

Figure 4-1 shows an illustration of temperatures and pressures distribution of a single stage H_2O-LiBr absorption refrigeration cycle.
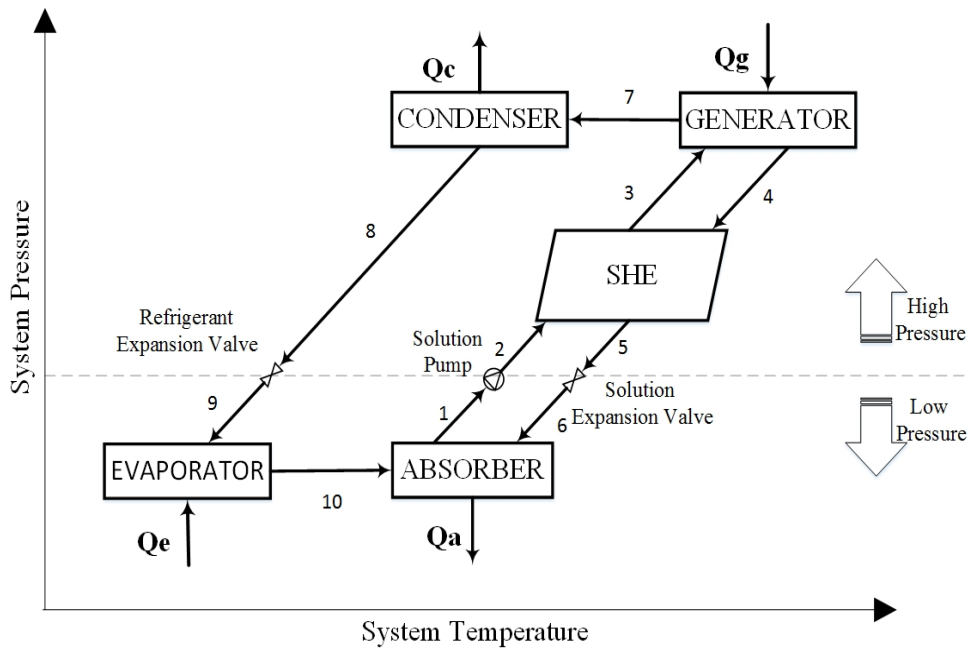
Figure 4-1 Temperature and pressure distribution over a single stage H_2O-LiBr absorption refrigeration system

The description for H_2O–LiBr absorption subsystem and the governing equations with the theoretical validation used are discussed in the following sections. In addition, a parametric study will be conducted to select the best parameters for a higher performance.

The identification of any state in aqueous LiBr absorption system is considered by knowing the relation between temperature, pressure, and concentration of lithium bromide in H_2O–LiBr solution as shown in Figure 4-2. Moreover, crystallization curve (red curve) is presented where precaution must be taken to avoid this phenomenon as LiBr solution beyond this curve is converted to solid crystals that decrease the system performance [40]. This phenomenon occurs when LiBr concentration increases over a certain limit or the solution temperature decreases, where point A

(lower concentration) moves to B (higher concentration), so crystallization phenomenon may possibly occur. Crystallization probably may occur in the entrance of the high concentration solution in the absorber.
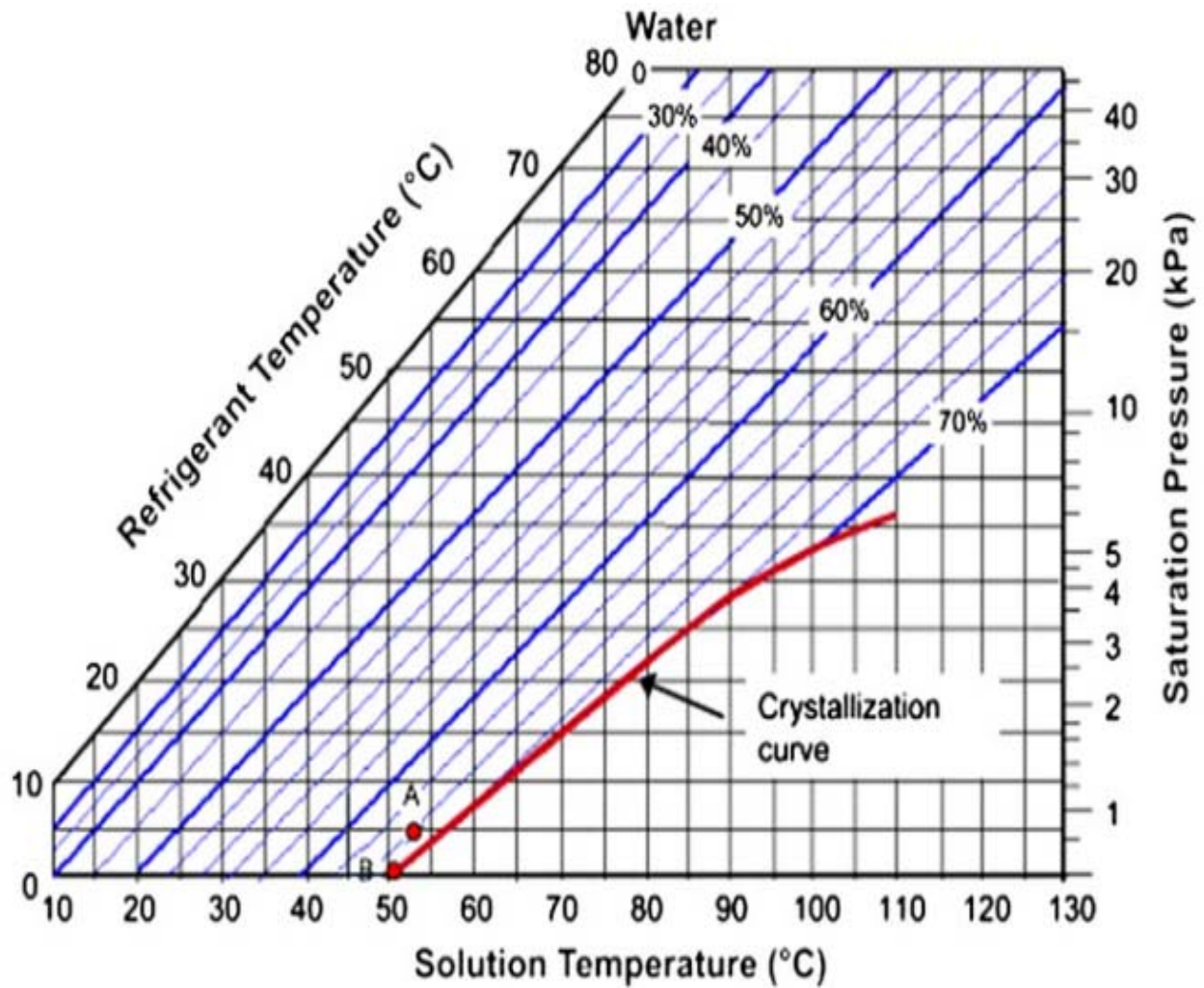
Figure 4-2 Vapor pressure and LiBr concentration chart [40]

4.1.1 System Description

Single Stage H_2O-LiBr Absorption Cooling Subsystem
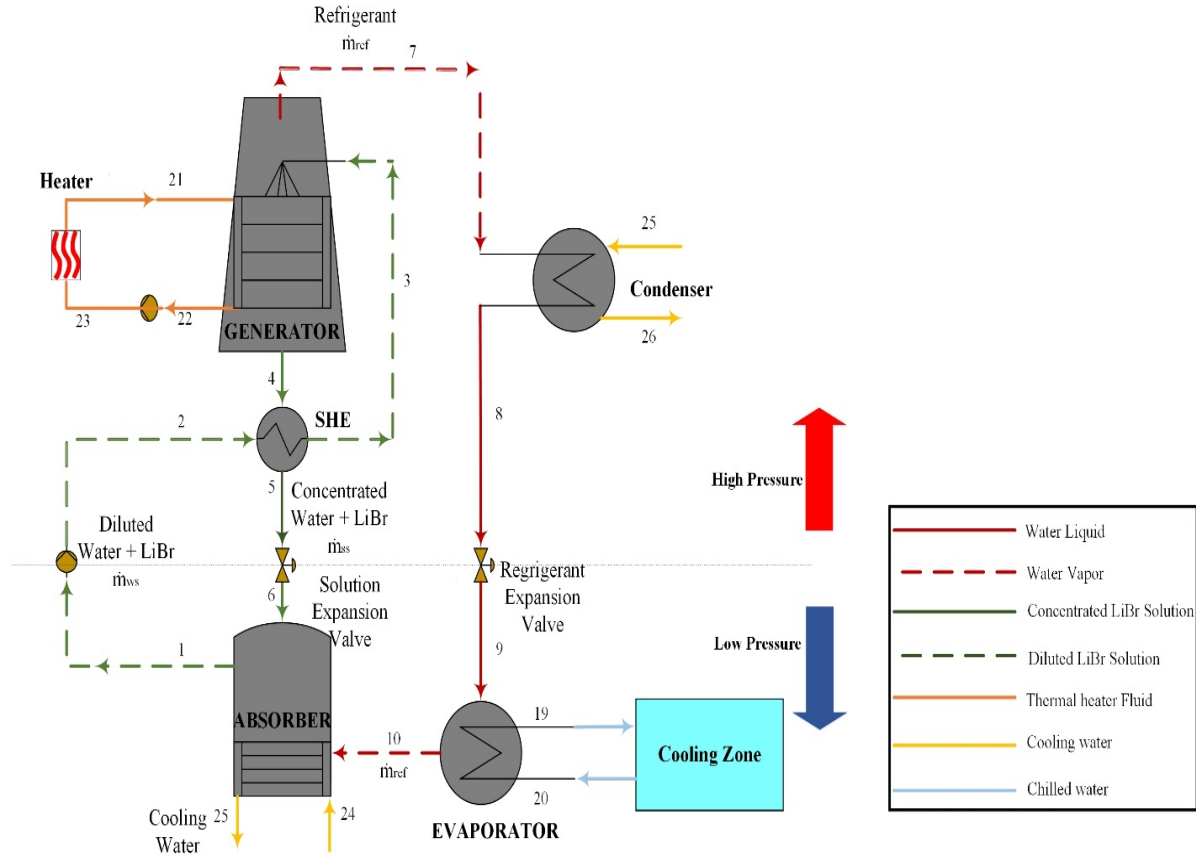
Figure 4-3 Configuration of H_2O-LiBr single stage absorption refrigeration subsystem

Figure 4-3 shows the system configuration of H_2O-LiBr single stage absorption refrigeration subsystem and illustrates the operation of the cycle as follow;

A heater is used heating the hydrous lithium bromide solution in the generator and evaporating water (refrigerant), that leaves the generator at state (7).

51

The vapor refrigerant (water) enters the condenser, losing its latent heat to the cooling water and leaves the condenser as saturated/subcooled at state (8). Furthermore, it enters the expansion valve to decrease its pressure to the absorber/evaporator pressure and leaves the expansion valve at state (9). Thereafter the refrigerant flows into the evaporator for the cooling process where it absorbs heat from the room (place to be conditioned), keeping the space within the comfort zone. The refrigerant vapor, which gains heat from the room, leaves the evaporator and enters into the absorber at low pressure at state (10). The low-pressure refrigerant (10) is mixed and absorbed by the concentrated (rich-in-lithium-bromide) mixture of water and lithium bromide (H_2O-LiBr) solution that leaves the generator at state (6). During absorption and mixing, the reaction is exothermic, where the generated heat is removed using cooling water in the absorber, resulting in a more homogeneous mixture at point (1). The cooling water enters the absorber at (25). The diluted (weak-in-lithium-bromide) saturated/subcooled solution liquid H_2O-LiBr solution at state (1) is pumped to the generator using a small recycling pump. After the pump, the solution is preheated by a heat exchanger before it enters the generator through receiving energy from the hot fluid leaving the generator at state (4). The weak solution enters the generator at state (3). When the solution is heated, by the heaters, the refrigerant evaporates and leaves the generator at state (7), whereas the concentrated H_2O-LiBr solution (rich-in-LiBr) returns back to the absorber at state (4). This concentrated solution loses its sensible heat to preheat the coming diluted solution (weak-in-LiBr) charge at point (2) within the heat exchanger. The strong solution flows through the expansion valve (5) to decrease its pressure to the absorber pressure (6) until it mixes again with the refrigerant at the absorber.

The relation between the enthalpy and the concentration for each state of single stage H_2O-LiBr absorption system is shown in Figure 4-4. This figure shows the enthalpy-concentration

diagram for each state of single stage H_2O-LiBr absorption system. The subcooled weak solution at state 1 is pumped to a higher pressure to state 2, then heat is added as sensible heat to increase the solution temperature. Afterward, more energy is added to the solution until it reaches to the saturation condition at state 4, where water vapor has evaporated and escaped through line 7 and the rest of the solution will return again to the absorber. The evaporated water vapor will lose its latent heat to be saturated liquid at state 8 and then decrease its pressure to be almost saturated liquid at state 9. Then, water vapor regains latent heat from the zone to be conditioned, it leaves as saturated vapor at state 10. The strong solution at state 4 is directed to the absorber, where the concentrated solution loses its sensible heat through heat exchange with the diluted solution to be at the subcooled region at state 5. Subsequently, the concentrated solution is directed to an expansion valve to reach the saturation region to be mixed with water vapor in the absorber.
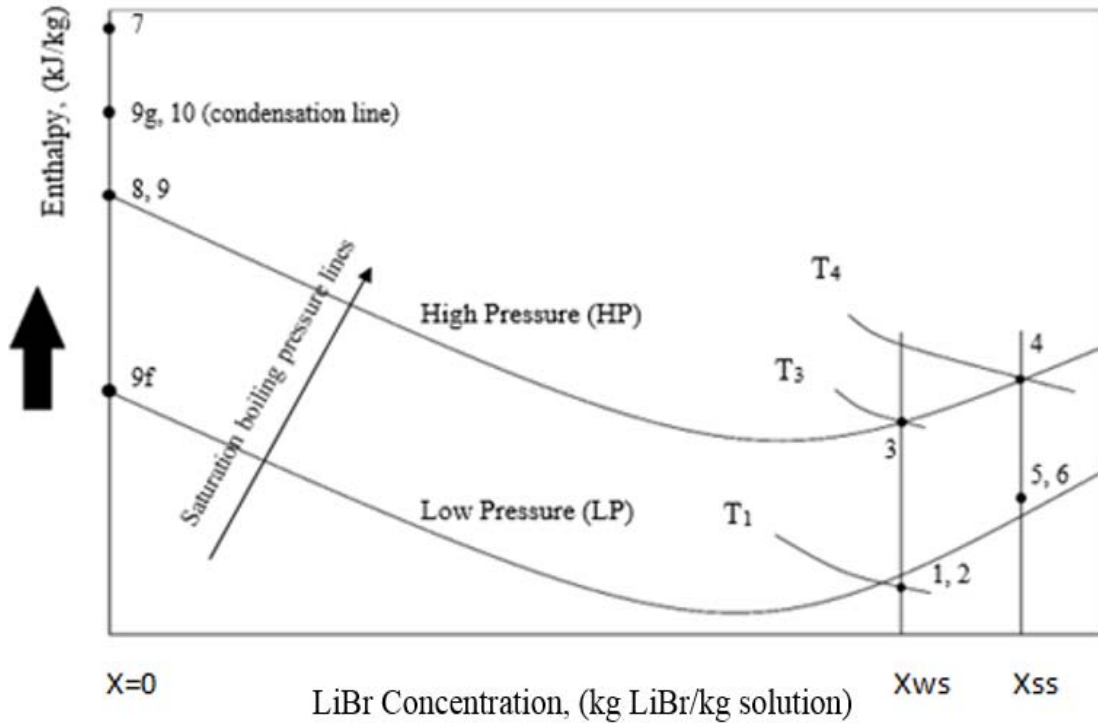
Figure 4-4 Enthalpy diagram of single stage H_2O-LiBr absorption system

4.2 Mathematical model

4.2.1 Assumptions

Thermodynamic analysis is carried out through mass and energy balance equations under the following assumptions:

- The cycle operates under steady-state and steady-flow conditions.

- No heat loss from the heat exchangers to the ambient.

- The mixture in the absorber is a homogenous solution.

- No pressure drop across the piping and fittings.

- Only pure water vapor is evaporated from the generator.

4.2.2 Governing equations

4.2.2.1 Mass Balance

Mass balance is performed at different parts of the H_2O-LiBr subsystem, where mass entering the system equals mass leaving the system.

Mass balance across the generator.

$$\dot{m}_{ws} = \dot{m}_{ss} + \dot{m}_{ref} \tag{4-1}$$

Concentration of LiBr solution across the generator.

$$\dot{m}_{ws} \times X_{ws} = \dot{m}_{ss} \times X_{ss} + \dot{m}_{ref} \times X_{ref} \tag{4-2}$$

where, $X_{ref} = 0$

Mass ratio between the weak concentration solution to the refrigerant vapor produced in the generator .

$$CR = \dot{m}_{ws} / \dot{m}_{ref}$$

$$= \frac{Xss}{Xss - Xws}$$

(4-3)

4.2.2.2 Energy Balance

Energy balance is written at different parts of the H_2O-LiBr subsystem, where energy input to the system equals energy output of the system.

The Absorber

Heat balance is written for the absorber, where heat is rejected from the mixing chamber to a cooling system for a homogenous LiBr solution.

$$Q_{abs} = (\dot{m}_{ref} \times h_{10}) + (\dot{m}_{ss} \times h_6) - (\dot{m}_{ws} \times h_1) \qquad (4-4)$$

$$Q_{abs} = \dot{m}_{25} \times Cp_{cw} \times (T_{25} - T_{24}) \qquad (4-5)$$

Solution Pump

Work needed to drive the solution pump is given by

$$W_{sp} = \dot{m}_{ws} \times (h_2 - h_1) \qquad (4-6)$$

$$W_{sp} = \dot{m}_{ws} \times (HP\text{-}LP) / (\rho_{ws} \times \eta_{pump}) \qquad (4-7)$$

Solution Heat Exchanger (SHE)

Heat balance is written for heat transfer between weak and strong LiBr solutions, and the effectiveness of the heat exchanger is shown below.

$$Q_{SHE} = \dot{m}_{ws} \times (h_3 - h_2)$$

$$= \dot{m}_{ss} \times (h_4 - h_5)$$

(4-8)

$$\varepsilon_{SHE} = \frac{T_4 - T_5}{T_4 - T_2}$$

(4-9)

Generator

Heat balance is written for the generator, where an external source is providing heat, either by thermal solar heaters or waste heat.

$$Q_{gen} = (\dot{m}_{ref} \times h_7) + (\dot{m}_{ss} \times h_4) - (\dot{m}_{ws} \times h_3)$$

(4-10)

LiBr Condenser (Desalination Evaporator)

Heat is rejected from LiBr condenser which is gained by the desalination subsystem.

$$Q_{Desal.evap} = \dot{m}_{ref} \times (h_7 - h_8)$$

(4-11)

Refrigerant Expansion Valve

A reducing pressure valve with a constant enthalpy.

$$h_8 = h_9$$

(4-12)

LiBr Evaporator

Heat balance is done on the cooling zone, where the $Q_{cooling}$ is the needed cooling effect.

$$Q_{cooling} = \dot{m}_{house} \times Cp_{cw} \times (T_{20}-T_{19})$$

(4-13)

$$Q_{cooling} = \dot{m}_{ref} \times (h_{10}- h_9)$$

(4-14)

4.2.2.3 Performance Analysis

The performance of LiBr absorption refrigeration subsystem is evaluated using the following parameters;

Coefficient of Performance (COP)

The ratio of the output evaporative cooling capacity to the energy added to the system.

$$COP = \frac{Qcooling}{Qgen+Wsp}$$

(4-15)

Circulation Ratio (CR)

The ratio of mass flow rate for the diluted solution entering the generator to the mass flow rate of the evaporated refrigerant out of the generator.

$$CR = \dot{m}_{ws} / \dot{m}_{ref}$$

(4-16)

Carnot Coefficient of Performance (COP_c)

The maximum possible coefficient of performance of vapor absorption refrigeration system.

$$COP_c = \left(\frac{Tgen-Tabs}{Tgen}\right) \times \left(\frac{Tcond}{Tcond-Tevap}\right)$$

(4-17)

System Efficiency/ Efficiency Ratio

The practical coefficient of performance of the system compared to Carnot coefficient of performance.

$$\eta_{ra} = COP / COP_c$$

<div align="right">(4-18)</div>

4.3 Validation

To establish confidence in the model presented for H_2O-LiBr absorption subsystem, results produced by this model are compared with the thermodynamic analysis developed by Wonchala, et al [34]. The input parameters for H_2O-LiBr absorption subsystem are presented in Table 4-1. The maximum value is less than 2% in all cases. The validation of the cycle solution procedure has been performed using data taken from the theoretical and experimental study by Wonchala, et al [34] as shown in Table 4-1.

Table 4-1 Input parameters data by Wonchala, et al [34]

Input Parameter	Quantity
Q_{gen}	14.2 kW
T_1	34.9 °C
T_4	90 °C
T_7	85 °C
T_8	44.3 °C
T_9	6 °C
ε_{SHE}	0.522

Table 4-2 Validation between Wonchala, et al [34], and proposed code

Output Parameters	Wonchala, et al Model	Current Model	Deviation (%)
Q_{evap} (kW)	10	9.883	1.1
Q_{cond} (kW)	10.69	10.51	1.6
Q_{abs} (kW)	13.51	13.55	0.2
COP	0.71	0.697	1.8

The developed EES code results show an excellent agreement with the case shown by Wonchala, et al [34] through a maximum deviation of 1.8% as shown in Table 4-2. Consequently, the validation is accepted over the study.

4.4 Parametric Study of H_2O-LiBr subsystem

A parametric study is performed using EES software to evaluate the performance of H_2O-LiBr absorption subsystem. The following inputs are considered constant during the study as shown in Table 4-3. Assuming temperature of the generator, and the evaporator is at saturation conditions.

Table 4-3 Input parameters to H_2O-LiBr absorption subsystem

Input Data	Quantity
$\dot{m}_{ws}$	0.05 kg/s
ε_{SHE}	0.7

T_1	35 °C
T_4	90 °C
T_8	35 °C
T_{10}	4 °C
Quality of water in LiBr solution leaving the absorber (Qa_1)	0
Quality of water in LiBr solution leaving the generator (Qa_4)	0
Quality of saturated vapor refrigerant leaving the generator (Qa_7)	1
Quality of saturated vapor refrigerant leaving the condenser (Qa_8)	0
Quality of saturated vapor refrigerant leaving the evaporator (Qa_{10})	1

Figure 4-5 shows the effect of the generator temperature on the LiBr solution concentrations through the cycle. LiBr concentration mainly depends on pressure and temperature of the mixture, hence, the weak solution concertation (diluted-in-LiBr) will remain constant as the evaporator pressure and temperature are fixed. On the other hand, the strong solution concentration (concentrated-in-LiBr) depends on condenser pressure and generator temperature with an inverse relation [23]. Moreover, the increase in the input energy rate to the generator would increase the refrigerant evaporation rate. Consequently, the refrigerant mass flow rate increased, and concentrated LiBr mass flow rate decreased at a constant diluted mass flow rate as shown in Equation (4-1), and the strong solution concentration increased as shown Equation (4-2). Therefore, the strong solution concentration increased by increasing the generator temperature at constant condenser temperature.
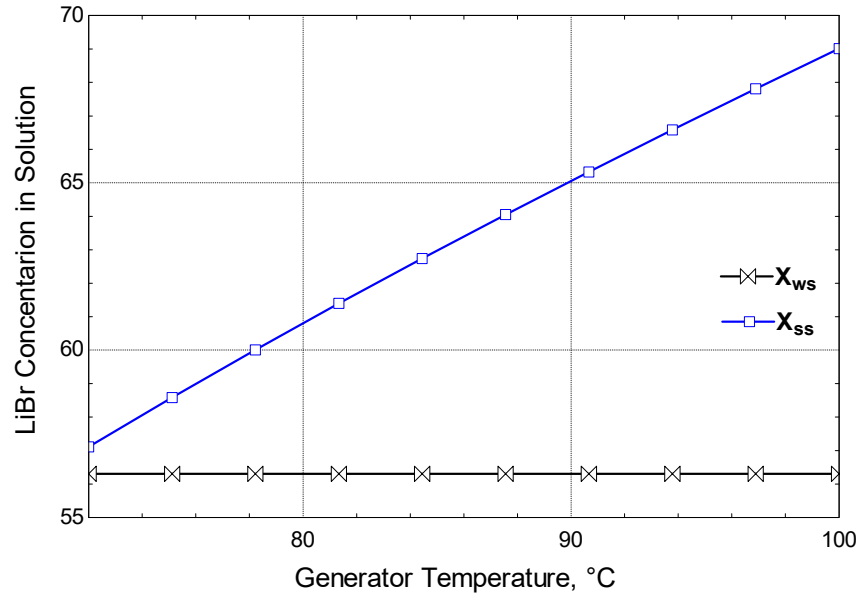
Figure 4-5 Effect of generator temperature on the LiBr solution concentration

Figure 4-6 shows the effect of condenser temperature of the LiBr concentration with the variation of absorber temperature. As discussed in Figure 4-5, the strong solution concentration (X_{ss}) depends on generator temperature and condenser pressure with an inverse relation, hence, (X_{ss}) decreased by increasing condenser temperature. However, the weak solution concentration (X_{ws}) is a function of evaporator pressure and absorber temperature with a direct relation [23], hence, (X_{ws}) increased with increasing absorber temperature, regardless the increase of condenser temperature.
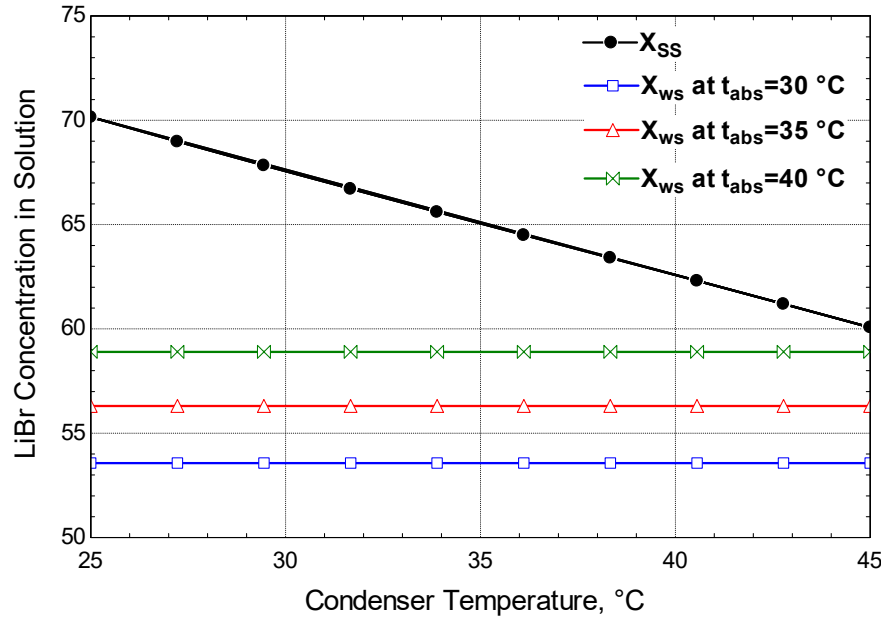
Figure 4-6 Effect of condenser temperature on LiBr concentration at different absorber temperature

Figure 4-7 shows the effect of generator temperature variation on the heat transfer of the absorption system components. Heat transfer of generator, absorber, condenser, and evaporator, increased by increasing the generator temperature as heat difference between the generator outputs (state 4, 7) with the generator input state 3 increases. Moreover, heat transfer across the LiBr condenser increases as refrigerant temperature increases (T_7), so the enthalpy difference on the condenser increased (h_7-h_8). In addition, the refrigerant mass flow rate across the system increases heat transfer across the absorber and the evaporator at a constant condenser, evaporator, and absorber temperatures. However, heat transfer across the SHE is almost constant since the LiBr mass flow rates ($\dot{m}_{ss}, \dot{m}_{ws}$) and temperature difference between the solution inputs (T_2, T_4), and

outputs (T_3, T_5) across SHE are almost constant assuming the evaporated water-vapor refrigerant flow rate is very small compared to the diluted/concentrated LiBr mass flow rate.
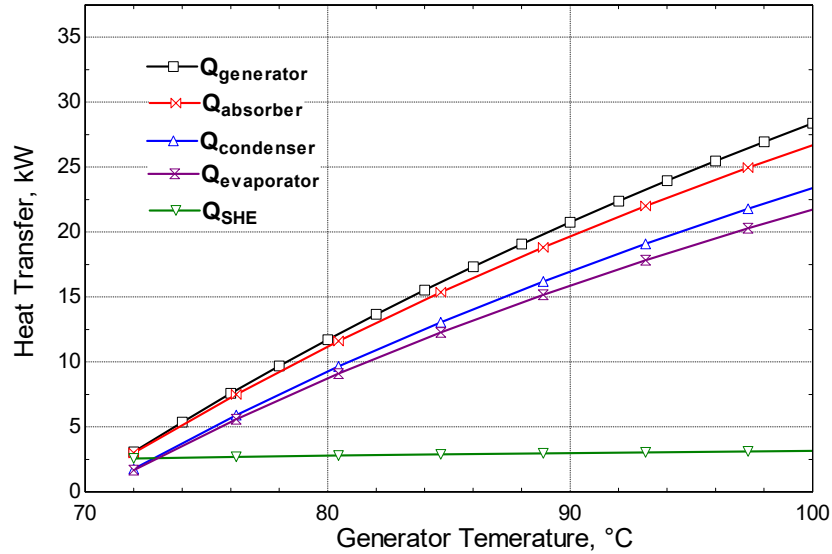
Figure 4-7 Effect of generator temperature on heat transfer across the absorption system

Figure 4-8 shows the effect of generator temperature on the COP and CR. The COP increased by increasing the generator temperature as the evaporated refrigerant mass flow rate increases by extra heat input to the generator that increased generator output temperature. Consequently, the refrigerant evaporation rate increased. On the other side, the cooling effect depends mainly on refrigerant mass flow rate at constant evaporator temperature, therefore the higher refrigerant flow rate increases the cooling capacity with a higher rate than the heat added to the generator, hence, the COP increased. The COP increases from 0.544 to 0.76 by increasing the generator temperature from 75 °C to 100 °C, receptively. However, the CR decreased as the refrigerant mass flow rate increases with constant weak solution mass flow rate (X_{ws}) as discussed in Equation (4-16).
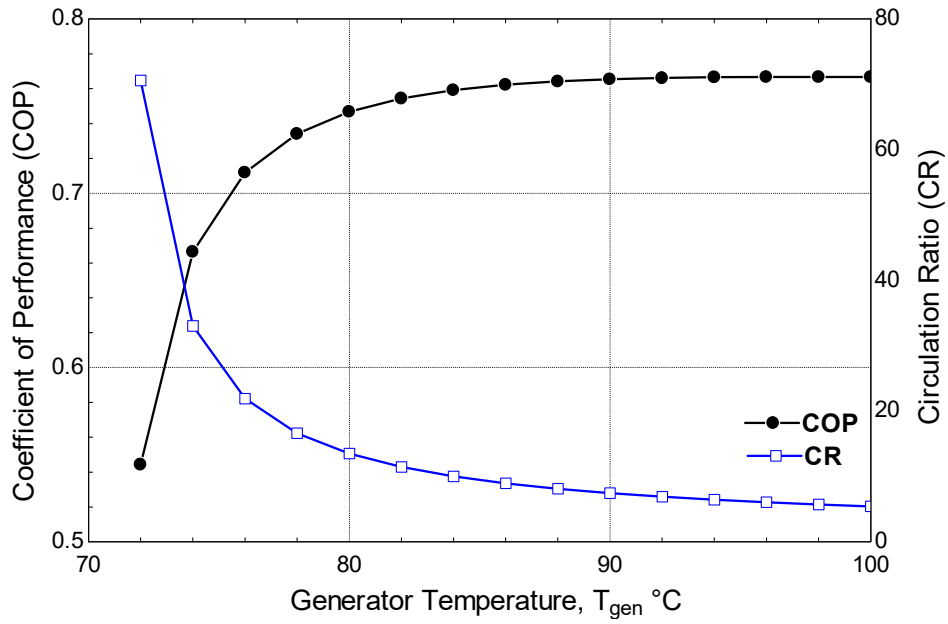
Figure 4-8 Effect of generator temperature on COP and CR

Figure 4-9 shows the effect of the solution heat exchanger (SHE) effectiveness on the COP of the system. The COP increased significantly with increasing the unit effectiveness because, the needed energy input to the generator decreased as the heat-exchanger preheats the weak-solution to a higher temperature before it enters the generator through state 3. This reduction in the input energy increases the performance of the system at constant cooling effect, hence, the COP will increase.
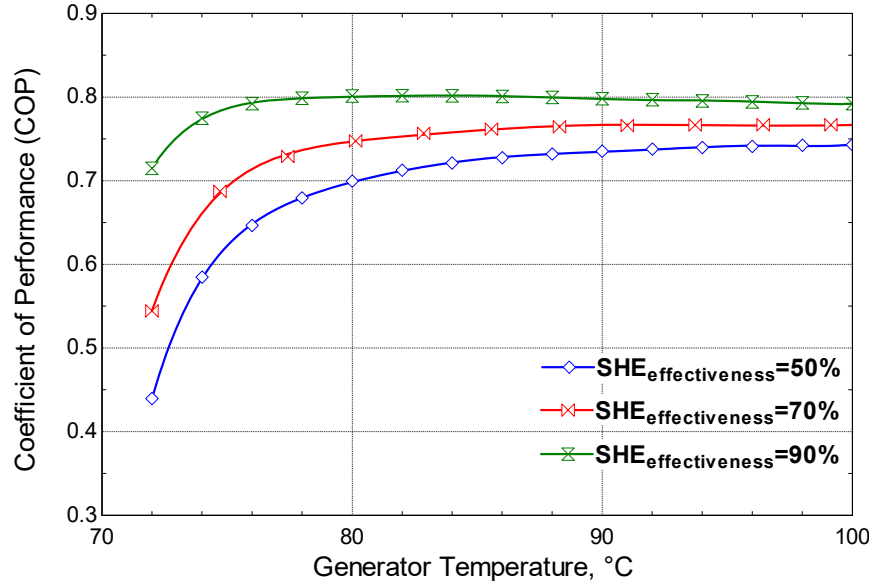
Figure 4-9 Effect of generator temperature on COP with different SHE effectiveness

Figure 4-10 shows the variation of condenser temperature on the COP and CR. The system high pressure is a function of condenser temperature, where the condenser pressure can be found at the saturation condition of the condenser outlet temperature at state (8). Moreover, the strong solution concentration (X_{ss}) has an inverse proportion with the system high pressure [23], so (X_{ss}) decreases by increasing condenser temperature through increasing condenser pressure. Therefore, the strong LiBr mass flow rate increased at constant diluted LiBr mass flow rate and concentration as discussed in Equation (4-2), that leads to a decrease in the evaporated refrigerant mass flow rate as discussed in Equation (4-1). For that reason, the cooling capacity decreases at constant input heat rate to the generator, so the COP decreased. On the other side, the refrigerant mass flow rate decreased at constant diluted LiBr mass flow rate, hence, the CR increases as described in Equation (4-16)
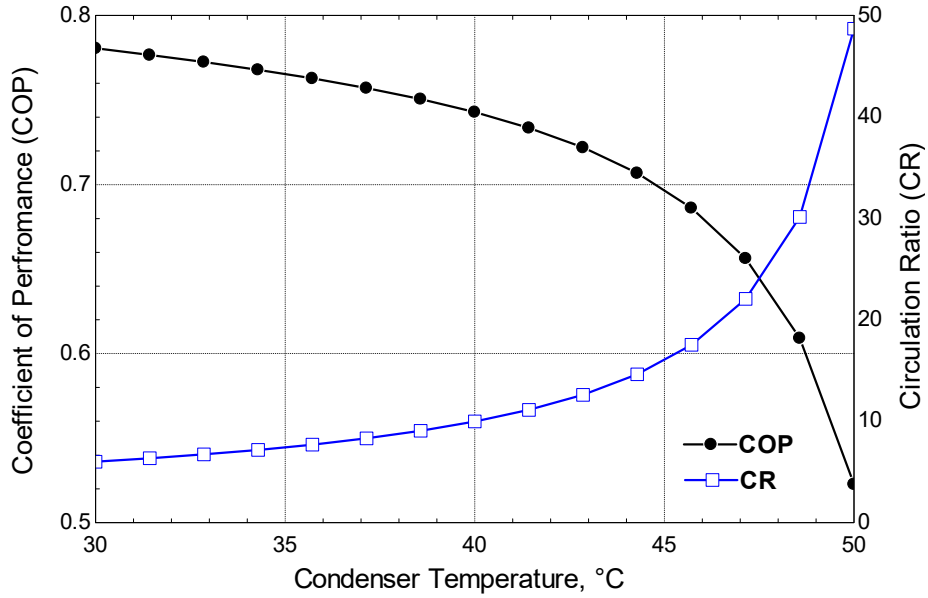
Figure 4-10 Effect of condenser temperature on COP and CR

Figure 4-11 shows the effect of the evaporator temperature on COP and CR. The system low pressure is a function of evaporator temperature, where the evaporator pressure can be found at the saturation condition of the evaporator outlet temperature at state (10). Moreover, the diluted solution concentration (X_{ws}) has an inverse proportion [23] with the system low pressure, so (X_{ws}) decreases by increasing evaporator temperature through increasing the evaporator pressure. Therefore, the strong LiBr mass flow rate decreased at constant diluted LiBr mass flow rate and concentrated LiBr concentration as discussed in Equation (4-2), that leads to an increase in the evaporated refrigerant mass flow rate as discussed in Equation (4-1). For that reason, the cooling capacity increases at constant input heat rate to the generator, so the COP increased. On the other side, the refrigerant mass flow rate increased at constant diluted LiBr mass flow rate, hence, the CR decreases as described in Equation (4-16).
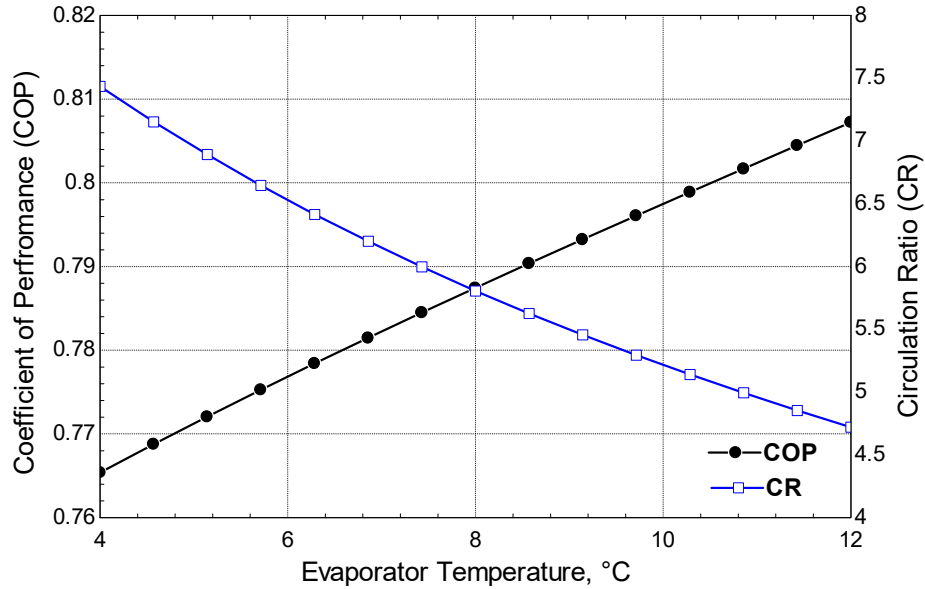
Figure 4-11 Effect of evaporator temperature on COP and CR

Figure 4-12 shows the effect of generator temperature on the COP at different absorber temperature. The diluted LiBr concentration (X_{ws}) is a function of the absorber temperature and system low pressure, hence, the concentration of the diluted LiBr solution increases by increasing absorber temperature [23]. Moreover, the strong LiBr mass flow rate increases to cancel the effect of the diluted LiBr concentration related to Equation (4-2), hence, the evaporated water vapor decreases as described in Equation (4-1). Consequently, the COP decreased by increasing absorber temperature.
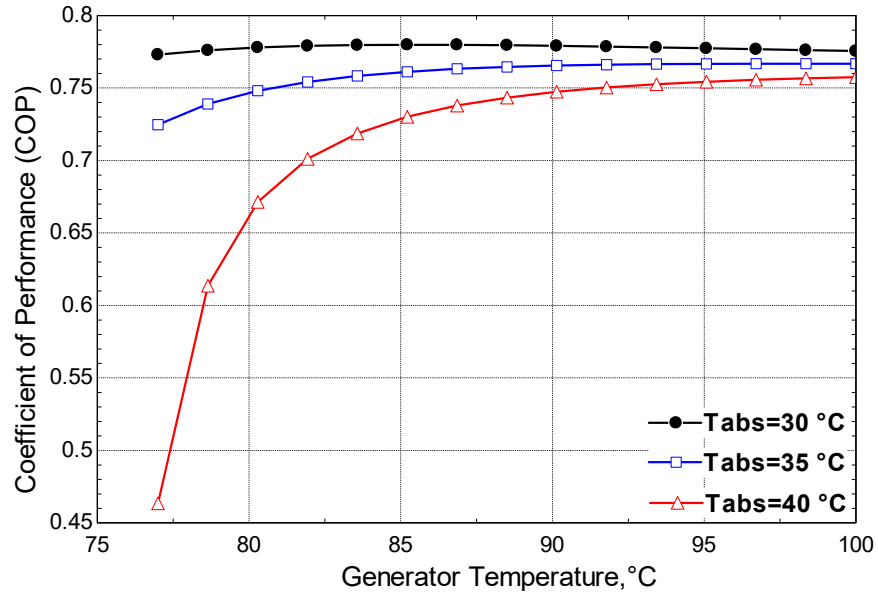
Figure 4-12 Effect of generator temperature on COP with different absorber temperature

Figure 4-13 shows the effect of generator temperature variation on COP at different condenser temperature. The results show that COP decreases by increasing the condenser temperature. The concentrated LiBr concentration (X_{ss}) is a function of system high pressure with an inverse proportionality [23], hence, X_{ss} decreases by increasing the condenser temperature and pressure. Consequently, the strong LiBr mass flow rate decreased at constant diluted LiBr concentration and mass flow rate as described in Equation (4-2). In addition, the evaporated refrigerant mass flow rate decreases by increasing strong LiBr mass flow rate solution as described in Equation (4-1). For that reason, the cooling capacity decreased with respect to the heat input to the generator, hence, the COP decreased.
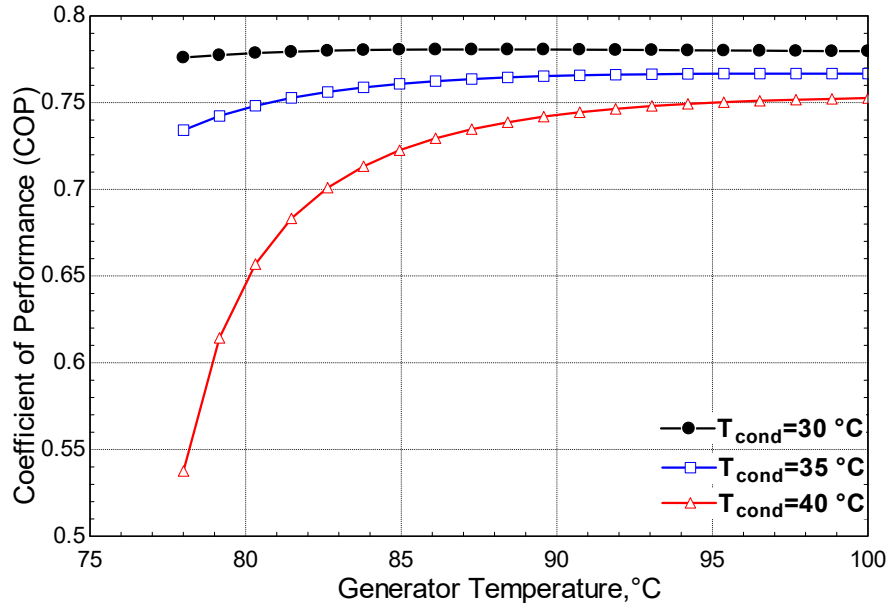
Figure 4-13 Effect of generator temperature on COP at different condenser temperature

Figure 4-14 shows the effect of generator temperature on the evaporator heat transfer energy. The heat transfer rate across the evaporator increases by increasing the generator temperature as the evaporated water vapor refrigerant from the generator increased at constant evaporator temperature.
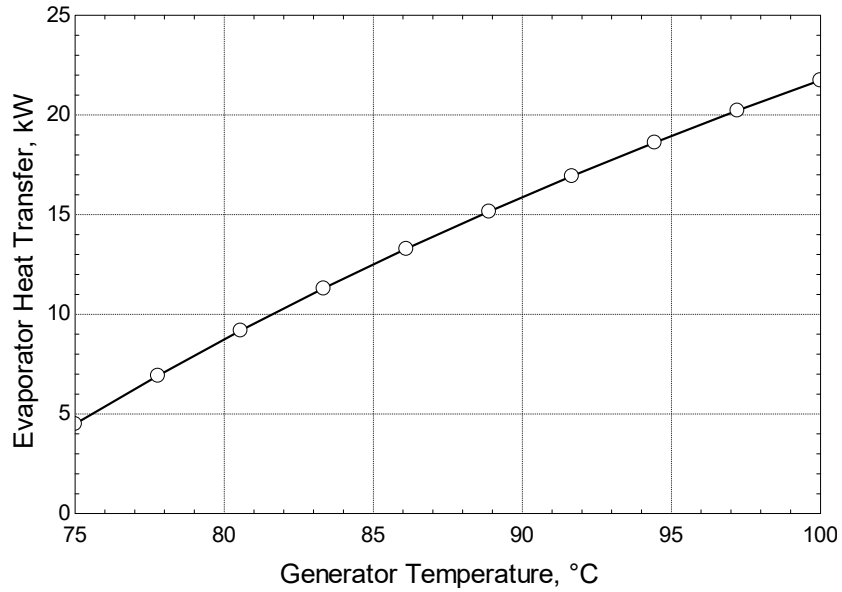
Figure 4-14 Effect of generator temperature on the evaporator heat transfer

Figure 4-15 shows the effect of generator temperature on the COP and system efficiency. The COP increased with increasing the generator temperature as discussed in Figure 4-6. However, the system efficiency increased to a certain value then a significant reduction occurs by increasing the generator temperature. At high temperature, Carnot coefficient of Performance (COP_c) increases with a higher rate than COP. Moreover, exergy loss increases as the temperature variation between the generator and ambient increases. The maximum efficiency of the system is 0.67 that occurs at T_{gen}=78 °C. In addition, the further increase in generator will decrease the COP as the (X_{ss}) may enter the crystallization zone, hence, performance will deteriorate.
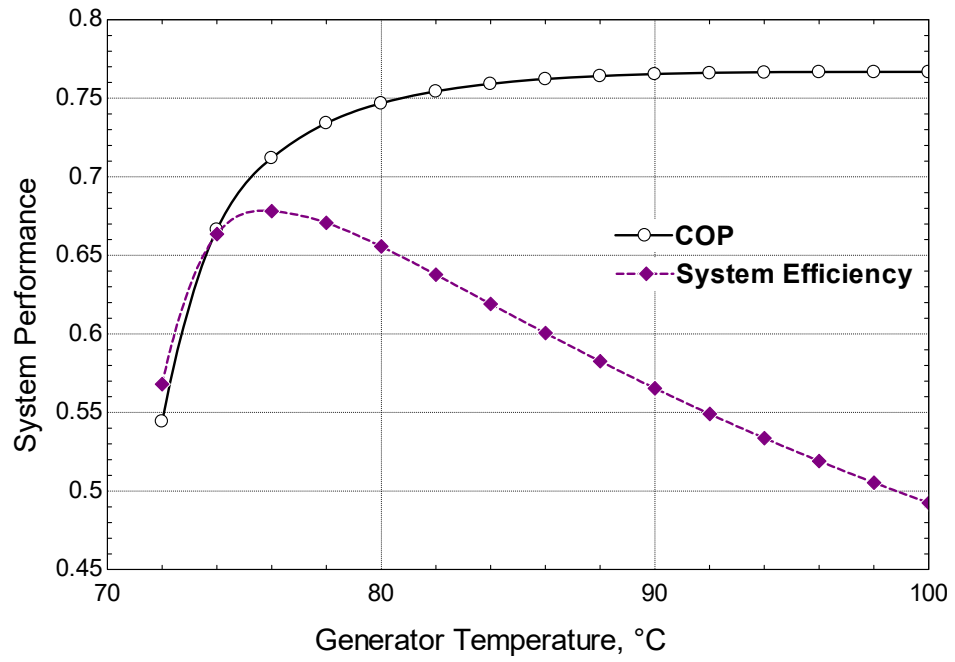
Figure 4-15 Effect of generator temperature on the system performance

Chapter 5: **Hybrid Single Stage H₂O-LiBr Absorption and Single Effect Desalination System**

5.1 Introduction

In this section, the analyzed system includes three main components, heating section, single stage H_2O-LiBr absorption subsystem, and single effect desalination subsystem for fresh water production. These cycles are coupled together as shown in Figure 5-1. Each cycle was mathematically modeled and validated in Chapters 3 and 4. The output parameters of the combined system as the cooling effect through the absorption evaporator, and the pure water will be supplied to a facility to decrease the needed input energy to produce those outputs.

The combination of the two subsystems is made through utilizing and directing the rejected heat from the absorption condenser to the desalination evaporator as shown in Figure 5-1. This hybrid system will have many advantages as follow;

- The rejected heat to the environment from the absorption condenser is utilized in the desalination plant as an input heat to produce potable water, hence, decreasing the environmental thermal load.

- The overall system efficiency is increased.

The coefficient of performance, performance ratio and the useful output energy for the two cycles is discussed through a parametric analysis. The analysis is performed at steady state operation with different input values.

5.2 System Description

Figure 5-1 shows the configuration of the whole combined H_2O-LiBr single stage and SEE subsystems. The high rejected heat from the absorption condenser is used to produce potable water by using SEE desalination system. Figure 5-2 shows the amount of heat rejected from the condenser with variable generator temperature that is expelled out to the environment. This desalination subsystem utilizes the rejected condenser energy to heat and evaporates water-vapor from seawater to produce distilled water. Figure 5-2 illustrates the refrigerant and seawater mass flow rates, and the energy direction through LiBr condenser to desalination evaporator.
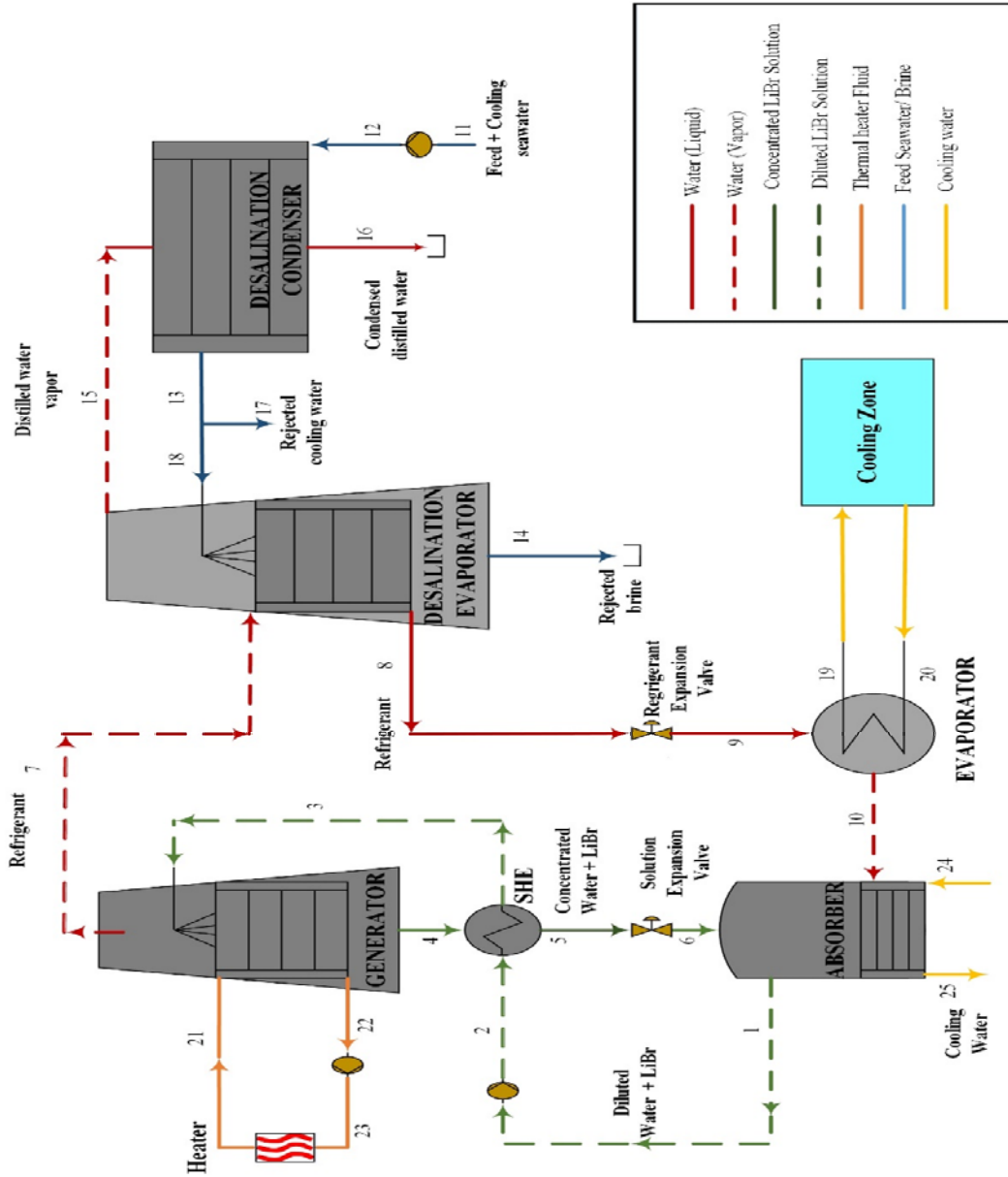
Figure 5-1 Hybrid single stage H_2O-LiBr absorption and single effect desalination system
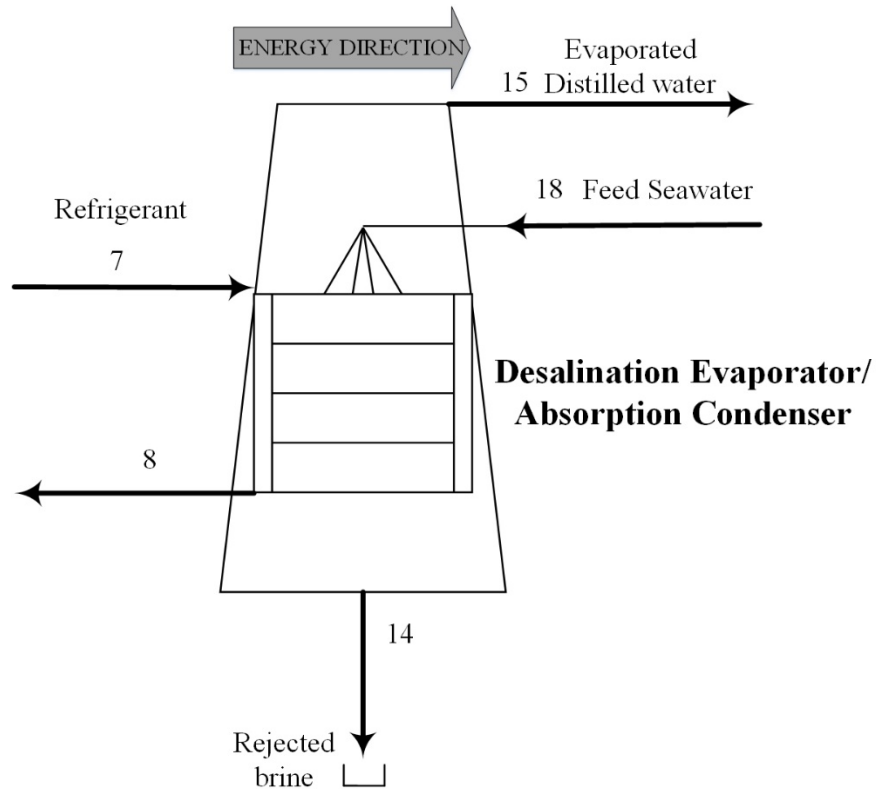
Figure 5-2 Configuration of desalination evaporator/ absorption condenser

5.3 Mathematical Model

5.3.1 Assumptions

The thermodynamic analysis is performed by mass and energy balance under the following assumptions:

- The combined system operates under steady-state and steady-flow conditions.

- No heat loss from the heat exchangers to the ambient.

- The mixture in the absorber is a homogenous solution.

- Neglecting pressure drop across the piping and fittings.

- The formed vapor is free of salt.

- Pressure is kept constant in the SEE subsystem.

- State 1, 4, 8, 16 are assumed to be at the saturation liquid conditions

- State 7, 10, 15 are assumed to be at the saturation vapor conditions.

5.3.2 Governing Equations

5.3.2.1 Mass balance

Mass balance equations are written for each component of the combined single stage H_2O-LiBr absorption and single effect desalination system similar to the equations written for each standalone subsystem. For SEE and LiBr refrigeration absorption standalone cycles, equations from (3-1) to (3-4), and equations from (4-1) to (4-3), respectively are used to evaluate the whole system mass balance.

Mass balance is performed for the desalination evaporator as shown in Figure 5-2.

Absorption Condenser/ Desalination Evaporator

$$\dot{m}_{18} = \dot{m}_{14} + \dot{m}_{15} \tag{5-1}$$

$$\dot{m}_{18} \times X_f = \dot{m}_{14} \times X_{salt\_brine} + \dot{m}_{15} \times X_d \quad \text{(Evaporator)} \tag{5-2}$$

$$\text{where,} \quad X_d = 0 \quad \quad \text{(Vapor is salt-free)}$$

5.3.2.2 Energy Balance

Energy balance is performed for each component of the combined single stage H_2O-LiBr absorption and single effect desalination system. The energy balance equations are written in a similar manner to the standalone subsystems written earlier. For the SEE and LiBr refrigeration absorption standalone cycles, equations from (3-5) to (3-13), and equations from (4-4) to (4-14), respectively are used to evaluate system energy balance.

Heat balance is made for the desalination evaporator as shown in Figure 5-2.

Absorption Condenser/ Desalination Evaporator

$$Q_{abs.cond} = Q_{desal.evap} \tag{5-3}$$

$$Q_{abs.cond} = \dot{m}_{ref} \times (h_7 - h_8) \tag{5-4}$$

$$Q_{desal.evap} = (\dot{m}_d \times h_{15}) + (\dot{m}_b \times h_{14}) - (\dot{m}_f \times h_{18}) \tag{5-5}$$

5.3.2.3 Exergy Balance

Exergy of fluid stream is defined as

$$\Psi = (h_i - h_o) - T_o \times (S_i - S_o) \tag{5-6}$$

The exergy balance of a steady flow system is expressed as

$$Ex_{destoyed} = \sum_{in}(\dot{m} \times \Psi) - \sum_{out}(\dot{m} \times \Psi) + \sum_{in} Q \times (1 - \frac{To}{T}) \tag{5-7}$$

$$-\sum_{out} Q \times (1 - \frac{To}{T}) - W$$

5.3.2.4 Performance Analysis

The performance of the combined single stage H_2O-LiBr absorption and single effect desalination system is evaluated by considering the PR and COP as shown in Equation (3-14) and (4-15), respectively. Moreover, the following performance parameter is considered as follow;

Overall Energy Utilization Factor (EUF)

EUF is the output energy from the system (cooling effect and distilled water) over the input energy to the system which is mainly the heat input to the generator [54].

$$EUF = (Q_{cooling} + Q_{desal.cond})/(Q_{gen} + W_{pumps}) \tag{5-8}$$

Exergy efficiency is described as the following

$$\text{Exergy Efficiency} = \frac{Q_{evap} \times \left(1 - \left(\frac{T_o}{T_{evap}}\right)\right)}{Q_{gen} \times \left(1 - \left(\frac{T_o}{T_{gen}}\right)\right) + W_{sp}} \tag{5-9}$$

5.4 Solution Procedures

Figure 5-3 shows the procedure for solving the combined subsystems in a simple way by inserting the input parameters to the developed code, then the program will use its built-in functions and formulae to calculate the thermodynamic properties and the system`s performance parameters.

Step 1	• Insert input data (T1, T4, T8, T9, T11, Q1, Q4, Q7, Q8, $\dot{m}_{ws}$, $\dot{m}_f$, X_f, $SHE_{effectivness}$, $Pump_{eff}$, $SEE_{pressure}$, $m_{percentage}$,)
Step 2	• Compute (HP, LP, Xws, Xss, Sp_vo_{ll})
Step 3	• Compute (h1, h2, h4, h7, h8, h10)
Step 4	• Compute ($\dot{m}_{ss}$, $\dot{m}_{ref}$, h9, Q9, h3, T3)
Step 5	• Compute (P_{ws}, $Q_{she-cold}$, $Q_{she-hot}$, Q_{gen}, Q_{cond}, Q_{evap}, Q_{abs})
Step 6	• Compute (T_v, BPE, $m_{newfeed}$)
Step 7	• Compute (h_{11}, h_{12}, h_{15}, h_{16})
Step 8	• Compute (T_b, X_{brine}, P_{sw})
Step 9	• Compute (h_{14}, $Q_{desal.cond}$, $Q_{desal.evap}$, $\dot{m}_{brine}$, $\dot{m}_d$)
Step 10	• Compute (h_{13}, T_{13})
Step 11	• Compute cycle (Temperature, Enthalpy, Entropy)
Step 12	• Compute System Performance (COP, PR, EUF, Exergy Efficiency)

Figure 5-3 EES solving procedures

5.5 Result and Discussion

5.5.1 Parametric Study of Combined H₂O-LiBr Absorption and SEE System

A parametric study is carried out for the performance analysis of combined H**₂**O-LiBr absorption and SEE system. Output parameters such as COP, PR, distillate water mass flow rate ($\dot{m}_d$) are evaluated at different operating conditions. Table 5-1 shows the input parameters to the combined system.

Table 5-1 Input parameters of cooling and desalination hybrid system

Input Parameters	Cycle	Value
Generator temperature (T_7)	LiBr	90 °C
Condenser temperature (T_8)	LiBr	35 °C
Evaporator temperature (T_{10})	LiBr	4 °C
Absorber temperature (T_1)	LiBr	35 °C
Diluted LiBr solution mass flow rate ($\dot{m}_{ws}$)	LiBr	0.07 kg/s
Absorber outlet water quality (Qa_1)	LiBr	0
Generator outlet water quality (Qa_4)	LiBr	0
Generator outlet refrigerant quality (Qa_7)	LiBr	1
Condenser outlet water quality (water state) (Qa_8)	LiBr	0

Evaporator outlet water quality (Qa_{10})	LiBr	1
Input feed seawater + Cooling water flow rate ($\dot{m}_{11}$)	SEE	0.14 kg/s
Percentage of feed water to the desalination-evaporator	SEE	30%
Inlet seawater temperature (T_{11})	SEE	30 °C
Feed salinity (X_f)	SEE	42 g/kg
Desalination system pressure	SEE	60 kPa
Absorber cooling water inlet temperature (T_{24})	LiBr	25 °C
Absorber cooling water mass flow rate ($\dot{m}_{24}$)	LiBr	0.4 kg/s
Inlet chilled water temperature (to evaporator) (T_{20})	LiBr	25 °C
Chilled water mass flow rate ($\dot{m}_{20}$)	LiBr	0.4 kg/s

Figure 5-4 shows the effect of the generator temperature on the heat transfer rate of the combined system components. Heat transfer across the generator increases with increasing the generator temperature as the enthalpy difference between the generator outputs (state 4, 7) with the generator input state 3 increases, as discussed in Figure 4-7. Moreover, heat transfer across the LiBr condenser increases as refrigerant temperature increases (T_7) so the enthalpy difference across the condenser increased (h_7-h_8) at constant condenser temperature. In addition, the refrigerant mass flow rate across the system increases by increasing the generator temperature. So, heat transfer across the absorber and the evaporator increases.

The heat transfer across the desalination condenser increases as the heating refrigerant mass flow rate and enthalpy difference (h_7-h_8) increased that increases the evaporated distilled water. However, heat transfer across the SHE is almost constant since the LiBr mass flow rates ($\dot{m}_{ss}$, $\dot{m}_{ws}$) and temperature difference between the solution inputs (T_2, T_4), and outputs (T_3, T_5) across SHE are almost constant assuming the evaporated water-vapor refrigerant flow rate is very small compared to the diluted/concentrated LiBr mass flow rate. Noted that, the heat transfer rate of the desalination condenser is zero at generator temperature less than of 78 °C, as no distilled water is produced. This fact is because of the small temperature difference between the top brine temperature and condenser input temperature (T_7), therefore all the heat transfer rate in the desalination evaporator would be consumed as sensible heat of seawater.
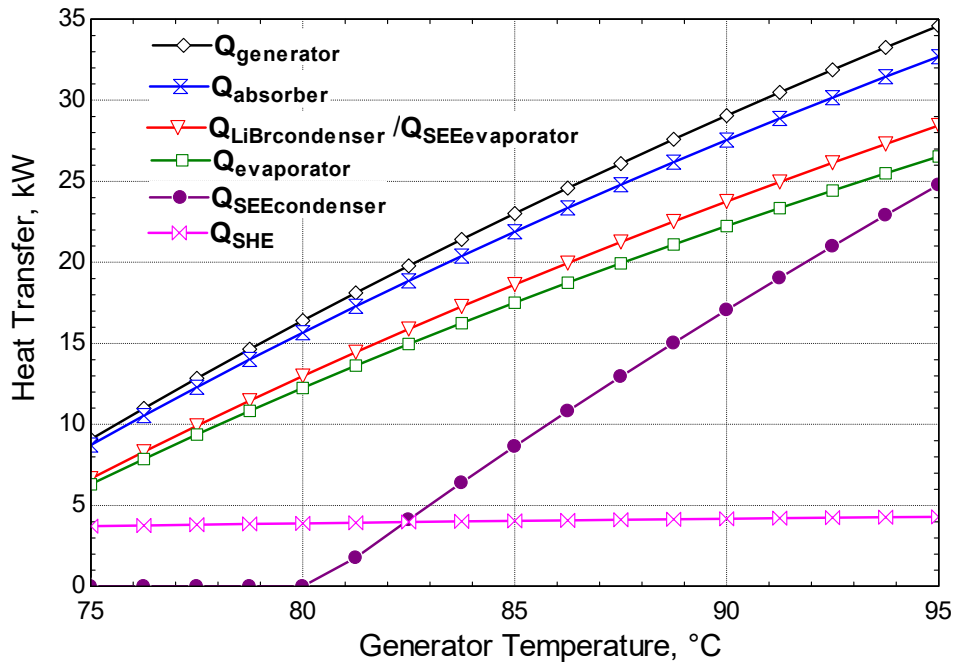
Figure 5-4 Effect of generator temperature on the heat transfer of different component of the combined system

Figure 5-5 shows the effect of changing the generator temperature on the refrigerant and distilled water flow rate at different desalination cycle pressures. The refrigerant flow rate increases with increasing the generator temperature as the evaporation rate increases with more input heat energy, Consequently, the distilled water flow rate increases as the input temperature (T_7) to the LiBr condenser increases at constant desalination system pressure. The evaporation in the desalination cycle depends mainly on system pressure, where the saturation temperature of the water vapor has a direct relation with the pressure. Therefore, the amount of distilled water increases by decreasing the saturation temperature –decreasing the saturation pressure- from 80 to 40 kPa. Note that, desalination plant has a temperature limit, where generator output vapor temperature should be $\geq$ 78 °C, at desalination pressure of 40 kPa to produce potable water. Otherwise, the desalination subsystem will not produce water as discussed before.
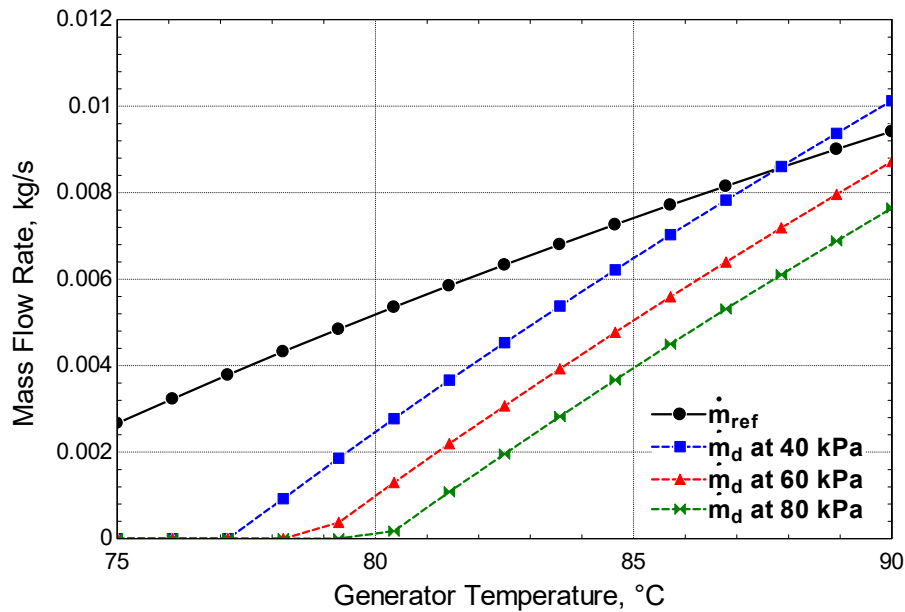
Figure 5-5 Effect of generator temperature on refrigerant and distilled water flow rates at different desalination cycle pressures

Figure 5-6 shows the effect of changing the generator temperature on the COP and PR at different desalination cycle pressures. The COP of the system increases by increasing the generator temperature as the cooling capacity in the evaporator increases –by increasing the refrigerant flow rate- with a higher rate than the generator heat transfer rate as discussed in Figure 4-7. Moreover, the PR increases with increasing the generator temperature as the evaporated distilled water increased as discussed in Figure 5-5. In addition, the desalination pressure can boost the PR more by decreasing the saturation pressure (brine boiling temperature), at a certain value of the generator temperature the PR can exceed a value 1 at low saturation pressure. Note that, the desalination subsystem cannot be operated with a generator temperature less than 78 °C, at desalination pressure of 40 kPa. The combined system show promising results for the distilled water, as the PR increases at a generator temperature of 90 °C.
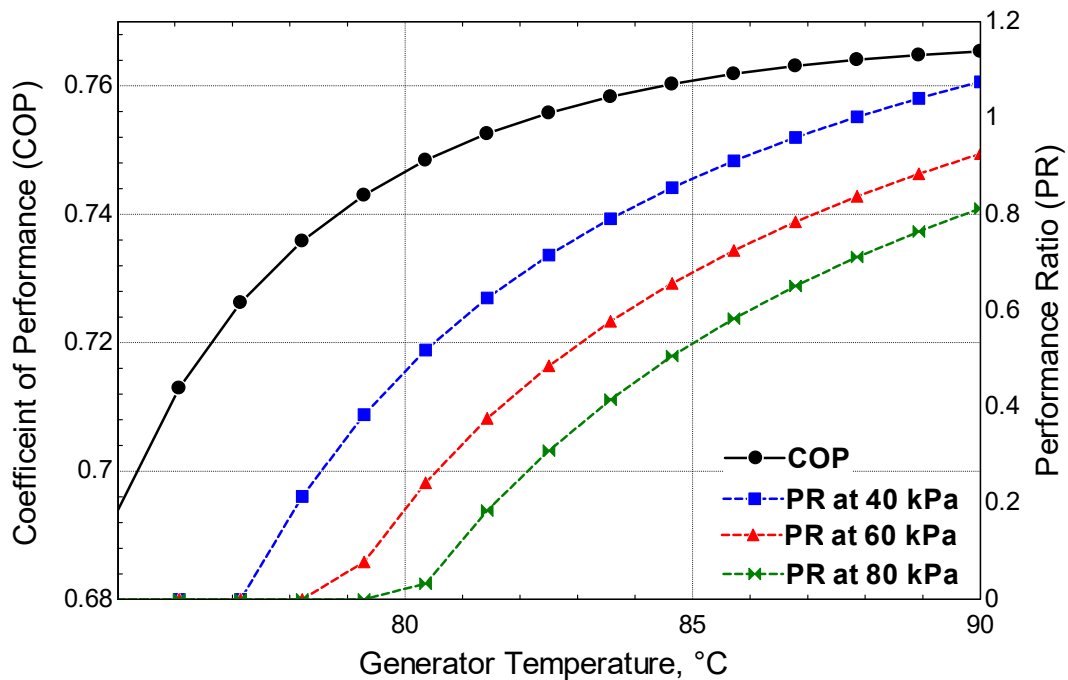
Figure 5-6 Effect of generator temperature on COP and PR at different desalination cycle pressures

Figure 5-7 shows the effect of generator temperature on the generator heat transfer rate at different SHE effectiveness. It is obvious that the minimum required heat transfer rate in the generator occurs at the highest effectiveness where the diluted LiBr solution (state 3) gains the maximum amount of heat from (state 5) through SHE. The required heat transfer rates through the generator are 27, 28.7 and 30 kW with SHE effectiveness 100, 75, and 50%, respectively at a constant generator temperature of 90 °C. Consequently, the needed input energy decreased by using SHE by 25.37% with SHE effectiveness of 100%. Moreover, the needed cooling water flow rate decreased as the concentrated LiBr solution (state 5) transferred the unwanted sensible energy to the diluted LiBr solution (state 3) before it enters the absorber, hence, less thermal energy removed from the absorber for a homogenous mixture.
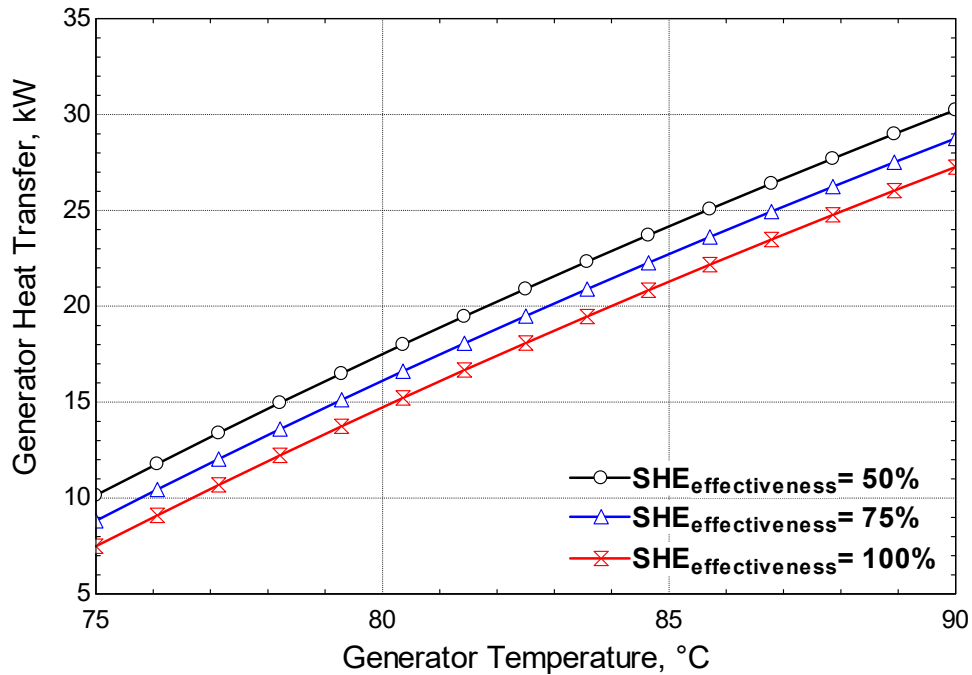
Figure 5-7 Effect of generator temperature on generator heat transfer at different SHE effectiveness

Figure 5-8 shows the effect of generator temperature on the absorber heat transfer rate at different values of SHE effectiveness. The lowest absorber heat input occurs at the highest SHE effectiveness, where the concentrated LiBr solution (state 5) loses the maximum amount of heat through SHE. Therefore, the required rejected heat from –the exothermic reaction of- the absorber decreases to its minimum value.
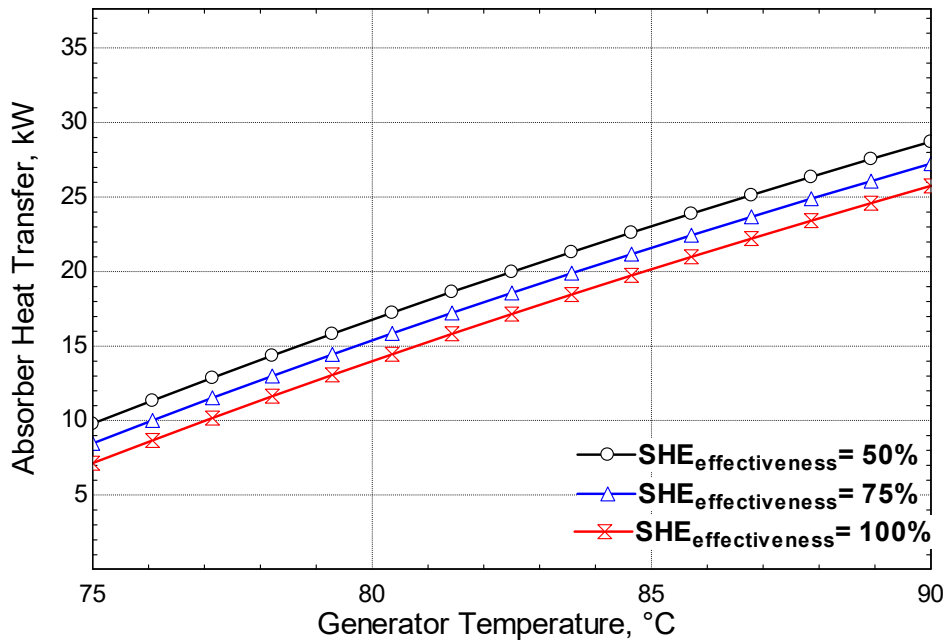
Figure 5-8 Effect of generator temperature on absorber heat transfer at different SHE effectiveness

Figure 5-9 show the variation of condenser temperature on refrigerant and distilled water flow rates. The refrigerant mass flow rate decreases by increasing the condenser temperature since the concentrated LiBr solution (X_{ss}) depends on the condenser temperature with an inversely proportional relation [23], hence, the concentrated LiBr solution decreased by increasing condenser temperature. Consequently, the concentrated LiBr mass flow rate increased at constant diluted LiBr solution (X_{ws}) and mass flow rate ($\dot{m}_{ws}$) as shown in Equation (4-2). The evaporated

refrigerant mass flow rate decreased at constant generator temperature as shown in Equation (4-1). On the other hand, the evaporated distilled water decreased for two reasons; the first reason is the decreasing of the evaporated refrigerant vapor flow rate as discussed before. The second reason is the lessening in the enthalpy difference between the generator vapor and condenser outlets (h_7-h_8) at constant generator temperature.

Figure 5-9 Effect of condenser temperature on refrigerant and distilled water flow rates

Figure 5-10 shows the effect of condenser temperature on the COP and PR of the system. As discussed in Figure 5-9, both refrigerant and distilled flow rates decrease with increasing the condenser temperature. Consequently, the evaporator cooling capacity decreased as it depends on the refrigerant mass flow rate, therefore the COP decreased with respect to the generator heat transfer rate. On the other hand, the reduction of the refrigerant mass flow rate and the condenser heat transfer rate decreased the evaporated distilled water mass flow rate ($\dot{m}_d$), hence, the PR decreased.

Figure 5-10 Effect of condenser temperature on COP and PR

Figure 5-11 shows the variation of evaporator temperature on refrigerant and distilled water flow rates. The refrigerant mass flow rate increased by increasing the evaporator temperature since the diluted LiBr solution (X_{ws}) depends on the evaporator temperature with an inversely proportional relation [23], hence, the diluted LiBr solution decreased by increasing evaporator temperature. Consequently, the concentrated LiBr mass flow rate decreased at constant concentrated LiBr solution (X_{ss}) (constant condenser temperature) as shown in Equation (4-2). Finally, the evaporated refrigerant mass flow rate increased at constant generator temperature as shown in Equation (4-1). On the other hand, the evaporated distilled water increased as the condenser heat transfer rate increased through the increase of the refrigerant mass flow rate.
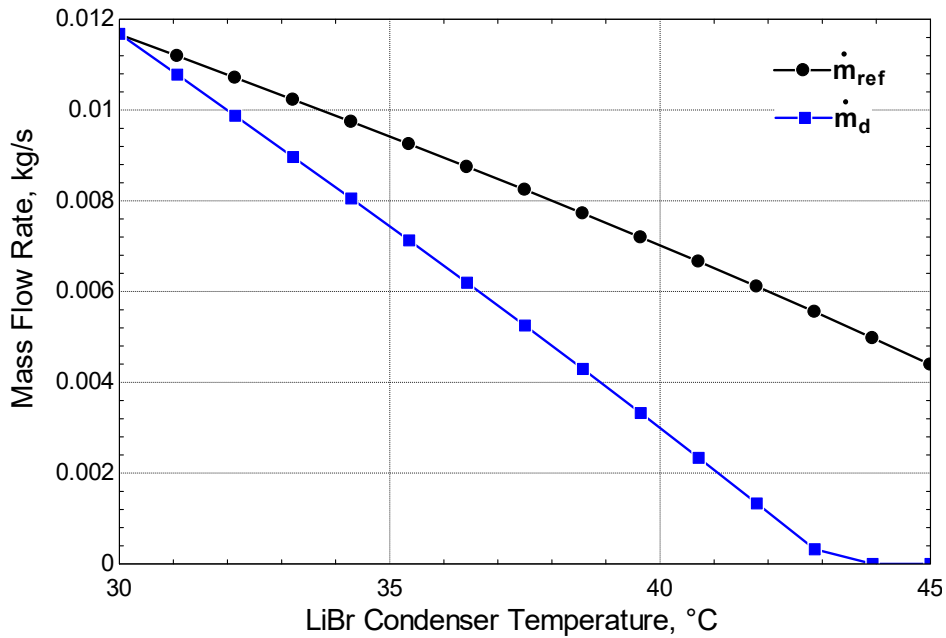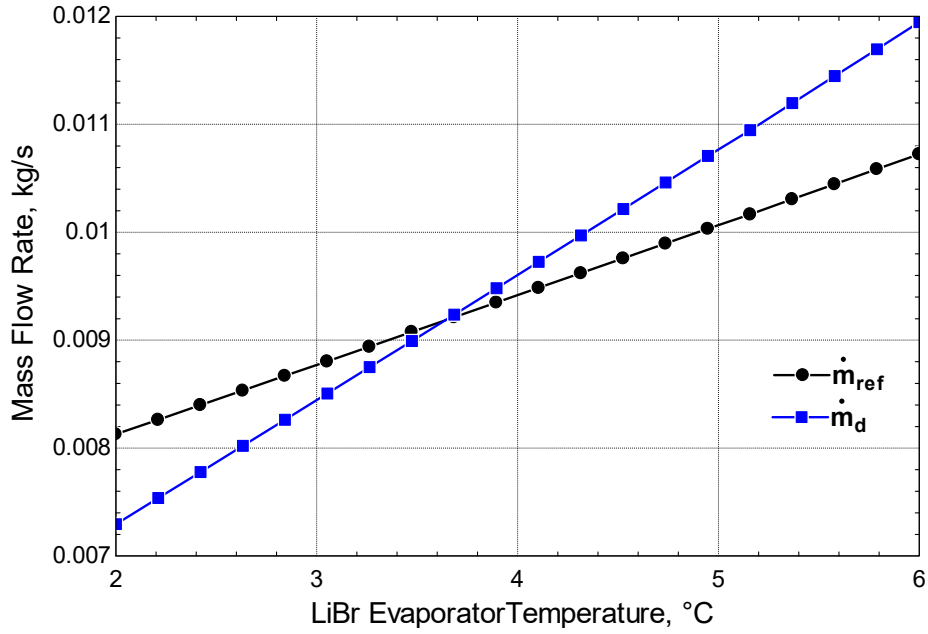
Figure 5-11 Effect of evaporator temperature on refrigerant and distilled water flow rates

Figure 5-12 shows the effect of evaporator temperature on the COP and PR of the system. As discussed in Figure 5-11, both the refrigerant and distilled flow rates increase with increasing the evaporator temperature. Consequently, the evaporator cooling capacity increased as it mainly depends on the refrigerant mass flow rate, therefore the COP increased with respect to the generator heat transfer rate. On the other hand, the increase of the refrigerant mass flow rate and the evaporator heat transfer rate boosted the evaporated distilled water mass flow rate ($\dot{m}_d$), hence, the PR increased.
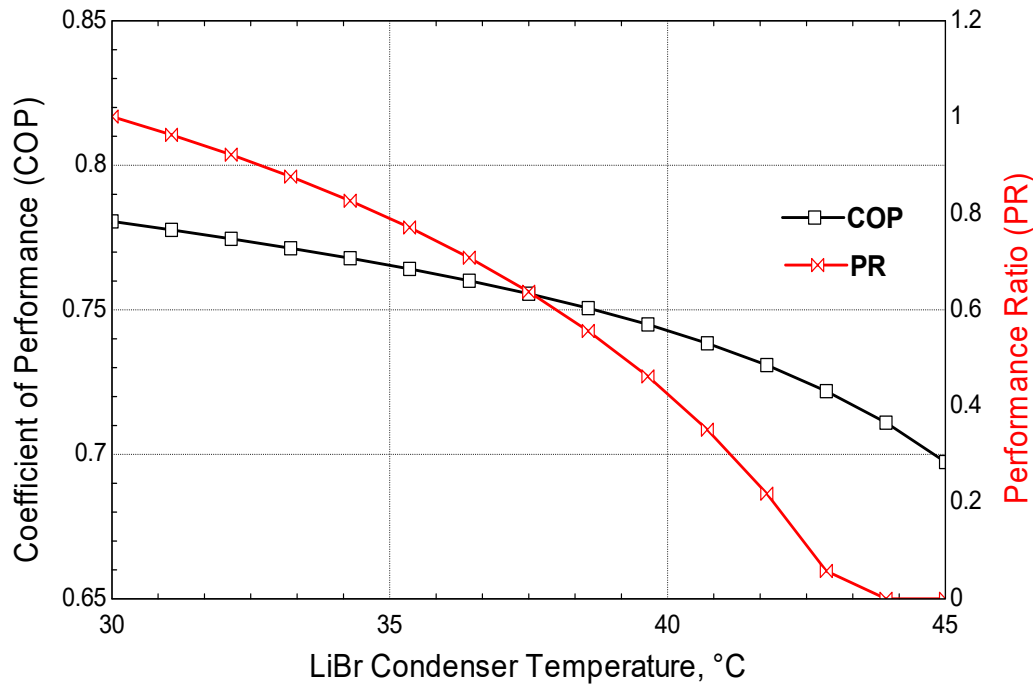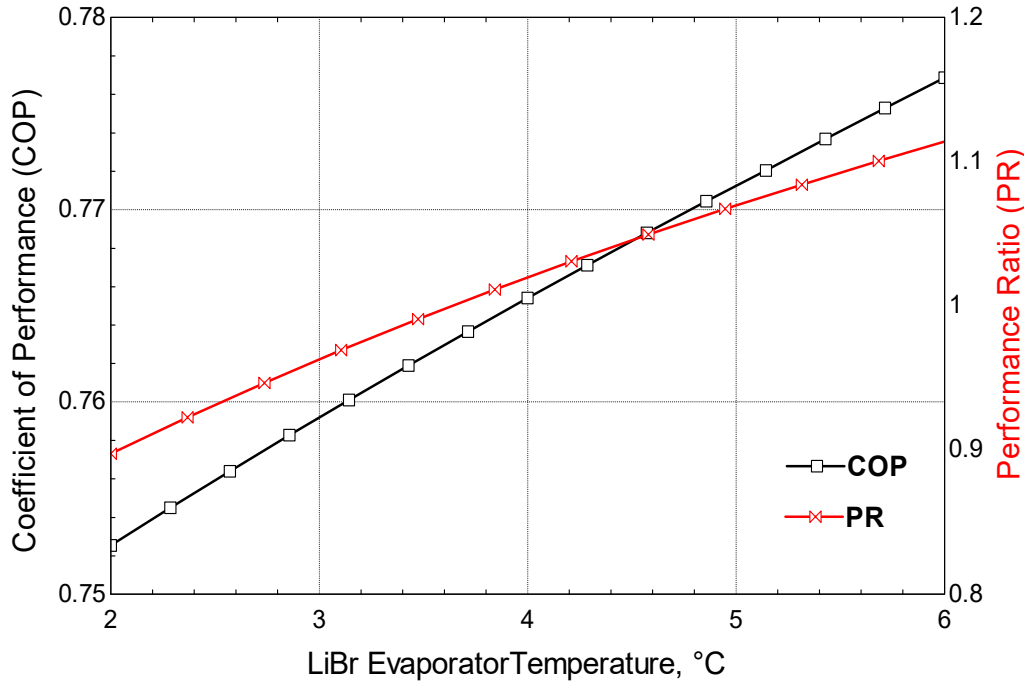
Figure 5-12 Effect of evaporator temperature on COP and PR

Figure 5-13 shows the effect of absorber temperature variation on refrigerant and distilled water flow rates. The refrigerant mass flow rate decreases by increasing the absorber temperature as the weak LiBr concentration (X_{ws}) increases at constant weak LiBr solution flow rate and strong LiBr concentration [23]. Consequently, the strong LiBr mass flow rate increases as indicated by Equations (4-1) and (4-2). Afterward, the produced distilled water vapor mass flow rate decreases as the input energy to the desalination evaporator decreased through the decrease of refrigerant mass flow rate.
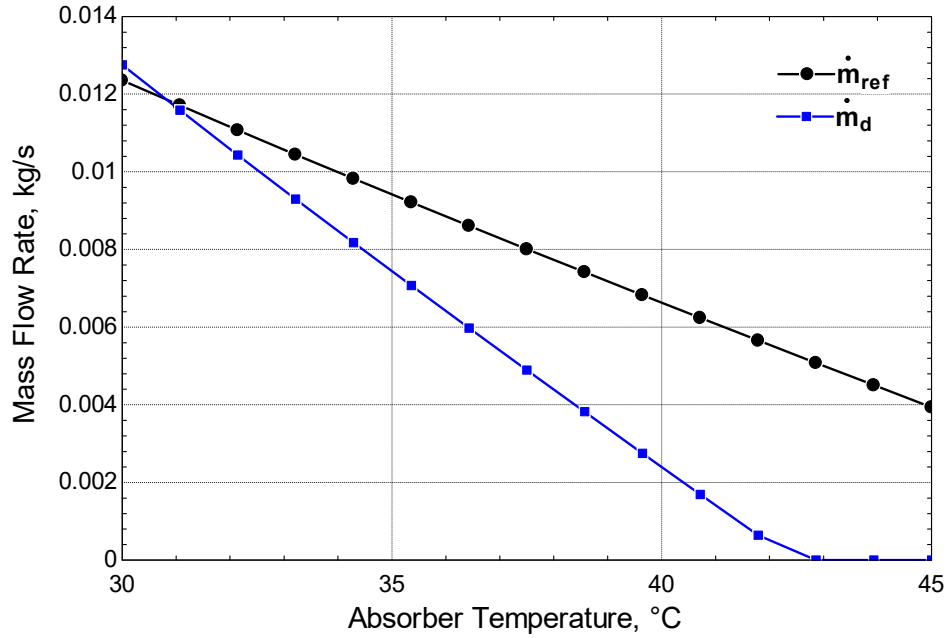
Figure 5-13 Effect of absorber temperature on refrigerant and distilled water flow rates

Figure 5-14 shows the effect of absorber temperature variation on the COP and PR of the system. As discussed in Figure 5-13, both refrigerant and distilled flow rates decrease by increasing the absorber temperature. Consequently, the cooling capacity of the evaporator decreased with respect to the generator heat input rate, hence, the COP decreased at constant evaporator temperature. On the other hand, the PR decreased by increasing the absorber temperature as the heat transfer rate to the desalination evaporator decreased significantly due to the reduction of refrigerant mass flow. Consequently, the effect of decreasing evaporated distilled flow rate increased.
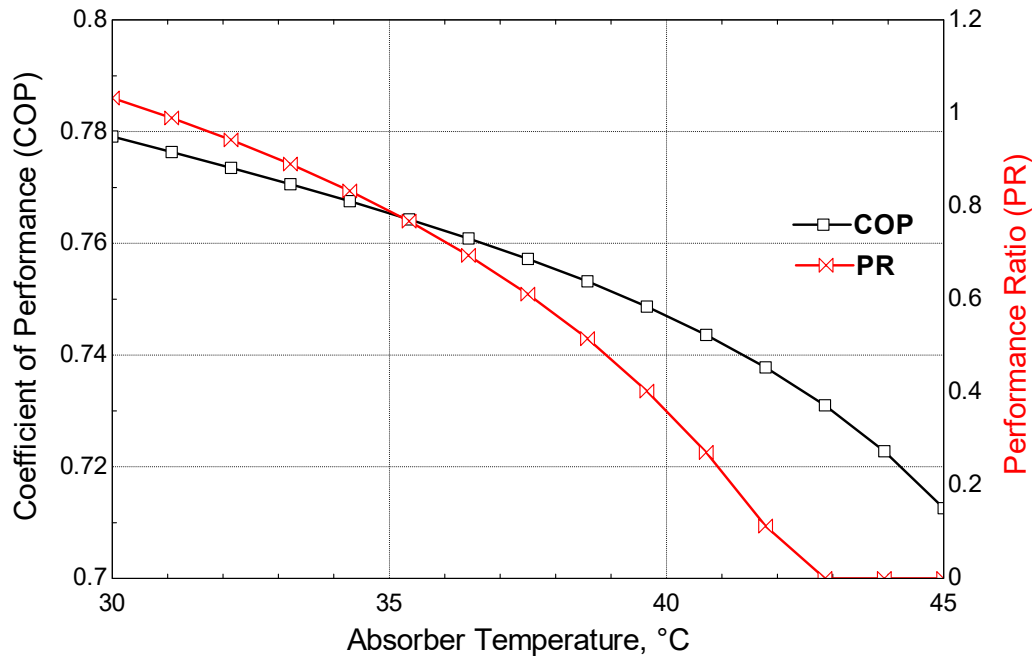
Figure 5-14 Effect of absorber temperature on COP and PR

Figure 5-15 shows the effect of generator temperature on EUF at different evaporator temperature where, it is clear that EUF increased by increasing generator temperature as the cooling effect ($Q_{cooling}$) and the distilled heat transfer rate across the desalination evaporator increased because of the increase of refrigerant and produced distilled water mass flow rates as discussed in Figure 5-5. Moreover, the decrease in evaporator temperature has a negative effect on the system performance, where the refrigerant mass flow decreased by decreasing evaporator temperature as discussed in Figure 5-11. Consequently, it is advisable to work at a high evaporator temperature for a higher system performance. On the other hand, the sharp increasing of EUF at generator temperature of 83.5 °C, at absorber temperature of 2 °C, as the desalination subsystem will not operate before the stated temperature, due to the low energy added to the desalination cycle. Noted that, the refrigerant mass flow rate has a major effect on the cooling capacity, and the

heat transfer rate to the desalination subsystem that is responsible for the distillate water production., hence, the PR will be insignificant at a generator temperature less than 83.5 °C

Figure 5-15 Effect of generator temperature on EUF at different evaporator temperature

Figure 5-16 shows the effect of generator temperature on EUF at different evaporator temperature where the system`s performance EUF increased significantly with the increase of generator temperature as discussed in Figure 5-15 from a value of 1.2 to 1.6 at a condenser temperature of 30 °C. The effect of changing condenser temperature on the EUF is more than the effect of changing evaporator temperature, as the input heat rate to the desalination evaporator increased by increasing distilled water flow rate and latent energy (h_7-h_8). Consequently, the produced distilled water is increased, which enhanced the desalination heat rate. Similarly, the increase in the condenser temperature to 40 °C has decreased the input heat transfer rate to the desalination evaporator (enthalpy of vaporization) (h_7-h_8). The required minimum generator temperature is 86 °C to produce potable water through SEE system
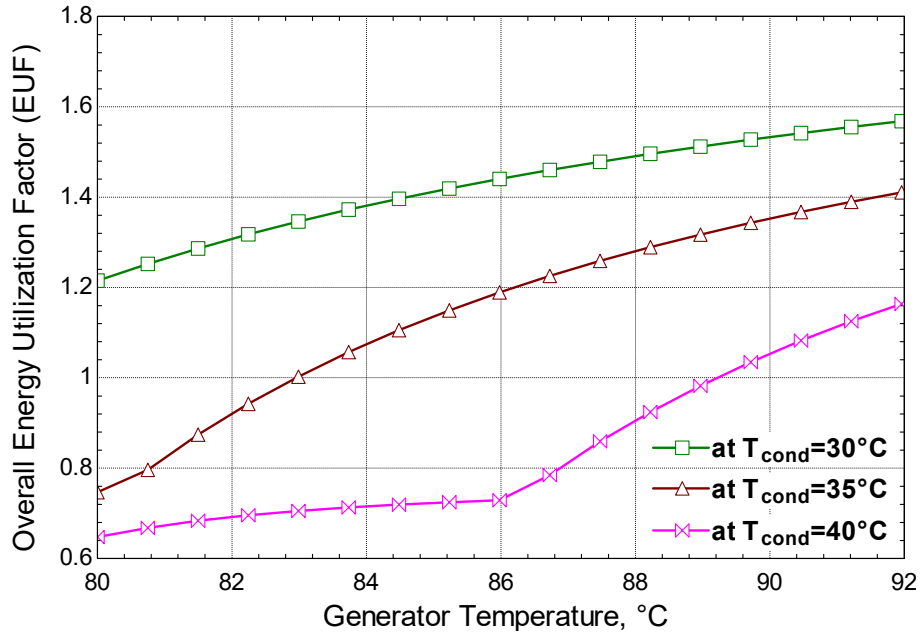
Figure 5-16 Effect of generator temperature on EUF at different condenser temperature

Figure 5-17 shows the effect of generator temperature on EUF at different absorber temperature where the EUF increased by increasing generator temperature as discussed in Figure 5-15. The temperature increase in the absorber has almost the same influence in decreasing the refrigerant mass flow rate as the temperature increase in the condenser. The generator temperature must be over 86.9 °C to operate desalination plant.

Figure 5-18 shows the effect generator temperature on COP and LiBr exergy efficiency. The COP of the system increases by increasing the generator temperature as discussed in Figure 5-6. However, LiBr exergy efficiency decreases by increasing the generator temperature as the temperature difference between generator and ambient temperatures increases. [58].
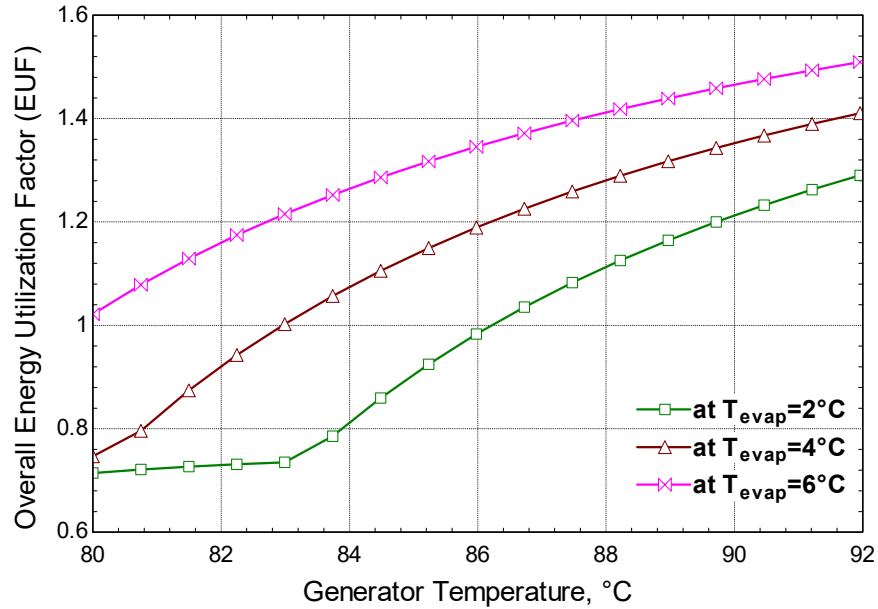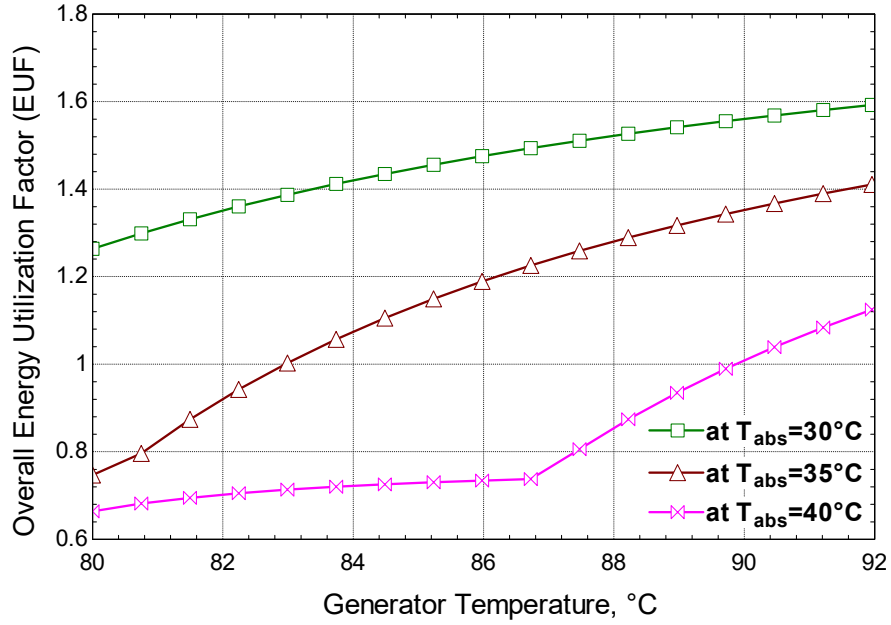
Figure 5-17 Effect of generator temperature on EUF at different absorber temperature
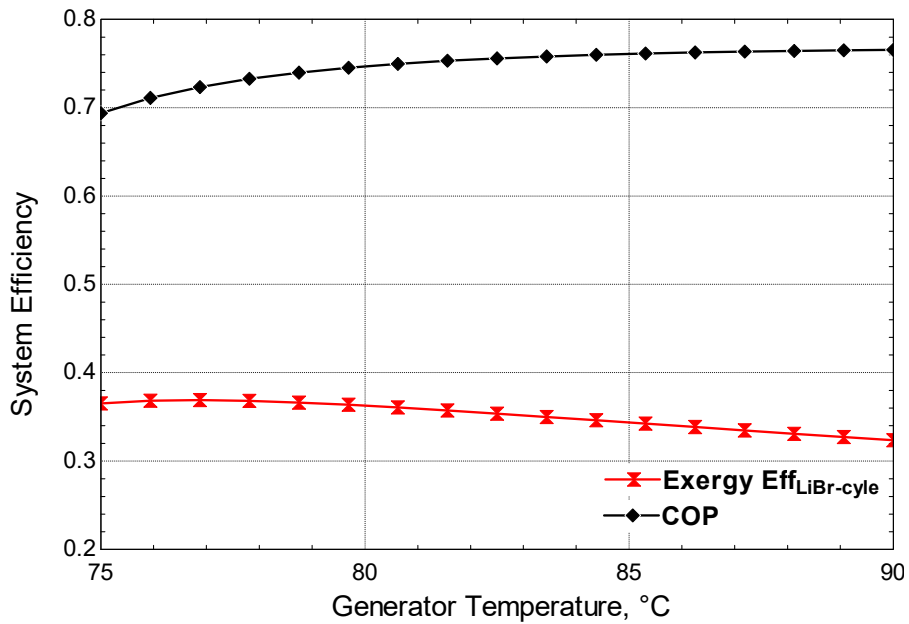
Figure 5-18 Effect of generator temperature on COP and LiBr exergy efficiency

Figure 5-19 shows exergy losses across the different combined system components. The results are important to decrease exergy losses in the system especially in the generator and the absorber. This high exergy loss in the generator is because of two reasons. The first reason is because of the high energy consumption in the generator to evaporate water from the concentrated solution, which is greater than the energy needed to evaporate the refrigerant in its pure form. The second reason is that more heat can be added to the generator, where the refrigerant evaporates with a high degree of superheat. Hence, extra losses from the generator. Moreover, the high degree of superheat leads to extra cooling requirements in the condenser. These results are quite similar to the study investigated by Zadeh and Bozorga [58].

Figure 5-20 shows the contribution of exergy losses of each component in the whole system. The generator and absorber have the highest exergy losses influence with a share of 34.34%, 20.99%, respectively.
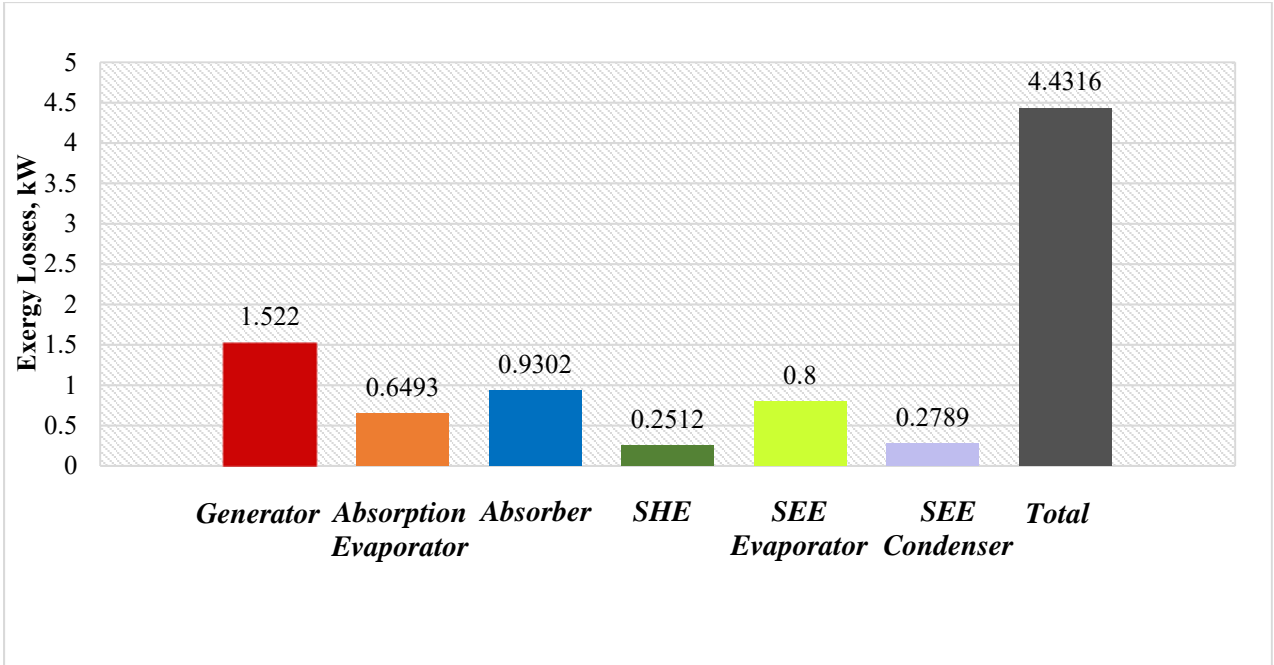
Figure 5-19 Exergy losses across each component in the hybrid system
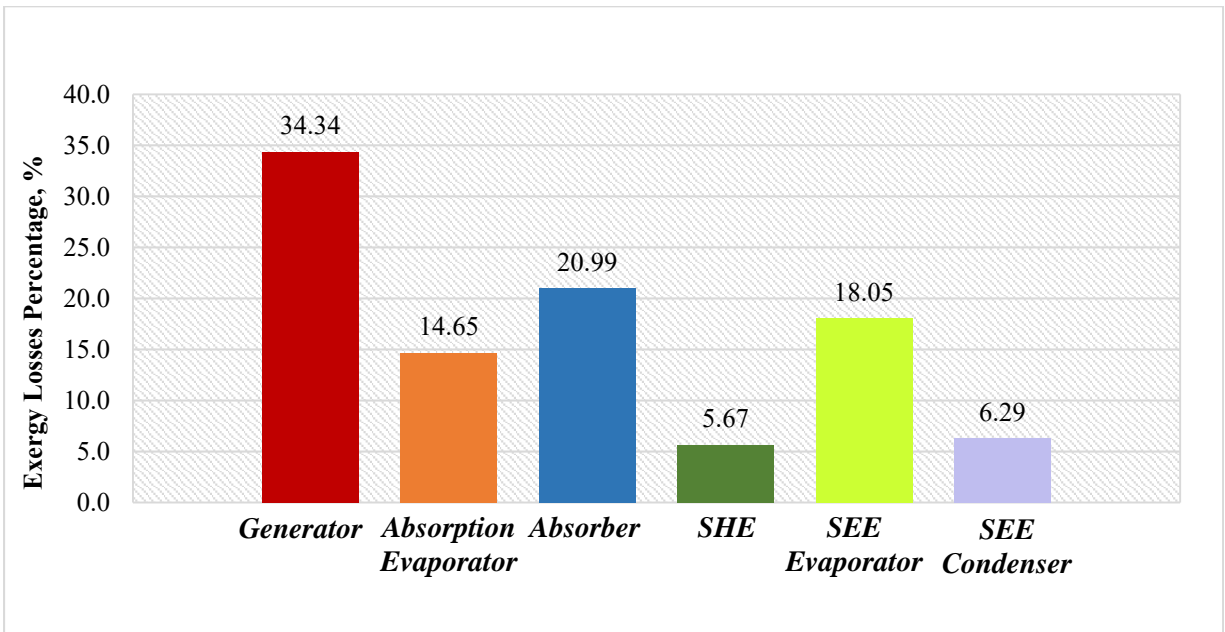
Figure 5-20 Exergy losses percentage of each component

5.6 Case Study

In this section, a case study is considered to investigate the outputs from the combined H_2O-LiBr absorption and SEE system. In gulf region especially in summer, the temperatures are quite high during the whole season where passive cooling cannot tolerate the thermal mass effect and the enormous summer temperature. Therefore, active cooling is required. Absorption refrigeration system is used instead of a vapor compression (VC) system to reduce the electric energy consumption and reduce GHG emissions. A combined H_2O-LiBr absorption and SEE system is operated to provide the required cooling effect and potable water especially during the day time. Table 5-2 presents the input data for the absorption and desalination hybrid system. A program is written using EES platform to calculate the cooling capacity, distilled water produced and the overall system efficiency. Moreover, the temperature, specific enthalpy, and mass flow rate for the whole system are discussed through Table 5-3. Afterward, the system`s performance is evaluated by computing the PR, CR, and COP through Table 5-4.

Table 5-2 Input parameters of cooling and desalination system case study

Input Parameters	Cycle	Value
Generator temperature (T_7)	LiBr	90 °C
Condenser temperature (T_8)	LiBr	30 °C
Evaporator temperature (T_{10})	LiBr	5 °C
Absorber temperature (T_1)	LiBr	30 °C

Diluted LiBr solution mass flow rate ($\dot{m}_{ws}$)	LiBr	0.02 kg/s
Absorber outlet water quality (Q_{a1})	LiBr	0
Generator outlet water quality (Q_{a4})	LiBr	0
Generator outlet refrigerant quality (Q_{a7})	LiBr	1
Condenser outlet water quality (water state) (Q_{a8})	LiBr	0
Evaporator outlet water quality (Q_{a10})	LiBr	1
Input feed seawater + Cooling water flow rate ($\dot{m}_{11}$)	SEE	0.5 kg/s
Percentage of feed water to the desalination-evaporator	SEE	50%
Inlet seawater temperature (T_{11})	SEE	30 °C
Feed salinity (X_f)	SEE	42 g/kg
Desalination system pressure	SEE	60 kPa
Absorber cooling water inlet temperature (T_{24})	LiBr	25 °C
Absorber cooling water mass flow rate ($\dot{m}_{24}$)	LiBr	0.4 kg/s
Inlet chilled water temperature (to evaporator) (T_{20})	LiBr	25 °C
Chilled water mass flow rate ($\dot{m}_{20}$)	LiBr	0.4 kg/s

Table 5-3 Thermodynamic properties of cooling and desalination hybrid system

State Point	Pressure (kPa)	Temperature (°C)	Specific Enthalpy (kJ/kg)	Mass Flow Rate (kg/s)	Concentration (kg LiBr /kg Solution)
1	0.87	30	66.3	0.02	52.9
2	4.24	30	66.3	0.02	52.9
3	4.24	56.83	123.3	0.02	52.9
4	4.24	90	249.1	0.0156	67.56
5	4.24	48	176.4	0.0156	67.56
6	0.87	57.96	176.4	0.0156	67.56
7	4.24	90	2669	0.00433	0
8	4.24	30	125.7	0.00433	0
9	0.87	5	125.7	0.00433	0
10	0.87	5	2510	0.00433	0
11	-	30	118.5	0.05	-
12	-	30	118.5	0.05	-
13	-	79.45	322.6	0.05	-

14	40	86.69	341.5	0.02	-
15	40	85.95	2653	0.0046	-
16	40	85.95	359.9	0.0046	-
17	40	79.45	322.6	0.025	-
18	-	79.45	322.6	0.025	-

Table 5-4 Output parameters for cooling and desalination hybrid system

Output Parameters	Cycle	Value
Generator load	LiBr	13 kW
Condenser load	LiBr	11 kW
Evaporator load	LiBr	10 kW
Absorber load	LiBr	12.3 kW
SHE load	LiBr	1.14 kW
Desalination evaporator load	SEE	11 kW
Desalination condenser load	SEE	10.7 kW
COP	LiBr	0.794
PR	SEE	1.078

EUF	LiBr/SEE	1.6
BPE	SEE	0.738 °C
$\dot{m}_d$	SEE	0.0044 kg/s
CR	LiBr	4.62
Brine salinity	SEE	51.64 g/kg
Brine temperature	SEE	86.69 °C
Rejected cooling water temperature	SEE	79 °C

The results are shown in Table 5-4,where the cooling load is 10 kW, which is enough to be delivered to a small area with a reasonable thermal load. Moreover, the produced distilled water is 0.0044 kg/s which is about 15.6 L/h that is enough for the regular person in the daily requirements according to World Health Organization (WHO) [59]. WHO estimated that during the moderate physical activity and over the average temperature, the minimum amount of water to take care of basic hygiene needs and basic food hygiene is 20 L/day/capita. The system performance COP and PR are 0.79, 1.087, respectively. These outputs are more than the range of the highest performance of the standalone subsystems in the literature.

5.6.1 Cost analysis

In this section, the life cycle cost analysis (LCCA) of the combined H_2O-LiBr absorption and SEE system is presented and compared with ordinary Vapor Compression System in Saudi Arabia.

The LCCA is the calculation of the total cost of the system over its lifetime. The LCCA depends on present worth value cost method (PWC), where the total PWC is determined by counting the initial, operation, maintenance, replacement, and salvage costs [60]. Note that the value of the money is a function of available interest, and inflation rates.

The life cycle cost analysis (LCCA) is calculated by Equation (5-10) [60].

$$LCCA = C_A + (A \times C_O) + (A \times C_M) + (B \times C_R) - (B \times C_S) \qquad (5\text{-}10)$$

Where C_A, C_O, C_M, C_R, C_S are initial, operation, maintenance, replacement, and salvage costs, respectively.

$$A = \frac{(1+i)^n - 1}{i(1+i)^n} \qquad (5\text{-}11)$$

$$B = \frac{1}{(1+i)^n} \qquad (5\text{-}12)$$

Where A, B are constants and i, and n are the discount rate and project life time, respectively.

Initial Cost

The system initial cost consists of the asset and installation prices of the hybrid system components. such as the solar collectors array, H_2O-LiBr absorption system, desalination system, piping, control system, and Pumping units. The input energy to the system is assumed to be from thermal solar collectors, where the type of the collector depends on the desired generator temperature. Flat plate/ evacuated tube collectors are suitable for single stage absorption refrigeration system, while parabolic troughs collectors are proper for higher temperature applications such as double stage absorption refrigeration system.

Operation Cost

The system operation cost includes the spare-parts, wages, electricity consumption costs, and any running cost needed in the operation. The Kingdom of Saudi Arabia electric tariffs are estimated to be 5 halala/kWh (1.33 Cent/kWh) for a consumption less than 1000 kWh for the residential sector [61].

Maintenance Cost

The maintenance program is an important sector to insure a high reliability and efficiency operation. Maintenance program are divided into predictive, preventive, and corrective (failure) maintenance. Preventive maintenance cost will be focused on the running machines as pumps. Maintenance cost cited in previous studies for absorption cooling systems are estimated by a value between 1-2% of the total capital cost [60].

Replacement Cost

Replacement cost includes any addition money needed to replace any auxiliary equipment during project life time.

Salvage Value

Salvage value means the price of the fixed asset at the end on the project life time, where the salvage value is estimated to be 5% of the total initial cost [60].

5.6.1.1 The Combined System Case Study

In this section, the cost analysis of the combined H_2O-LiBr absorption and SEE system is investigated, where the projected life time is assumed to be 20 years. The proposed system cooling

capacity is 10 kW, and the distilled water productivity is 15.62 L/h. The initial cost for the whole

system is shown in Table 5-5.

Table 5-5 Total Initial Cost of the combined H_2O-LiBr absorption and SEE system

Component	Cycle	Price
Heater	Heating	1500 $ [62]
Generator	LiBr	430 $ [29]
Condenser	LiBr/ SEE	1100 $ [29]
Evaporator	LiBr	1100 $ [29]
Absorber	LiBr	1100 $ [29]
Desalination Condenser	SEE	430 $ [29]
Control, Sensors and valves	LiBr/ SEE	860 $ [29]
LiBr Pump	LiBr	500 $ [29]
LiBr salt	LiBr	700 $ [29]
Seawater pump (Stainless steel)	SEE	200 $ [63]
Chiller Pump	LiBr	100 $ [63]
Total Cost		8020 $

The operation cost is calculated by summing pumps electricity consumption during the project life time, and spare-parts that will be used like bearings and greasing (500 $). The working hours are assumed to be 8 hours per day during the project lifetime.

Electricity cost will be 1.33 Cent/kWh as the monthly consumption is low, and the total power consumption is estimated to be 2 kW.

Electricity cost = (1.33) * (2* 8 * 30 * 12 * 20)

$$= 1540 \text{ \$}$$

Hence, the total operation cost is approximately 2000 $.

Maintenance cost is estimated to be around 500 $ as the system has high durability. And labor cost will be 500 $.

Replacement cost will include the pump replacement, system sensors and valves once

Replacement cost = 1* (100+200+500+860)

$$=1660 \text{ \$}.$$

Salvage Value is estimated at the end of the project life time by 5% from the initial cost.

Salvage Value = 400 $. Then,

C_A = 8020 $ C_O =2000 $

C_M = 1000 $ C_R = 1660 $

C_S = 400 $

Then, the total life cycle cost can be determined using equations (5-7) to (5-9) assuming discount rate (i) and life time (n) as 5 % and 20 years:

$$A = \frac{(1+i)^n - 1}{i(1+i)^n} = \frac{(1+0.05)^{20} - 1}{0.05(1+0.05)^{20}} = 12.46$$

$$B = \frac{1}{(1+i)^n} = \frac{1}{(1+0.05)^{20}} = 0.376$$

$$LCCA = C_A + (A \times C_O) + (A \times C_M) + (B \times C_R) - (B \times C_S)$$

$$= 8020 + (12.46 \times 2000) + (12.46 \times 1000) + (0.376 \times 1660) - (0.376 \times 400)$$

$$= 8020 + \quad 24920 \quad + \quad 12460 \quad + \quad 624.16 \quad - \quad 150.4$$

$$= 45,874.16 \text{ \$}$$

Finally, the total life cost for the proposed combined system is 45,874 $ during 20 years, to produce cooling effect of 10 kW and distilled water 15.62 L/h during the solar 8 hours.

5.6.2 Vapor Compression System and Governmental Water

The cost analysis of both Wall Mount Mini Split Air Conditioner and governmental water system is investigated, where the projected life time is assumed to be 20 years. The proposed system cooling capacity is 10 kW, and the fresh water consumption is 15.62 L/h. The initial cost for the cooling system is mainly the air conditioning units, where 3 units of GREE RIO 12HP115V1A [64] is used with a cooling capacity, and rated power consumption of 3*3.45 kW (3*11,800 BTU/h), and 5.2kW, respectively, that costs 3*723 $. Consequently, the total fixed cost of split system is 2169 $.

Electricity cost will be 1.33 Cent/kWh as the monthly consumption is low, and the total power consumption is estimated to be 5.3 kW.

Electricity cost = (1.33) * (5.2* 8 * 30 * 12 * 20)

= 4000 $

Hence, the total operation cost is approximately 4000 $.

Maintenance labor cost is estimated to be around 1000 $.

Replacement cost will include the whole system once every 15 years [65].

Replacement cost = 1* (2169)

=2169 $.

Salvage Value is estimated at the end of the project life time by 5% from the initial cost, and salvage cost of the dilapidated system is added.

Salvage Value = 108+108

= 217

Then,

C_A = 2169 $ C_O =4000 $ C_R = 2169 $

C_M = 2000 $ C_S = 217 $

Then, the total life cycle cost can be determined using equations (5-7) to (5-9) assuming discount rate (i) and life time (n) as 5 % and 20 years:

$$A = \frac{(1+i)^n - 1}{i(1+i)^n} = \frac{(1+0.05)^{20} - 1}{0.05(1+0.05)^{20}} = 12.46$$

$$B = \frac{1}{(1+i)^n} = \frac{1}{(1+0.05)^{20}} = 0.376$$

$$LCCA = C_A + (A \times C_O) + (A \times C_M) + (B \times C_R) - (B \times C_S)$$

$$= 2169 + (12.46 \times 4000) + (12.46 \times 1000) + (0.376 \times 2169) - (0.376 \times 217)$$

$$= 2169 + \quad 49840 \quad + \quad 12460 \quad + \quad 814 \quad - \quad 81$$

$$= 64{,}202 \ \$$$

Secondly, the fresh water consumption will be 15.62 L/h (124.96 L/day) for 8 solar working hours, hence the water tariff will be 0.1 SR/m^3 as the monthly consumption is 3.8 m^3/day [66]

Hence water consumption cost per 20 years is

Water consumption cost = (0.1) * (3.8* 365 * 20) = 2774 SR (737 $)

Water Consumption after 20 years is $(A \times C_O)$

Water Consumption after 20 = 8853 $

Finally, the total cost for the split air unit and governmental water supply is (8853+64202), that is equals 73,055 $.

The hybrid LiBr absorption and SEE system has reduced the LCCA by 27,181 $

Chapter 6: **Conclusions**

Thermodynamic analysis of the proposed integrated H_2O-LiBr absorption cycle with single effect desalination (SEE) system have been carried out using EES software to measure the performance of the combined and standalone systems.

For SEE subsystem, the results showed that the distilled water increased from 0.76, 0.93 kg/s by decreasing the top brine temperature from 94 °C to 76 °C. Moreover, the produced distilled water increased by increasing the input steam/refrigerant temperature. Consequently, the PR increased at a constant steam flow rate. In addition, the increase of the input feed seawater temperature increases the evaporated water vapor that increased the PR at a constant steam flow rate, where the PR is boosted from 0.82 to 0.987 by changing inlet seawater from 15 °C to 30 °C, respectively. However, the increase of the input feed seawater temperature would double the condenser surface area which will increase the initial construction cost and subsystem volume. The increase in the top brine temperature greatly affects the evaporator and condenser surface areas, the evaporator surface area decreased by increasing top brine temperature as the temperature difference between steam and top brine temperature (T_7-T_b) decreased with constant heat input to the system. However, the condenser surface area decreased as the rate of heat transfer through the condenser decreased by increasing the brine boiling temperature as the enthalpy of vaporization decreased by increasing system pressure.

For H_2O-LiBr absorption subsystem, the result showed that the generator temperature has a great impact on system performance, where the increase in generator temperature from 72 °C to 100 °C has increased the COP of the cooling system from 0.54 to 0.78, Moreover, the effectiveness of SHE played a big role in reducing the input energy as it boosted the COP by 14.2% with

changing SHE effectiveness from 50% to 90%. On the other hand, the COP decreased from 0.78 to 0.52 by increasing condenser temperature from 30 °C to 50 °C as strong LiBr solution concentration in inversely proportional to the condenser temperature, hence, the strong LiBr solution flow rate increased. Consequently, the evaporated refrigerant decreased that reduced the needed cooling effect and COP. However, the COP increased by increasing evaporator temperature.

The diluted LiBr solution concentration is inversely proportional to evaporator temperature, hence, the diluted LiBr solution concentration decreased that increased the strong LiBr solution flow rate. Consequently, the evaporated refrigerant increased which increases the cooling capacity and the COP. The system efficiency increased to a certain value then a significant reduction occurs by increasing the generator temperature, this is because of the high exergy losses as the temperature variation between the generator and ambient increases by increasing generator temperature. The highest system efficiency is 78% that occurs at $T_{gen}=78$ °C.

For the hybrid system, the results showed that the increase in generator temperature from 75 °C to 90 °C has increased the refrigerant mass flow rate and COP by 250%, and 10.86%, respectively. Moreover, the decrease in the desalination system pressure from 80 kPa to 40 kPa has boosted the distilled water flow rate and PR by 33.15% and 32.37%, respectively, at generator temperature of 90 °C. In addition, the generator input energy has decreased by 25.37% by using a SHE with 100% effectiveness, also the needed absorber cooling water pumping power has decreased as the concentrated LiBr solution lost a large quantity of energy through SHE.

The increase in the condenser temperature from 30 °C to 45 °C has decreased the refrigerant mass flow rate and COP by 60% and 11.67%, respectively. This temperature increase has reduced

distilled water evaporation to zero. Moreover, the increase of absorber temperature from 30 °C to 45 °C has the same influence on the system parameters, where the refrigerant mass flow rate and COP have decreased by 63% and 8.5%, respectively. This temperature increase has reduced distilled water evaporation to zero.

On the other hand, the increase in evaporator temperature from 2 °C to 6 °C has increased the refrigerant mass flow rate and COP by 31% and 3.2%, respectively. Moreover, the evaporator temperature increase has boosted the distilled water mass flow rate and PR by 73% and 31%, respectively. The EUF for the combined system has been improved with 70% by increasing generator temperature from 80 °C to 90 °C, respectively. Moreover, the combined system performance EUF is boosted to a value of 1.6 which is almost double the performance of the standalone absorption system with a COP value of 0.766. The exergy analysis showed that the generator has the highest exergy losses influence with a share of 34.34% also, the exergy efficiency decreases by increasing generator temperature as the temperature difference between generator and ambient temperatures increases.

Finally, this combined system has a promising output parameters where the cost analysis showed that the combined system has reduced the LCCA by 27,181 $ if compared with an ordinary VCS over a life time of 20 years. However, the desalination plant must be operated as long as the cooling plant is working to keep the cooling conditions for LiBr condenser, otherwise the cooling system will not work. Moreover, care must be taken in operating the desalination plant in the combined system, as the generator temperature must be over a certain limit to evaporate sufficient refrigerant mass flow rate to evaporate distilled water in the desalination system.

References

[1]   Y. Fan, L. Luo, and B. Souyri, "Review of solar sorption refrigeration technologies: Development and applications," *Renew. Sustain. Energy Rev.*, vol. 11, no. 8, pp. 1758–1775, 2007.

[2]   M. A. Dawoud, "The role of desalination in augmentation of water supply in GCC countries," *Desalination*, vol. 186, no. 1–3, pp. 187–198, 2005.

[3]   R. Al Hashemi, S. Zarreen, A. Al Raisi, F. . Al Marzooqi, and S. . Hasan, "A Review of Desalination Trends in the Gulf Cooperation Council Countries," *Int. Interdiscip. J. Sci. Res.*, vol. 1, no. 2, pp. 72–96, 2014.

[4]   L. García-Rodríguez, "Seawater desalination driven by renewable energies: A review," *Desalination*, vol. 143, no. 2, pp. 103–113, 2002.

[5]   S. G. Sundaresan, "Characterization of the CFC issues relating to the air conditioning and refrigeration industry part 2: standards for acceptable levels of contaminants in refrigerants," *Int. J. Refrig.*, vol. 11, no. 4, pp. 213–216, 1988.

[6]   S. A. K. Keith Herold, Reinhard Radermacher, *Absorption Chillers and Heat Pumps*, 1 edition. CRC Press, 1996.

[7]   B. Prasartkaew, "Performance test of a small size LiBr-H$_2$O absorption chiller," *Energy Procedia*, vol. 56, no. C, pp. 487–497, 2014.

[8]   P. Srikhirin, S. Aphornratana, and S. Chungpaibulpatana, "A review of absorption refrigeration technologies," *Renew. Sustain. Energy Rev.*, vol. 5, no. 4, pp. 343–372, 2000.

[9]   W. Pridasawas, "*Solar-driven refrigeration systems with tocus on the ejector cycle,*" no. October. 2006.

[10]   S. C. Kaushik and S. Chandra, "Computer modeling and parametric study of a double effect generation absorption refrigeration cycle," *Energy Convers. Manag.*, vol. 25, no. 1, pp. 9–14, 1985.

[11]   B. H. Gebreslassie, M. Medrano, and D. Boer, "Exergy analysis of multi-effect water-LiBr absorption systems: From half to triple effect," *Renew. Energy*, vol. 35, no. 8, pp. 1773–1782, 2010.

[12]   Z. . Li and K. Sumathy, "Technology development in the solar absorption air-conditioning systems," *Renew. Sustain. Energy Rev.*, vol. 4, no. 3, pp. 267–293, 2000.

[13]   I. S. Al-Mutaz, "Potential of nuclear desalination in the Arabian Gulf countries," *Desalination*, vol. 135, no. 1–3, pp. 187–194, 2001.

[14]   A.M. El Nashar, "The role of desalination in water resources management in Gulf Region," in *IV Iberian Congress on Management and Planning of the Water Science, Technique and Citizenship:Keys for a Sustainable Management of the Water*, 2004.

[15]   A. D. Khawaji, I. K. Kutubkhanah, and J. M. Wie, "Advances in seawater desalination technologies," *Desalination*, vol. 221, no. 1–3, pp. 47–69, 2008.

[16]   H. El-Dessouky and H. Ettouney, "Chapter 2 – Single Effect Evaporation," *Fundam. Salt Water Desalin.*, pp. 19–48, 2002.

[17]   S. Aphornratana and T. Sriveerakul, "Experimental studies of a single-effect absorption refrigerator using aqueous lithium-bromide: Effect of operating condition to system

performance," *Exp. Therm. Fluid Sci.*, vol. 32, no. 2, pp. 658–669, 2007.

[18]   E. Kurem and I. Horuz, "A comparison between ammonia-water and water-lithium bromide solutions in absorption heat transformers," *Int. Commun. Heat Mass Transf.*, vol. 28, no. 3, pp. 427–438, 2001.

[19]   I. Horuz and T. M. S. Callander, "Experimental investigation of a vapor absorption refrigeration system," *Int. J. Refrig.*, vol. 27, no. 1, pp. 10–16, 2004.

[20]   F. Asdrubali and S. Grignaffini, "Experimental evaluation of the performances of a H_2O-LiBr absorption refrigerator under different service conditions," *Int. J. Refrig.*, vol. 28, no. 4, pp. 489–497, 2005.

[21]   M. A. Hammad and M. S. Audi, "Performance of a solar LiBr-water absorption refrigeration system," *Renew. Energy*, vol. 2, no. 3, pp. 275–282, 1992.

[22]   V. Boopathi Raja and V. Shanmugam, "A review and new approach to minimize the cost of solar assisted absorption cooling system," *Renew. Sustain. Energy Rev.*, vol. 16, no. 9, pp. 6725–6731, 2012.

[23]   F. L. Lansing, "Computer modeling of a single-stage lithium bromide/water absorption refrigeration unit," *The Interplanetary Network Progress Report*, no. 42–32. 1976.

[24]   S. Bolocan, F. Chiriac, A. Serban, G. Dragomir, and G. Nastase, "Development of a Small Capacity Solar Cooling Absorption Plant," *Energy Procedia*, vol. 74, pp. 624–632, 2015.

[25]   A. Șencan, K. A. Yakut, and S. A. Kalogirou, "Exergy analysis of lithium bromide/water absorption systems," *Renew. Energy*, vol. 30, no. 5, pp. 645–657, 2005.

[26] O. Ketfi, M. Merzouk, N. K. Merzouk, and S. El Metennani, "Modeling and simulation of a single stage solar absorption cooling machine under Algerian climate," *Proc. 2015 IEEE Int. Renew. Sustain. Energy Conf. IRSEC 2015*, pp. 2–6, 2016.

[27] H. S. Majdi, "Performance evaluation of combined ejector LiBr/H2O absorption cooling cycle," *Case Stud. Therm. Eng.*, vol. 7, pp. 25–35, 2016.

[28] F. Agyenim, I. Knight, and M. Rhodes, "Design and experimental testing of the performance of an outdoor LiBr/H2O solar thermal absorption cooling system with a cold store," *Sol. Energy*, vol. 84, no. 5, pp. 735–744, 2010.

[29] G. A. Florides, S. A. Kalogirou, S. A. Tassou, and L. C. Wrobel, "Design and construction of a LiBr-water absorption machine," *Energy Convers. Manag.*, vol. 44, no. 15, pp. 2483–2508, 2003.

[30] S. Kaushik and S. Singh, "Thermodynamic Analysis of Vapor Absorption Refrigeration System and Calculation of COP," *I Jraset*, vol. 2, no. 2, pp. 73–80, 2014.

[31] A. I. Shahata, M. M. Aboelazm, and A. F. Elsafty, "Energy and Exergy Analysis for Single and Parallel Flow Double Effect Water-Lithium Bromide Vapor Absorption Systems," *Analysis*, vol. 2, no. 2, pp. 85–94, 2012.

[32] Y. Hu, "Advanced Exergy Analysis for a Solar Double Stage Absorption Chiller Advanced Exergy Analysis for a Solar Double Stage Absorption Chiller," 2012.

[33] M. I. Karamangil, S. Coskun, O. Kaynakli, and N. Yamankaradeniz, "A simulation study of performance evaluation of single-stage absorption refrigeration system using conventional working fluids and alternatives," *Renew. Sustain. Energy Rev.*, vol. 14, no. 7,

pp. 1969–1978, 2010.

[34] J. Wonchala, M. Hazledine, and K. Goni Boulama, "Solution procedure and performance evaluation for a water-LiBr absorption refrigeration machine," *Energy*, vol. 65, pp. 272–284, 2014.

[35] R. Gomri, "Second law comparison of single effect and double effect vapour absorption refrigeration systems," *Energy Convers. Manag.*, vol. 50, no. 5, pp. 1279–1287, 2009.

[36] S. C. Kaushik and A. Arora, "Energy and exergy analysis of single effect and series flow double effect water-lithium bromide absorption refrigeration systems," *Int. J. Refrig.*, vol. 32, no. 6, pp. 1247–1258, 2009.

[37] A. Al-Ugla, M. A. I. El-Shaarawi, and S. A. M. Said, "Alternative designs for a 24-hours operating solar-powered LiBr - Water absorption air-conditioning technology," *Int. J. Refrig.*, vol. 53, pp. 90–100, 2015.

[38] R. J. Romero, W. Rivera, I. Pilatowsky, and R. Best, "Comparison of the modeling of a solar absorption system for simultaneous cooling and heating operating with an aqueous ternary hydroxide and with water/lithium bromide," *Sol. Energy Mater. Sol. Cells*, vol. 70, no. 3, pp. 301–308, 2001.

[39] X. Liao and R. Radermacher, "Absorption chiller crystallization control strategies for integrated cooling heating and power systems," *Int. J. Refrig.*, vol. 30, no. 5, pp. 904–911, 2007.

[40] L. Garousi Farshi, S. M. Seyed Mahmoudi, and M. A. Rosen, "Analysis of crystallization risk in double effect absorption refrigeration systems," *Appl. Therm. Eng.*, vol. 31, no. 10,

pp. 1712–1717, 2011.

[41] Y. Kaita, "Thermodynamic properties of lithium bromide-water solutions at high temperatures," *Int. J. Refrig.*, vol. 24, no. 5, pp. 374–390, 2001.

[42] M. Shatat, M. Worall, and S. Riffat, "Opportunities for solar water desalination worldwide: Review," *Sustain. Cities Soc.*, vol. 9, pp. 67–80, 2013.

[43] S. A. Kalogirou, "Seawater desalination using renewable energy sources," *Prog. Energy Combust. Sci.*, vol. 31, no. 3, pp. 242–281, 2005.

[44] S. Casimiro, C. Ioakimidis, J. Mendes, and M. Giestas, "Modeling in TRNSYS of a single effect evaporation system powered by a Rankine cycle," *Desalin. Water Treat.*, vol. 51, no. 7–9, pp. 1405–1415, 2013.

[45] K. H. Mistry, M. A. Antar, and J. H. Lienhard V, "An improved model for multiple effect distillation," *Desalin. Water Treat.*, vol. 51, pp. 1–15. April 2013.

[46] A. Al-Ansari, H. Ettouney, and H. El-Dessouky, "Water-zeolite adsorption heat pump combined with single effect evaporation desalination process," *Renew. Energy*, vol. 24, no. 1, pp. 91–111, 2001.

[47] F. Al-Juwayhel, H. El-Dessouky, and H. Ettouney, "Analysis of single-effect evaporator desalination systems combined with vapor compression heat pumps," *Desalination*, vol. 114, no. 3, pp. 253–275, 1997.

[48] K. Parham, M. Yari, and U. Atikol, "Alternative absorption heat transformer configurations integrated with water desalination system," *Desalination*, vol. 328, pp. 74–82, 2013.

[49]   M. Ibrahim and I. Dincer, "Experimental performance evaluation of a combined solar system to produce cooling and potable water," *Sol. Energy*, vol. 122, pp. 1066–1079, 2015.

[50]   H. K. Abdulrahim and M. A. Darwish, "Thermal desalination and air conditioning using absorption cycle," *Desalin. Water Treat.*, vol. 55, no. 12, pp. 3310–3329, 2015.

[51]   C. Chiranjeevi and T. Srinivas, "Influence of vapor absorption cooling on humidification-dehumidification (HDH) desalination," *Alexandria Eng. J.*, vol. 55, no. 3, pp. 1961–1967, 2016.

[52]   K. Fathalah and S. E. Aly, "Theoretical study of a solar powered absorption/MED combined system," *Energy Convers. Manag.*, vol. 31, no. 6, pp. 529–544, 1991.

[53]   F. Mandani, H. Ettouney, and H. El-Dessouky, "H$_2$O-LiBr absorption heat pump for single-effect evaporation desalination process," *Desalination*, vol. 128, no. 2, pp. 161–176, 2000.

[54]   C. Chiranjeevi and T. Srinivas, "Combined two stage desalination and cooling plant," *Desalination*, vol. 345, pp. 56–63, 2014.

[55]   V. G. Gude and N. Nirmalakhandan, "Combined desalination and solar-assisted air-conditioning system," *Energy Convers. Manag.*, vol. 49, no. 11, pp. 3326–3330, 2008.

[56]   F. Alvarado and S. A. Klein, "EngineeringEquationSolver,F-ChartSoftware," *Middleton, WI, USA*, 1999.

[57]   James L. Threlkeld, *Thermal Environmental Engineering*, Second Edi. Prentice-Hall, 1970.

[58]   P. Zadeh, "The energy and exergy analysis of single effect absorption chillers," *Mech. Eng.*, vol. 4, no. 4, 2011.

[59]   "World Health Organization." [Online]. Available: http://www.who.int/en/.

[60]   S. Yongprayun, N. Ketjoy, W. Rakwichian, and S. Maneewan, "Techno-economic Analysis of a LiBr-H_2O Solar Absorption Cooling System in Thailand," vol. 2, no. 2, 2007.

[61]   "Kingdom of Saudi Arabia Electricity Tariffs.Saudi Electricity Company," 2015. [Online]. Available: https://www.se.com.sa/en-us/customers/Pages/TariffRates.aspx.

[62]   Www.alibaba.com, "greentechnology (Heater)." .

[63]   Www.alibaba.com, "https://www.alibaba.com/product-detail/STAINLESS-STEEL-SEA-WATER-PUMP_60235768518.html?spm=a2700.7735675.30.1.JbZFb9&s=p." .

[64]   GREE, "Online DC inverter-driven ductless split systems 16 SEER." [Online]. Available: http://resource.comfortup.com/is/content/Watscocom/article_1391689035744_en_ss?fmt=pdf.

[65]   G. Rosenquist, K. Coughlin, L. Dale, J. Mcmahon, and S. Meyers, "Life-cycle Cost and Payback Period Analysis for Commercial Unitary Air Conditioners," no. March, 2004.

[66]   "Saudi Aabia water tariff," Page 1. September, 2012.

VITAE

Name	Ahmad Mohammad Shaaban
Nationality	Egyptian
Date of Birth	17/01/1990
Email	ahmadshbn@hotmail.com
Mobile Number	+201007472249
Permanent Address	165 Tiba St. Sporting, Alexandria, Egypt
Academic Background	M.S. in Mechanical Engineering March, 2017 KFUPM, Saudi Arabia. B.S. in Mechanical Engineering September, 2012 Alexandria University, Egypt
Publications	**Ahmed M. Shaaban**, Maged A.I. El-Shaarawi, M.A. Antar. Thermodynamic Analysis of Combined H_2O-LiBr Absorption and Single Effect Evaporation Desalination system. Energy Conversion and Management. (Status: Ready to submit) Sherif S. Rashwan, **Ahmed M. Shaaban**, Fahad Al-Suliman. A comparative study of a small-scale solar PV power plant in Saudi Arabia. Renewable & Sustainable Energy Reviews. (Status: Under 2nd review).